TECHNICAL REPORT ECOM 01207-F September 1967

ERROR REDUCTION IN LOOP DIRECTION FINDERS

FINAL REPORT

1 MARCH 1967 TO 30 JUNE 1967

Report No. 8

CONTRACT NO. DA 28-043 AMC-01207(E)
DA PROJECT NO. 5A6-79191-D902-0103

Prepared By
H. H. JENKINS and R. W. MOSS
ENGINEERING EXPERIMENT STATION
GEORGIA INSTITUTE OF TECHNOLOGY
ATLANTA, GEORGIA

For

U. S. ARMY ELECTRONICS COMMAND
FORT MONMOUTH, N. J.

G. T. A.

FOREWORD

This report was prepared at the Georgia Tech Engineering Experiment Station on Contract DA 28-043 AMC-01207(E). The work covered by this report was performed within the Electronics Division and under the general supervision of Mr. D. W. Robertson, Head of the Communications Branch. The report summarizes the activities and results of a twenty-seven month effort directed to an investigation of bearing error reduction in HF direction finders equipped with electrically-small vertical loop antennas.

The authors gratefully acknowledge the assistance of Mr. W. B. Warren for his technical counsel; Mr. L. P. Cole for his assistance in fabrication, measurement, and data reduction; and Mr. D. W. Gore for his contributions to data reduction.

ABSTRACT

Techniques for reducing bearing errors in vertical loop HF direction finders for ionospherically propagated signals were developed and operationally evaluated. The investigation was concerned with the determination of specific characteristics of the incident signal and the subsequent use of these characteristics to restrict the display of the bearing information to the conditions that produce minimum bearing error.

The techniques were implemented in an exploratory dual-channel HF/DF system. The main channel produced a bearing display from the output of a rotating vertical loop; the auxiliary channel unblanked the bearing display when conditions were favorable for minimum bearing errors. A storage scope was also used for bearing display and memory.

Analyses of the error producing effects in loop systems showed that: (1) minimum bearing errors can be expected at or near the maxima of the vertical component of the incident signal; and (2) steady bearings normally possess less error than swinging bearings. Unblanking information was obtained by either detecting the fade crests of the vertical component of the incident signal or by using a swing rate discriminator to determine a steady bearing condition. Several modes of fade crest detection were included to optimize performance for a wide variety of signal and fade conditions.

Operational evaluation was performed in the field on signals from 5 to 20 MHz over path lengths exceeding several hundred miles. Primary consideration was given to transitional ionospheric conditions. Overall test results show that a large majority of the unblanked bearings can be restricted to within $\pm 15^{\circ}$ of the great circle bearing when the optimum mode of operation is used. Average bearing errors of 10° or less are typical.

Operational comparison of the exploratory system and the AN/PRD-5 showed that the exploratory system's performance is superior with a 2 to 1 reduction in bearing spreads, standard deviations, and RMS errors. Improvement is most significant in the presence of polarization fading.

A mathematical model was devised defining both bearing error and swing rate for polarization rotation of the incident signal. Test data showed that measured bearing errors and swing rates closely matched predicted errors from the model.

The advantages of the storage scope are discussed with emphasis on display memory and processing.

Investigations on specially-wound and doubly-loaded loops are described. Compensated loop techniques are discussed.

ABSTRACT (Continued)

Operational evaluation was performed in the field on signals from 5 to 20 MHz over path lengths exceeding several hundred miles. Primary consideration was given to transitional ionospheric conditions. Overall test results show that a large majority of the unblanked bearings can be restricted to within $\pm$ 15° of the great circle bearing when the optimum mode of operation is used. Average bearing errors of 10° or less are typical.

Operational comparison of the exploratory system and the AN/PRD-5 showed that the exploratory system's performance is superior with a 2 to 1 reduction in bearing spreads, standard deviations, and RMS errors. Improvement is most significant in the presence of polarization fading.

A mathematical model was devised defining both bearing error and swing rate for polarization rotation of the incident signal. Test data showed that measured bearing errors and swing rates closely matched predicted errors from the model.

The advantages of the storage scope are discussed with emphasis on display memory and processing.

Investigations on specially-wound and doubly-loaded loops are described. Compensated loop techniques are discussed.

TABLE OF CONTENTS

TABLE OF CONTENTS (Continued)

TABLE OF CONTENTS (Continued)

TABLE OF CONTENTS (Continued)

LIST OF FIGURES

LIST OF FIGURES (Continued)

LIST OF FIGURES (Continued)

LIST OF FIGURES (Continued)

LIST OF TABLES

1.0 INTRODUCTION

HF loop DF systems are susceptible to large bearing errors when used for ionospherically propagated signals. This report describes the results of an investigation conducted to develop and evaluate techniques for reducing these bearing errors.

The report consists of several major sections. The first section surveys the sources of errors with emphasis on the interaction of the loop and the incident signal. Determination of the error sources permitted development of specific techniques for error reduction. These techniques were implemented in a dual-channel HF/DF exploratory system which was operationally evaluated under field conditions. Major sections are devoted to a description of the specific techniques, the exploratory system, and the field test phase. Test results are presented and analyzed, and optimum modes of operation are defined. A section comparing the exploratory system's performance with the AN/PRD-5 HF/DF system illustrates the significant error-reducing capabilities of the exploratory system.

Other sections describe brief investigations conducted on special loop antenna configurations and compensated antenna systems.

2.0 FACTUAL DATA

2.1 Statement of the Problem - Sources of Bearing Errors in Loop Direction Finders

2.1.1 Introduction

There are three major error producing effects: abnormal polarization, wave interference, and path deviation. The following discusses these effects with emphasis on the character and magnitude of the bearing errors produced in the loop system. This discussion does not treat instrumental and site (environmental) errors, but discusses only those errors produced by the interaction of the loop with the incident signal.

2.1.2 Polarization Errors[1]

Loop DF accuracy depends upon the existence of a correct and constant relationship between the direction of propagation and the polarization of the E field vector. The correct polarization occurs when the incident E field contains no horizontal components perpendicular to the direction of propagation. In this case, which generally occurs with ground-wave signals, no polarization error exists, and the measured bearing will be the true great circle bearing (GCB). However, an E field polarization tilt creating horizontal components perpendicular to the direction of propagation results in bearing error.

A signal propagated via the ionosphere (sky-wave signal) is depolarized into a time-variant, elliptically polarized form. Polarization tilt introduces voltages in the loop that are not zero when the plane of the loop is perpendicular to the GCB. As the loop is rotated, the resulting null indicates a bearing which is incorrect. Such bearing errors are a function of the vertical angle of incidence, Φ, and polarization tilt angle, ψ. The general expression for the total induced voltage, V, in a small vertical loop (diameter less than about 0.1λ) located in free-space is given by

$$V = KE\,[\sin\theta\cos\psi - \cos\theta\cos\Phi\sin\psi] \qquad (1)$$

where

$K = \frac{2\pi}{\lambda}$ x(area of loop) x (number of turns),

θ = angle between direction of propagation and the normal to the plane of the loop,

λ = wavelength,

ψ = polarization tilt angle or the angle between the E-field vector and the vertical plane normal to the plane of the loop,

Φ = angle of vertical incidence of the wave or the angle between the direction of arrival of the incident wave and the plane of the loop,

and E = the electric field strength in volts/meter.

Figure 1 illustrates the above parameters.

If θ is not zero when a minimum value of V is obtained, a bearing error results. It is easily shown from equation (1) that the bearing error, θ_e, is given by

$$\theta_e = \tan^{-1} (\cos \Phi \tan \psi) \qquad (2)$$

when the loop is rotated until the receiver output is zero. Figure 2 depicts θ_e as a function of ψ for various selected values of Φ. Several factors are evident from figure 2. θ_e is a function of both Φ and ψ; hence, bearing accuracy can vary as the elevation angle-of-arrival changes even though polarization tilt is constant. Continuous uniform polarization rotation will create a continuously rotating bearing display with the rate of rotation, $\frac{d\theta_e}{d\psi}$, less near the true bearing, i.e., the bearings are steadiest near the GCB. However, for the worst case, $\Phi \equiv 0^\circ$, the bearing rotation is constant implying that the true bearing can not be ascertained based on an observation of the steadiness of a bearing display. For low angle signals ($\Phi \geq 80^\circ$), the variations in $\frac{d\theta_e}{d\psi}$ are more pronounced as ψ increases. For example, with ψ rotating between 0° and 45° θ_e is less than about 10° and changes slowly (bearing swing is slow), but as ψ increases, θ_e increases rapidly with ψ (bearing swing is fast).

Polarization tilt also decreases the sharpness or distinctness of the bearing null by decreasing the time-rate-of-change of the induced voltage as the antenna rotates through the null. This is manifested as a change in the slope of the null pattern. It may be shown that the relative change in slope is given by

$$\sqrt{1-\sin^2 \psi \sin^2 \Phi} \qquad (3)$$

which is plotted in figure 3 for selected Φ values. The most noticeable factor is that, for Φ values 0° to 30°, the null slope changes are less than about 12%. Above $\Phi = 30^\circ$, the change in slope increases rapidly.

Polarization errors are particularly prevalent when the sky-wave signal is experiencing Faraday rotation in the ionosphere and multi-

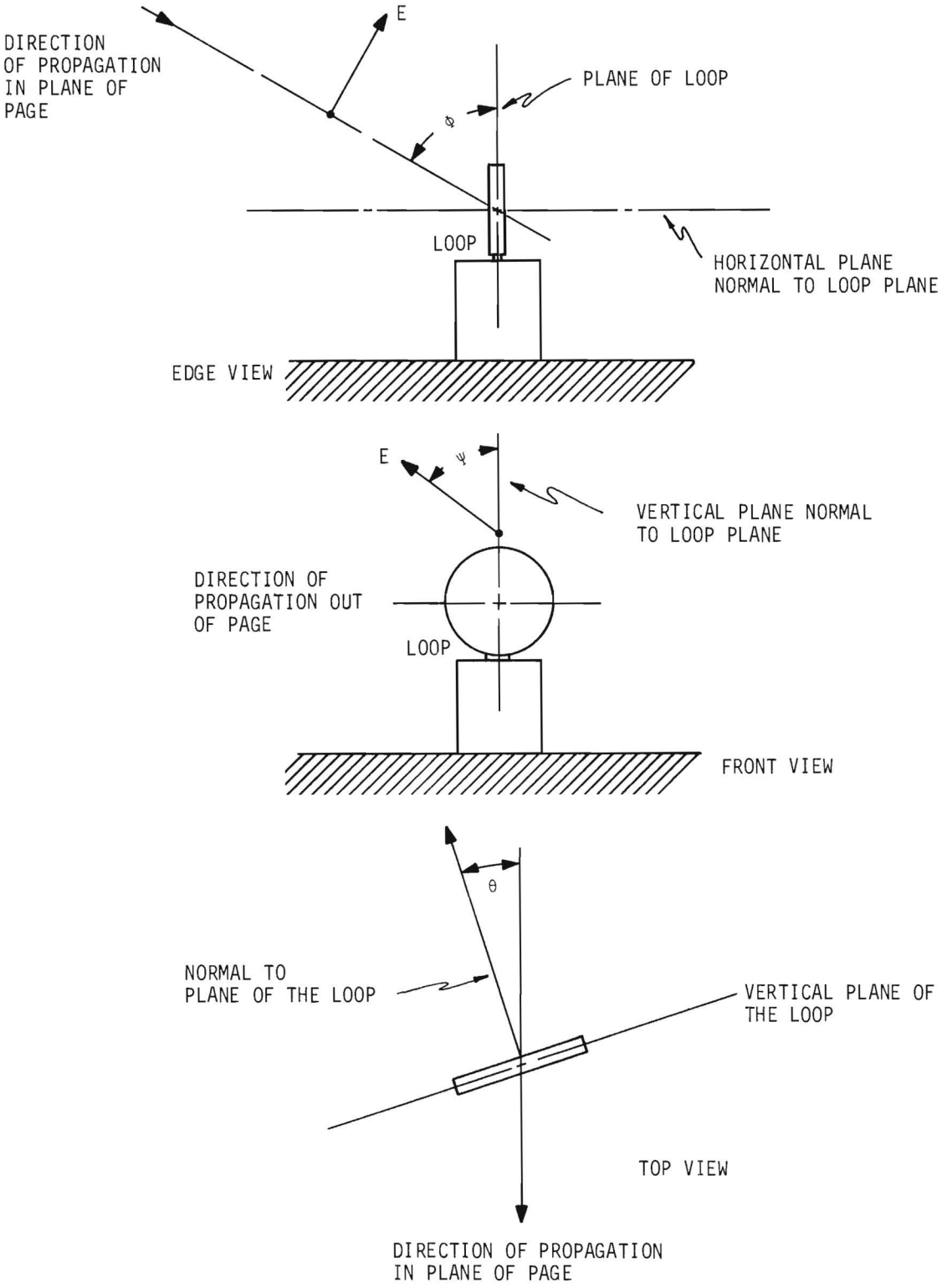

Figure 1. Diagrams of Parameters Pertinent to Equation (1).

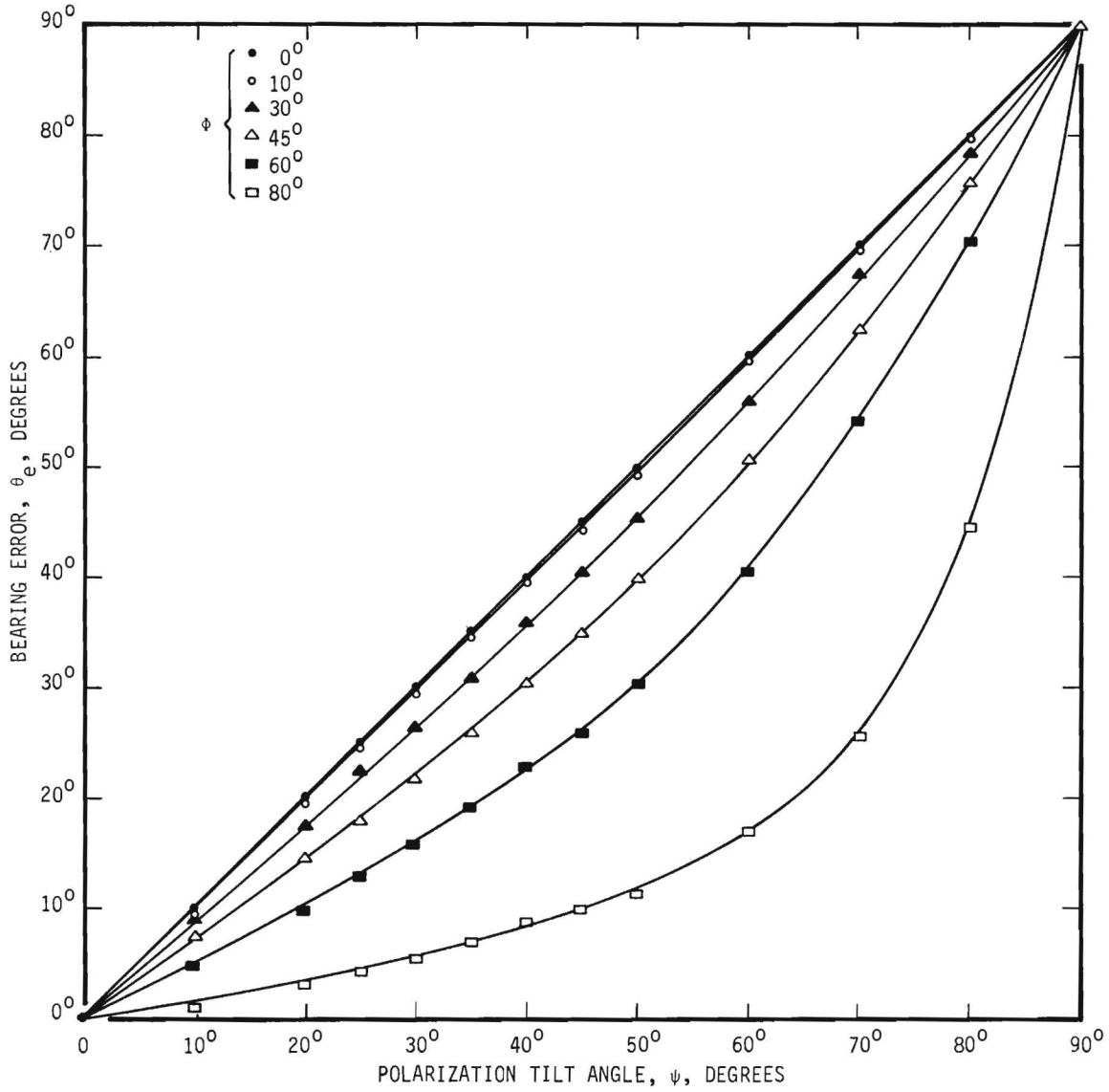

Figure 2. Bearing Error, θ_e, Versus Polarization Tilt Angle, ψ, for Fixed Vertical Angles of Incidence, Φ.

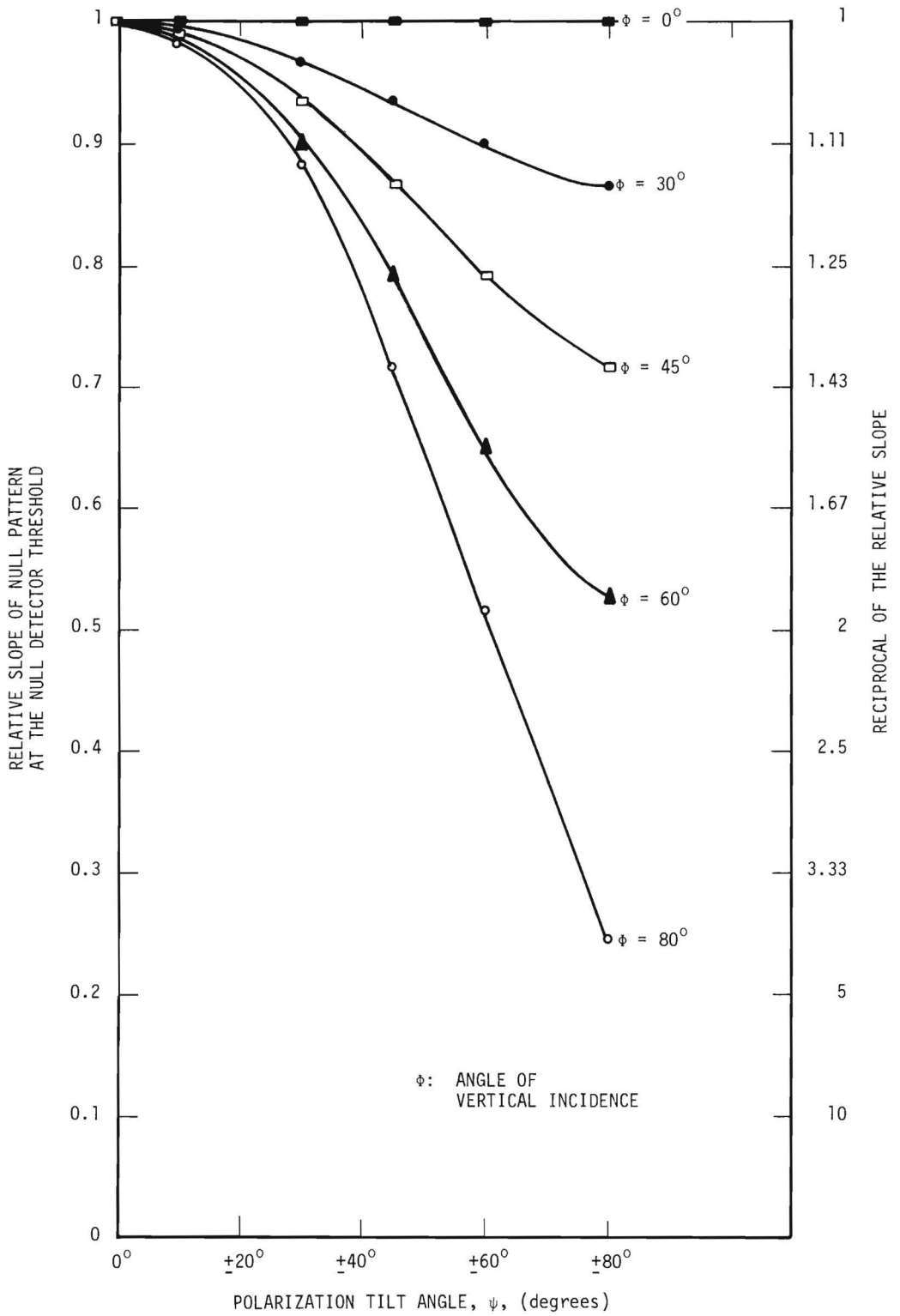

Figure 3. Relative Slope of Null Pattern as a Function of Φ and ψ.

path effects are minimal. This normally occurs near the MUF especially on a one-hop path. Faraday rotation leads to asynchronous polarization fading between the vertical and horizontal components of the incident signal with fade rates in the order of several per minute. This is illustrated by figure 4 which depicts the detected signals from a horizontal dipole (lower trace) and a 5 foot vertical whip (upper trace). The dipole had 7 foot elements and was boresighted on the GCB of the incident signal (VOA Greenville, N. C., on 9.5 MHz at 1225 GMT). The time base is 5 seconds per division. The asynchronous nature of the fading is evident in that the dipole nulls and peaks occur at whip peaks and nulls, respectively.

To summarize, bearing polarization rotation errors can be as large as $\pm 90^{\circ}$ from the GCB and are evidenced by swinging bearings and bearing display broadening with the slowest swing and minimum broadening near the GCB. However, as the elevation angle increases, the swing rate and bearing display characteristics become more uniform over a complete rotation cycle.

2.1.3 Wave-Interference Errors

Polarization errors are an inherent inadequacy of a loop antenna and can be reduced by using an entirely different DF antenna system, such as spaced loops or an Adcock. However, wave interference errors have their sources entirely external to the loop and are a source of bearing error for all DF systems. The loop is more susceptible to wave interference (or multipath) errors because it is an electrically-small, narrow-aperture device.

In practice, more than a single wave front at the same frequency is incident on a DF antenna. In fact, most of the energy is normally contained within discrete modes that arrive from many horizontal and vertical angles. The results of investigations[2] using wide-aperture, special-purpose antennas (such as the Wullenweber array) have delineated the complex, multimode structure of an ionospherically propagated signal. These studies have indicated that the discrete modes in the incident multimode signal are not only often of comparable amplitude but also arrive at different bearing angles. Also, the relative phases between the modes are time-variables. The resultant of all these variations is a corrugated phase front whose pattern is changing as a function of time. With a small-aperture loop antenna, the observed bearings at any instance will be normal to the phase surface at that point. Therefore, under wave interference effects, the bearings are constantly shifting and swinging. The effects can best be illustrated by a simple example.

Consider the case (figure 5) where two vertically polarized waves of the same amplitude are incident on the loop at A with the angles-of-arrival differing by 2θ. Assume that, at a given instant, the

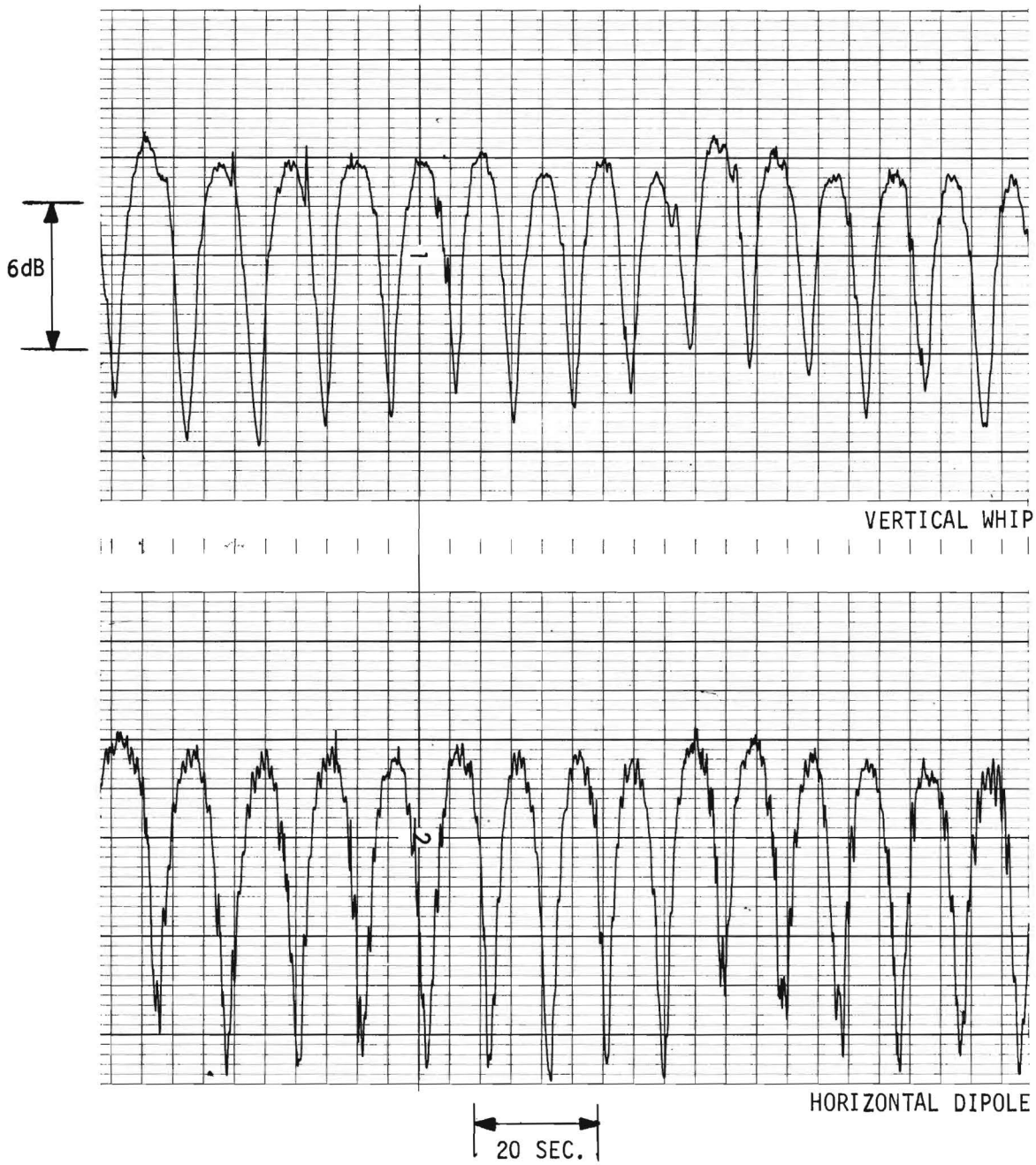

Figure 4. Example of Polarization Fading.

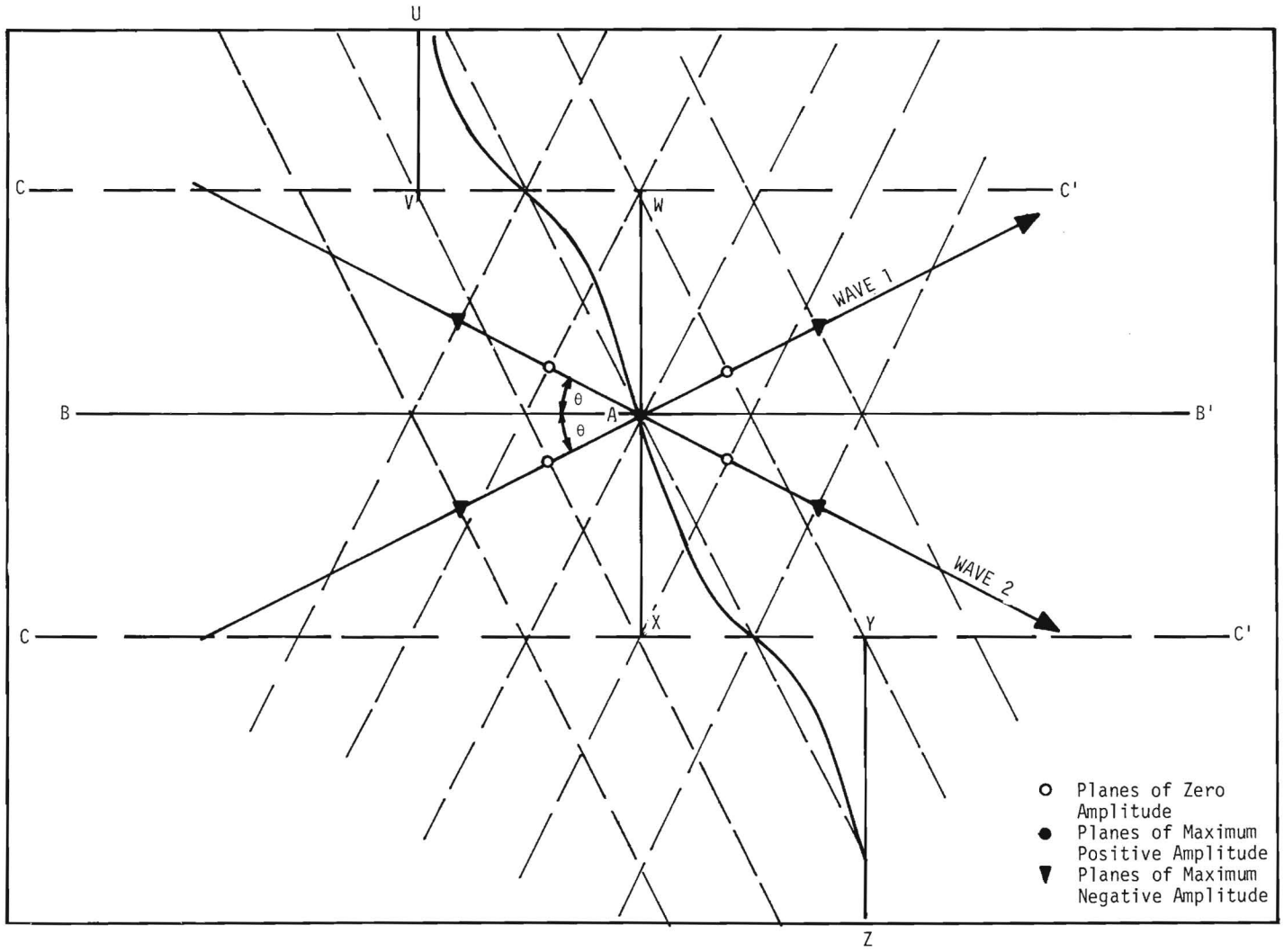

Figure 5. Wave Interference Patterns Depicting Phase-Front Distortion.

amplitudes are in phase and at a maximum value. At distances $\frac{\lambda}{2}$ from A along the directions of propagation, the amplitudes are zero; at distances of λ, the amplitudes are maximum negative. Planes of maximum and minimum amplitudes due to wave interference occur in planes parallel to the direction of the bisector (line B-B') of the angle 2θ between waves 1 and 2. For example, line B-B' is a line of maximum amplitude standing wave; lines C-C' are lines of minimum amplitude. In-phase signal planes intersect on B-B'; out-of-phase planes intersect on C-C'. The planes of maxima (and minima) are separated by $\left(\frac{\lambda}{2}\right)\left(\frac{1}{\sin\theta}\right)$. A corrugated phase front develops because of the intersection of the wavefronts.

As θ increases (decreases), the separation of the planes of amplitude maxima and minima decreases (increases). However, the separations between phase front deviations are all equal to or greater than $\frac{\lambda}{2}$, which is several orders of magnitude greater than the aperture of a loop DF antenna. The line segments U-V, W-X, and Y-Z illustrate the equiphase front for the case where the wave amplitudes are equal. The curved line through A illustrates a more general case where amplitudes are not equal. In this case, the amplitude of wave 1 is larger than that of wave 2. If wave 2 were larger, the wave front would scintillate about an equiphase front of wave 2. Note that along the line W-X, the intersecting planes are all in phase; however, at the minimum planes (lines C-C'), 180° phase difference occurs and a rapid bearing swing occurs. Also note that the curved equiphase line is more corrugated (more inaccurate bearings and faster bearing swings) at and near the minimum amplitude lines C-C'. Near line B-B' (maximum amplitude line) the corrugation is less severe and less swing occurs at or near a maximum amplitude line. As the phase delay and angle between waves 1 and 2 change with time, the pattern shifts creating a continuously swinging or shifting bearings. A small-aperture loop follows every corrugation and shift of the equiphase surface since the aperture is not sufficiently wide to average across corrugations. Large ($\pm 90^{\circ}$) bearing errors can occur due to wave interference even though no horizontal components exist in the incident field. Also, it may be noted that bearing deviations can occur without a phase delay between the waves because a change in θ can result in a shifting pattern.

Correlation between fading and bearing swing rate and error may also be seen from consideration of figure 5. Synchronous fading between the vertical and horizontal components of the waves occur during wave interference. Lines of minimum amplitude and maximum bearing swing (line C-C') correspond to the minima of a fade cycle where both vertical and horizontal polarized components are lowest and bearing swing rate and error are largest.

Figure 6 depicts the synchronous nature of multipath fading. The detected signals are from a horizontal dipole (lower trace) and a 5 foot vertical whip (upper trace). The dipole had 7 foot elements and was boresighted on the GCB of the incident signal (WWV on 10 MHz at 1240 GMT). The time base is 5 seconds per division. Dipole nulls and peaks occur at whip peaks and nulls, respectively, indicating the synchronous nature of the fading.

A major parameter from the viewpoint of system design is fade rate, i.e., how many times per unit time the signal level crosses a pre-set level. Investigators cite rates ranging from several per hour to several every tenth of a second; however, most experimental data indicate that rates on the order of several per minute are typical with several per second being stated as an upper limit for normal (e.g., non-auroral) propagation. Most investigators [3-9] state that the probability density distribution of the sky-wave amplitude is Rayleigh; Mitra[10] specifies a Gaussian distribution. However, McNicol[11] and Goldberg[12] state that the distribution is Rician, which allows for both Rayleigh and Gaussian distributions to occur as limiting states. The distribution is Rayleigh if the ionospheric wave is composed entirely of a series of waves with random phases and no specularly reflected, steady-state component. The distribution is Gaussian if the wave contains a steady-state component with an amplitude approximately three times larger than the fluctuating fading component. An infinite number of distributions between Rayleigh and Gaussian can occur depending upon the ratio of the amplitude of the steady-state component of the wave to the amplitude of the fading components. Experiments[3-12] have shown that the distribution is non-stationary.

2.1.4 Path Deviation Errors

When wave interference is the predominant effect, the bearing deviations are in a constant state-of-change. However, in some cases, a single wavefront will dominate with an azimuth angle-of-arrival different from the GCB. In this case, the bearing is relatively steady and appears to be an excellent, apparently accurate bearing.

Path deviation errors may be considered a special case of wave interference errors; however, the effects are considerably more deceptive and subtle since it may be accompanied by a relatively slow fade pattern producing steady, acceptable bearings for a long period of time (e.g., several minutes to hours).

The quantitative effects of path deviation on bearing error is difficult to define due to the variability of the ionospheric features that create path deviation. For example, azimuth deviations ranging

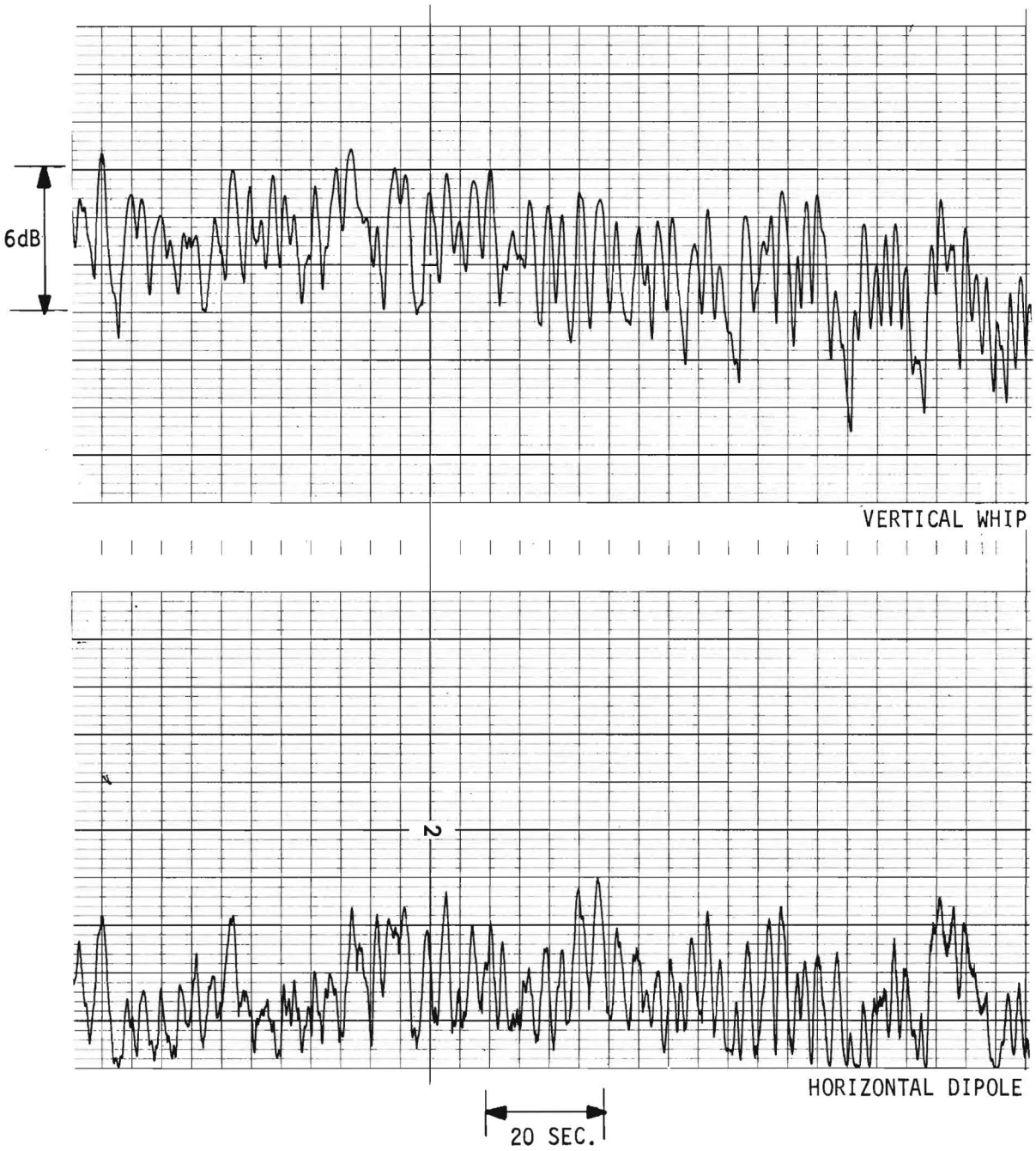

Figure 6. Example of Multipath Fading.

from 2° for random ionospheric irregularities to 60° for spread-F propagation are cited[13]. Deviations as large as 15° or 20° have been observed[13], especially at frequencies near the MUF, with north-south paths producing the larger deviations. In general, the errors decrease as the propagation distance increases with one-hop transmissions possessing the greatest deviations.

2.1.5 Conclusions

Of the three major sources of bearing errors in loop systems, path deviation error produces the smallest error, on the average. However, it is difficult to detect and virtually impossible to reduce. Polarization rotation error occurs far less often than wave interference errors, but the effect is worse because it produces rotating bearing displays with little or no pattern change. Both polarization rotation and wave interference can produce errors of $\pm 90^{\circ}$.

All errors are correlated with ionospheric propagation phenomena and, hence, are subject to wide variations that can only be described statistically.

2.2 Technical Approach to Error Reduction - First Phase

2.2.1 Introduction

The basic approach to error reduction was to consider techniques for unblanking a bearing display based on the determination of specific characteristics of the incident signal and the use of these characteristics to restrict the display of the bearing information to the conditions that tend to produce minimum bearing error. Attention was first given to using the horizontal component of the incident wave as an unblanking agent: bearings were to be displayed only when the amplitude dropped below an adjustable, pre-set threshold level.

A dual-channel HF/DF receiving system (figure 7) consisting of a main and auxiliary channel was developed. The main channel detected the null of a small, continuously rotating loop and displayed the null pattern on a CRT display synchronized with the rotating loop. Special circuitry was included to detect and display the loop nulls in the form of a propeller-type display. The auxiliary channel detected the envelope of the signal received by a small, stationary dipole (20 inches per element) and provided a real-time DC analog of the horizontal dipole level to a level detector. When the level dropped below a preset value, the level detector output gated the intensity modulation to the bearing display. When the level exceeded the pre-set value, the level detector gated out the signal that was intensity modulating the display.

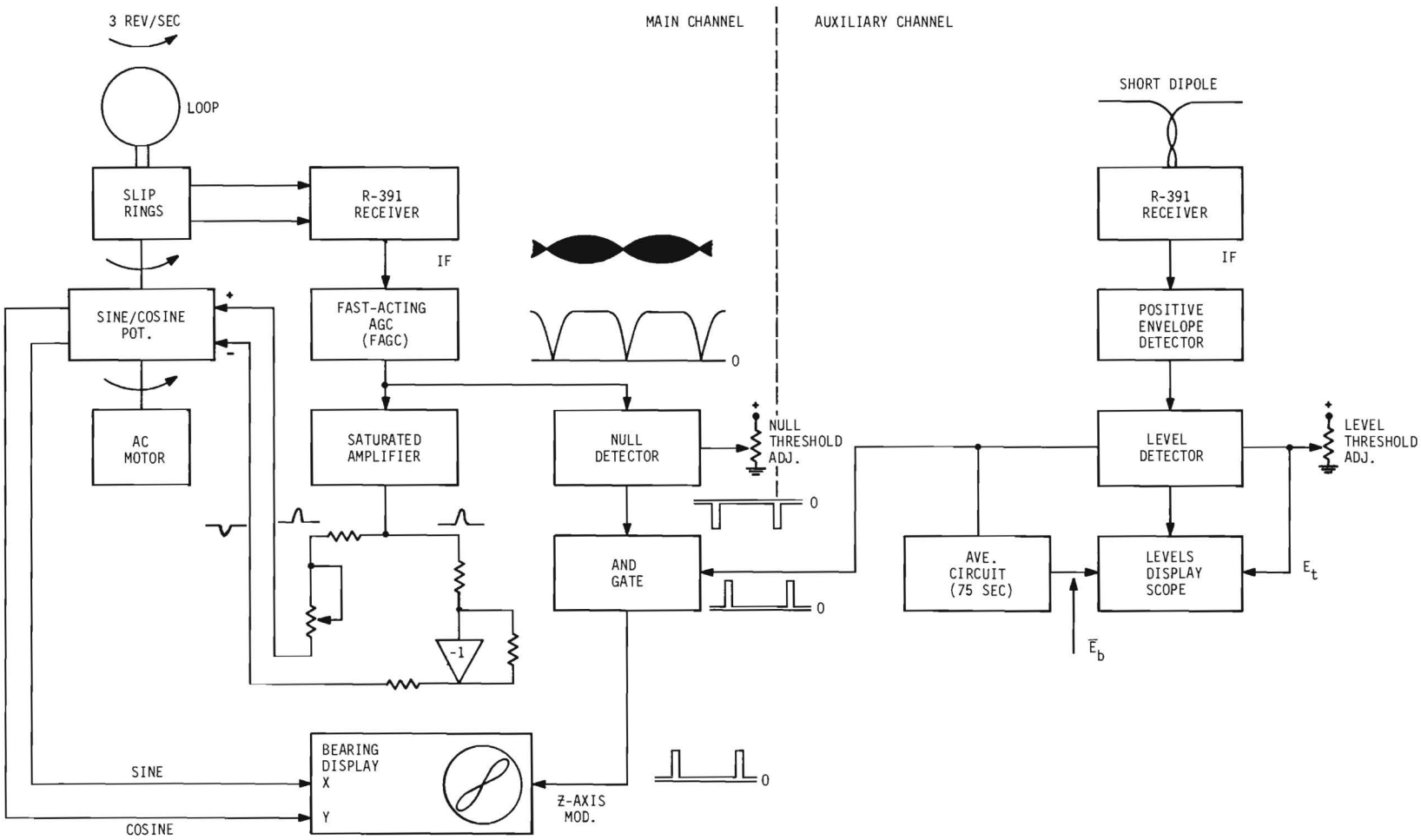

Figure 7. Block Diagram of the Initial Exploratory System.

Associated test instrumentation included the levels display scope, which permitted setting the level detector threshold, and the fade monitor scope, which provided a display of the loop and dipole null and fading patterns.

2.2.2 Functional Description of System

The following is a general, functional description of the system. Details may be found in quarterly reports 1-4.

In the main channel, an AC motor rotates both the loop and the shaft of a sine/cosine potentiometer at 3 rev/sec. The balanced loop output is transmitted through slip-rings to an R-391 receiver (AGC off) balanced antenna input. The R-391 IF output is modulated by the rotating loop antenna pattern.

The function of the post-IF circuitry is to detect and display the nulls of the scan modulation as a function of azimuth in order to obtain instantaneous bearings. The post-IF circuit design contains several features that differ from conventional methods for detecting and displaying null patterns. These features include (1) continuous, dynamic null detection by fast automatic gain control (FAGC), (2) separate display of each null of the rotating loop pattern, and (3) enhancement of the differences between "good" and "bad" bearing displays.

The fast AGC circuit is designed to detect the null pattern without deteriorating its sharpness or depth. The null pattern could be detected by a conventional envelope detector. However, at the low signal level of the null minima, the envelope detector diode operates in the square-law region which degrades the sharpness of the null. One method to reduce square-law effects is to increase the gain and maintain the level at the detector out of the square-law region for a longer portion of the null minima. A disadvantage of this procedure is circuit overload effects. A method to overcome this and still maintain the integrity of the null pattern is to reduce the gain on the signal peaks but maintain the gain at a high level during signal nulls. The FAGC circuit consists of (1) three IF amplifiers separated by two shunt diode attenuators between the first and second and second and third amplifiers, and (2) a conventional diode envelope detector that passes the positive portion of the IF signal. The envelope detector DC output is used to control the shunt diode attenuators. This produces a variable attenuation action. As the input level increases, the DC output of the low-pass filter increases the current through the diodes and decreases the overall gain. As the IF signal decreases, the reverse occurs, and the overall gain is increased. The result is a constant output level over a large portion of a scan period. However, as the input level continues to decrease into the null minima, the diodes lose control, and the output follows the null pattern. A conventional diode detector simply reproduces

the envelope of the normal IF signal and deteriorates the sharpness of the null. However, the detected output of the FAGC unit shows a much sharper null since the signal is maintained above the square-law region of the detector diode for a longer period of time.

The FAGC action is controlled only by the loop antenna scan modulation since the envelope detector low-pass filter, with a 55 Hz passband, rejects the signal modulation components but passes the scan modulation fundamental and those higher-order harmonics which greatly effect the sharpness and depth of the null minima. The 55 Hz passband was determined empirically as the highest value providing a maximum amount of null sharpness and depth with a minimum amount of signal modulation components.

The FAGC output is constant (± 1 dB) for input levels from -70 dBm to 0 dBm. Threshold sensitivity is about -80 dBm. The FAGC unit is untuned; hence, a wide range of intermediate frequencies can be accommodated.

The FAGC output is applied to a saturated amplifier, which is a common-emitter stage that operates in a saturated state until the null minima occur. The saturated amplifier acts as a clipper, inverter, and amplifier in that it amplifies and inverts the bottom portion of the null pattern. Only that portion of the null minima that drops below the saturation level is passed by the saturated amplifier. No output occurs when the nulls become obscured such that the FAGC output does not drop below the saturation level even though a null pattern may still exist. The circuitry following the saturated amplifier produces two signals of equal amplitude and opposite polarity for use as input signals to the sine/cosine potentiometer.

The positive and negative signals are applied to the input terminals of the sine/cosine potentiometer. The potentiometer outputs are applied to the phase-matched X and Y amplifiers of a conventional XY oscilloscope. When the positive and negative pulses occur, the sine/cosine potentiometer forms a half-propeller pattern on the oscilloscope with the tip of the propeller pointing to the bearing azimuth (or its reciprocal). The next null paints the remaining portion of the propeller pattern. Hence, each null is separately displayed, i.e., for one loop scan, each null paints only one-half of the propeller display. Most conventional DF displays provide a complete propeller pattern for each null. It is suggested that an individual null display is better because erroneous bearings are usually accompanied by skewed, asymmetrical patterns that are not evident on a conventional loop DF display.

The shape of the propeller pattern follows the shape of the null pattern and is determined by the sharpness and depth of the nulls at the output of the loop FAGC. If the nulls are not deep, the common-emitter stage may not be driven out of saturation, the sine/cosine

potentiometer will have no input, and no pattern will be displayed. This is a distinct advantage in that, if the nulls are not deep, the bearings are inaccurate and, hence, should not be displayed. Therefore, the pattern-forming circuitry automatically eliminates some of the inaccurate bearings.

The null detector is a level comparator that generates a negative pulse when the FAGC output drops below an adjustable reference level. As the reference level is adjusted lower, the pulse occurs closer to the null minima. When the nulls are obscured or filled-in (implying erroneous bearings), no level detector output pulse occurs. The null detector output pulse is one input to the AND gate that controls the intensity modulation of the bearing display.

The other AND gate input comes from the auxiliary channel and is obtained in the following manner. The amplitude of the IF output of the R-391 auxiliary channel is proportional to the level of the horizontal component in the signal incident on the loop. When the horizontal component fades to a minima, the envelope detector output, which is the input to the level detector, decreases. An output pulse is applied to the AND gate when the input is below as established threshold, which is set relative to a long-term average of the dipole level, in order to unblank at various levels on the horizontal component fade cycles. This allows for the recording of bearing data as a function of the level of the horizontal component.

Simultaneous inputs to the AND gate intensity modulates the long-persistency (0.4 second) display and indicates that (1) a null has occurred below the null threshold, and (2) the horizontal component of the incident field is below the established threshold level.

2.2.3 Operational Evaluation Results - First Phase

The effects of unblanking on horizontal component minimas were operationally evaluated during a three-month period and included 197 separate tests on 44 frequencies in the 5-17.8 MHz range. The transmissions came from 17 separate locations over propagation path distances from 21 km to 8600 km. A majority of the tests were conducted from 1600 to 2100 hours local time during periods of ionospheric change. Essentially all of the test transmissions were international short-wave broadcast stations and WWV. (Detailed descriptions of the test site, test methods and procedures, and data reduction and analysis may be found in quarterly reports no. 4 and no. 5).

The following is a listing of the major conclusions derived from the tests:

(1) Bearings taken on ionospherically propagated transmissions are in a continuous state-of-change.

(2) The amount and rapidity of bearing fluctuations are a function of the fading depth and rate. A definite correlation between bearing swings and the fading characteristics of the signal was noted on about 85% of the tests. Other investigators have also noted this relationship. Kanellakos[14] states that large deviations in bearing correspond quite well with the deep fades in the signal amplitude and that these results confirm the findings of Wale and Delves[15]; and Salamon, Harding, and Wasson[16]. These results are also consistent with the findings of the University of Illinois[17], Gething[18], and Bailey[19]. In general, bearing displays distort and broaden on a fade.

(3) On a large majority of the tests, the loop and dipole outputs faded synchronously. When the dipole channel output was low due to a fade, the loop channel level was also low. Loop and dipole signal peaks also tended to coincide.

(4) Bearings taken when the dipole channel output is either low or at a minima are more inaccurate and dispersed. In addition, a low SNR with co-channel interference will cause additional bearing inaccuracy at low dipole levels since the incident wave front is the vector sum of the desired signal, which has a lowered SNR, and the co-channel interference.

(5) In general, bearings taken on the crests or skirts of a fade cycle are more accurate and have less spread than bearings taken on or near the fade cycle minima.

(6) The most significant reduction (2 to 1 reductions were measured) in bearing errors can be obtained by taking bearings when both the loop and dipole levels are at their maxima value and in a steady-state condition, i.e., the levels are holding steady at the peak of a fade cycle. Also, the sharpest, deepest null patterns occur at the crests of the fade cycles.

(7) The F2MUF and direction of transmissions have very significant effects on operational reliability. If the operating frequency exceeds the F2MUF and/or the transmissions are beamed away from the receiving site, operational reliability decreases.

(8) On some tests, changes in fading characteristics were followed by changes in bearing characteristics. For example, on some tests, bearing sectors definitely shifted after changes in fade characteristics.

(9) In some cases, bearings on transmissions beamed away from the test site were characterized by definite bearing groupings to a sector (or sectors) significantly different from the true bearing. Bearings taken in the presence of significant interference also

exhibited this characteristic.

(10) Bearings taken on fade crests in the presence of RFI and/or a low SNR were more accurate than bearings taken on the fade crests and skirts.

To summarize, the test results disclosed that unblanking at the horizontal component minima is ineffective for significant, reliable bearing error reduction; however, in general, a considerable reduction in bearing error is possible if bearings are taken only when the signal is near the crest or peak of a fade and in a relatively steady condition.

2.3 Technical Approach to Error Reduction - Second Phase

2.3.1 Introduction

The investigations of the second phase of the project were based on the major implications of the error analysis and the empirical results of the first phase: bearing errors can be reduced by displaying only those bearings occurring at or near the vertical component signal strength maximas when the bearings are relatively steady at the crest of a fade cycle.

The major efforts of the second phase investigation were as follows:

(1) The design, development, and test of techniques to unblank the bearing display on fade crests. Four types (modes) of fade crest detectors were added to the auxiliary channel and evaluated to determine relative performance under a variety of signal and fading conditions including polarization and multipath fading, low SNR, and co-channel interference.

(2) The design, development, and test of a swing rate discriminator (SRD) using the time-rate-of-change of the bearing swings for unblanking. The SRD unblanks when eight consecutive bearings occur within a preset number of degrees from one another. The SRD can be used separately or in conjunction with the fade crest detectors.

(3) The evaluation of a variable persistency storage scope when used as a bearing display processor and memory unit.

(4) A comparison of the performance of the exploratory system (ES) and the AN/PRD-5 during simultaneous operation in the field.

(5) An operational comparison of the relative effectiveness of a loop and vertical whip when used with the auxiliary channel.

Several improvements in the exploratory system and the associated instrumentation were made. A major improvement in the instrumentation was the addition of an automatic bearing print-out (APO) technique.

The R-391 receivers were replaced by two HQ-145 receivers with the frequency tuning controls mechanically ganged and a common local oscillator. These features were added to simplify the tuning and operating procedures. The common local oscillator also equalized the receiver sensitivities.

The following section will discuss, first, the functional block diagram of the modified, dual-channel system, including the fade crest detectors, SRD, and storage scope. This is followed by a discussion of the fade crest detector's design and operational evaluation including detailed test results. Similar sections are included on the storage scope, antenna evaluations, and the comparisons of the exploratory system and the PRD-5. Additional sections are included comparing the test results based on other factors such as propagation conditions, SNR, and co-channel interference. The final section is a detailed treatment of the SRD.

2.3.2 Functional Block Diagram of Second Phase Dual-Channel Exploratory System (ES)

Figure 8 is a functional diagram of the dual-channel exploratory system (ES) used on the second phase. Several improvements were made on the main channel. A major one was the addition of AC coupling between the FAGC output and the null detector to reduce the number of spurious intensity modulation pulses that occurred on a fade. This resulted in removing a considerable number of inaccurate indications that cluttered the display.

A magnetic pick-up device provided an azimuth reference pulse, which could be made to occur at any convenient azimuth. This pulse was used to start the SRD and APO units. Another magnetic pick-up provided an output pulse for every 2° of loop rotation. These pulses were used as inputs to the APO.

The SRD was added and required three inputs: (1) the azimuth reference pulse for a start pulse; (2) the bearing pulses indicating the null azimuth; and (3) display unblanking pulses from the logic gates operating on the main and auxiliary channel outputs.

The auxiliary channel was completely redesigned with the major factors being the inclusion of four switchable types (modes) of fade crest detection and a variable persistency storage scope, HP141A, supplementing the conventional scope as a bearing display.

Gates No. 2 and 3 control the intensity modulation unblanking

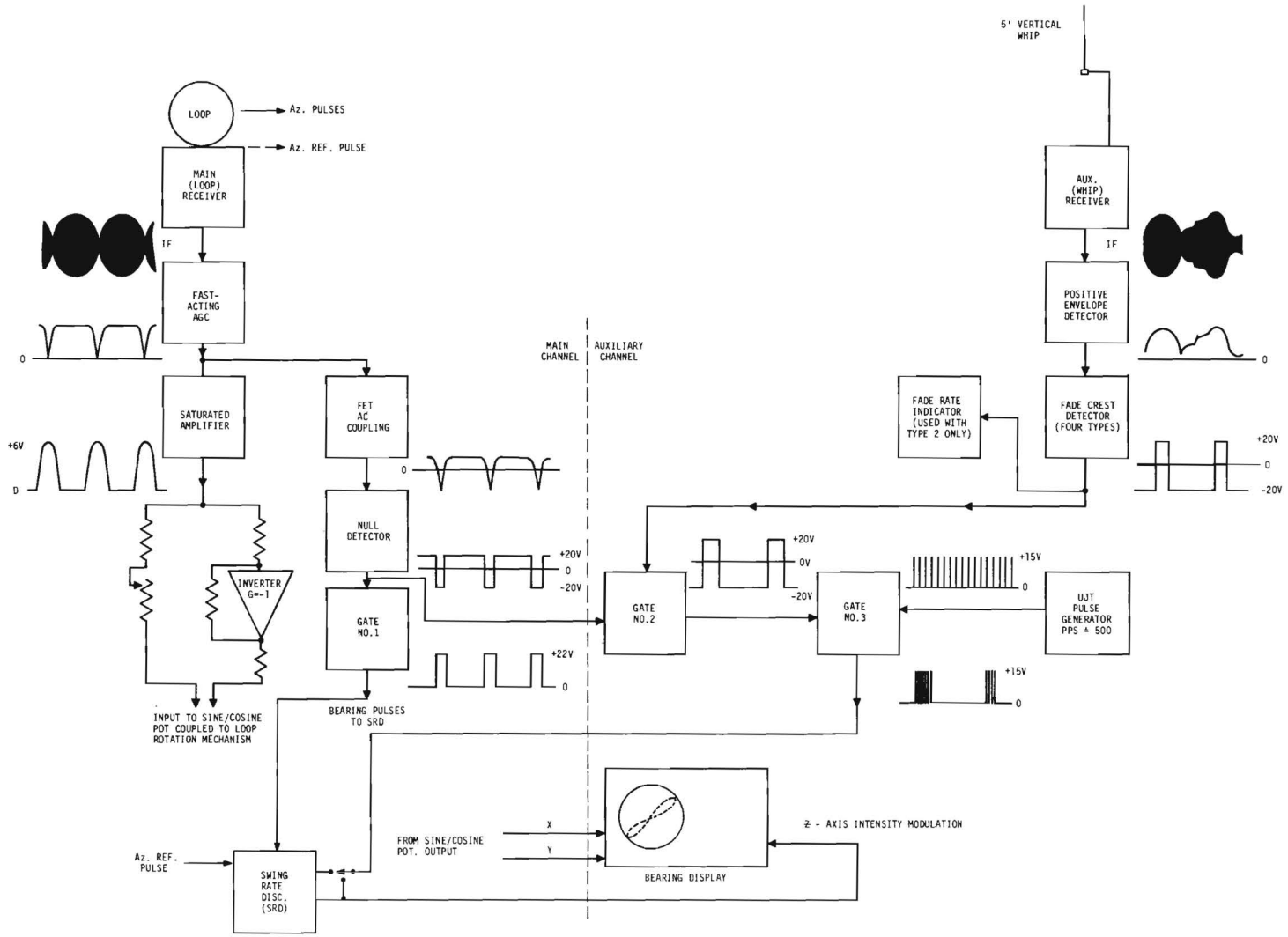

Figure 8. Functional Block Diagram of the Final Dual-Channel Exploratory System with Pertinent Waveforms.

pulses. If there is a null detector output (i.e., if the loop nulls are deep and unobscured) the fade crest detector output is gated through to gate No. 3. If the fade crest detector output is positive, the unblanking pulses are applied to either the display or the SRD, if it is being used. Hence, for display unblanking, the loop nulls must be deep, the signal must be near the crest of a fade cycle, and, if the SRD is operating, the bearing swing must be within a certain azimuth range. The major purpose of the field test phase was to experimentally determine if bearing errors could be reduced, for a variety of conditions, by using the above criteria for display unblanking.

2.3.3 Detailed Description - Fade Crest Detectors

2.3.3.1 Design Considerations

A major consideration is the existence of a wide variety of signal fading characteristics ranging from the orderly, regular pattern of polarization rotation to the erratic, irregular characteristics of multipath effects. Irregularity is increased by a low SNR or co-channel interference. The design had to consider fade rates in the range 0.01 to 1.0 per second and non-stationary statistical amplitude distributions. Therefore, it was decided to design and test several different types of fade detectors:

Mode 1 - Direct Differentiation
Mode 2 - Averaging and Comparison
Mode 3 - Peak Sample and Hold with a Slow Discharge
Mode 4 - Peak Sample and Hold with a Slow Discharge and Differentiation.

Modes 1 and 2 were designed for the more orderly fading characteristics with good SNR and slow fade rate conditions. Modes 3 and 4 were designed for (1) the erratic, irregular fade situations with higher fade rates, and (2) operation in low SNR and/or interference conditions.

2.3.3.2 Mode 1 - Direct Differentiation

This mode (figure 9) produces an output when the derivative of the fading signal is zero, e.g., at the fade peaks and null. This mode was designed to operate on fade rates up to about 0.2 Hz. Its main advantage is its simplicity; disadvantages are that output pulses are produced on fade nulls and plateaus, the performance is a function of the fade rate, and it is susceptible to spurious detection caused by noise and transients. Operation is illustrated in figure 10. E_{in} is the fading envelope; E_o is the zero-crossing detector output. Especially noticeable is the output pulse occurring

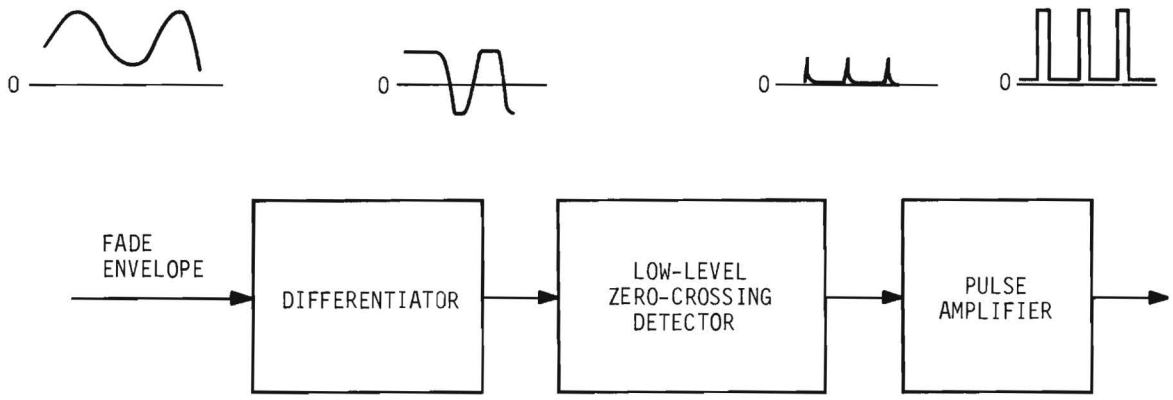

Figure 9. Fade Detector - Direct Differentiation.

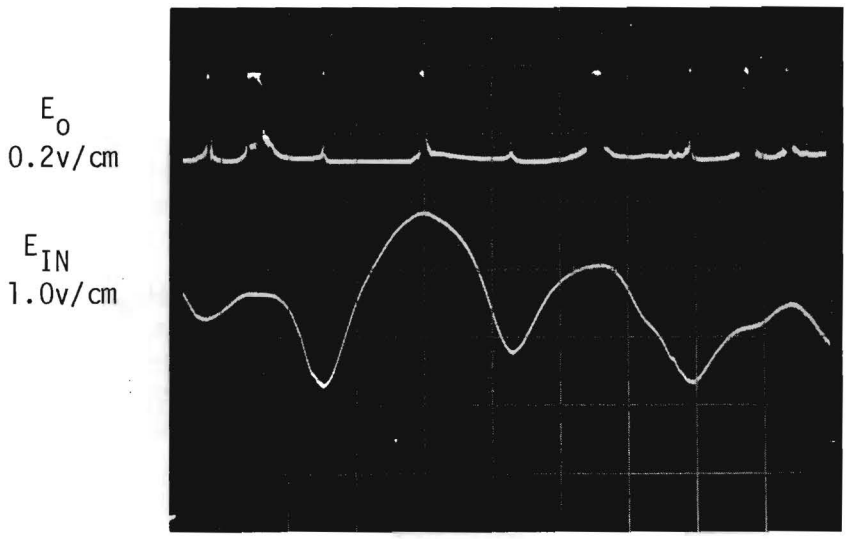

Figure 10. E_o and E_{IN} for the Differentiator.

at a fade plateau just prior to the last fade peak.

2.3.3.3 Mode 2 - Averaging and Comparison

This mode (figure 11) operates by (1) averaging the fading envelope, and (2) comparing the average value with a weighted envelope. An output occurs only if the weighted input exceeds the average value. The weighting factor is termed the fade margin and determines how far above the average value the input must rise before an output occurs. For example, with a 3 dB fade margin, an output occurs when the input is 3 dB or greater above the average.

An averaging time of 15 seconds was chosen based on an assumed minimum rate of four fade cycles per minute. The averaging time must be, at least, equal to the fade period. This is necessary since it requires at least one fade cycle to indicate the short-term statistical behavior.

The fade margins of 0, 1, 3, 6, and 10 dB were based on the anticipated range of the maxima relative to the average for both multipath and polarization fading. Multipath may be characterized by a Rician distribution which allows for the finite probability of having a fade crest of infinite amplitude. However, 10 dB was chosen as a practical upper limit since the percentage of time that this level is exceeded for Rician statistics is less than 0.01%. In order to predict the fade margin range for polarization fading, it was necessary to establish a mathematical model. Ideally, the amplitude-time variation of the vertical (or horizontal) component is identical to a full-wave rectified sine wave if the polarization fading is circularly polarized and the rotation rate is uniform ($\psi = kt$). It may be noted that the waveforms in figure 4 are very similar to a full-wave rectified sine wave. Since ψ is assumed to be uniform ($\psi = kt$), it was possible to define fade margin as a function of ψ as shown in figure 12. The fade margin, E, is the level in dB above the average or 0 dB level. For the model shown in the upper right hand corner of figure 12, the time base is converted to angular radians, ψ, where ψ is the polarization tilt angle referenced to the vertical. When ψ is 0°, the vertical whip output is a maxima; when $\psi \equiv 90^{\circ}$, the level is zero. At the average value, $\psi = 50^{\circ}$. Figure 12 is a continuous plot of fade margin as a function of ψ. It may be noted that a fade margin greater than about 3.8 dB exceeds the theoretical maxima of the fading signal. Also ψ changes more rapidly when E exceeds 3 dB. Based on this theoretical model, 3 dB was considered to be about the highest fade margin that could be reliably used for polarization fading. (Operational evaluation proved this to be true). For a given fade margin, figure 12 can be used with figure 2 to obtain an estimate of displayed bearing spread if the angle-of-arrival, Φ, can be estimated. For example, with a 3 dB fade margin, ψ from figure 12

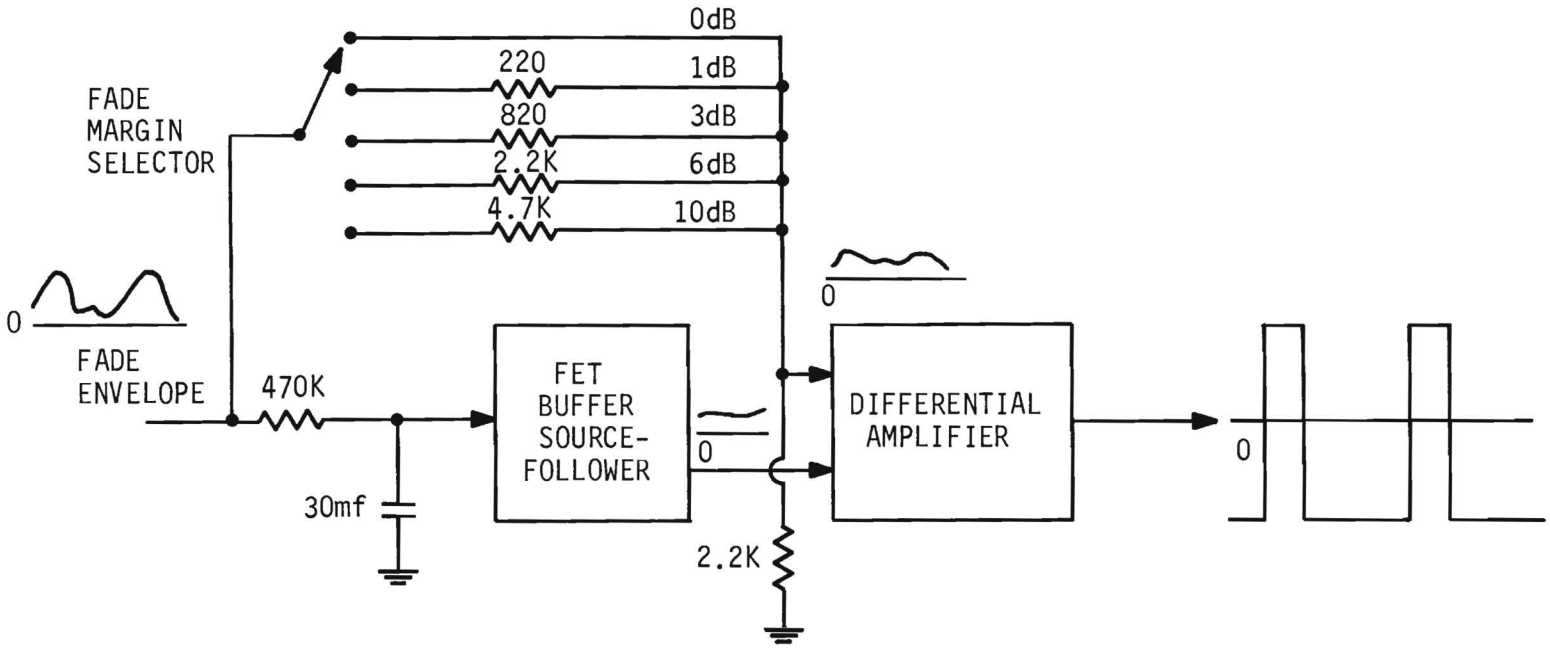

Figure 11. Fade Detector - Average and Comparison with Selectable Fade Margin.

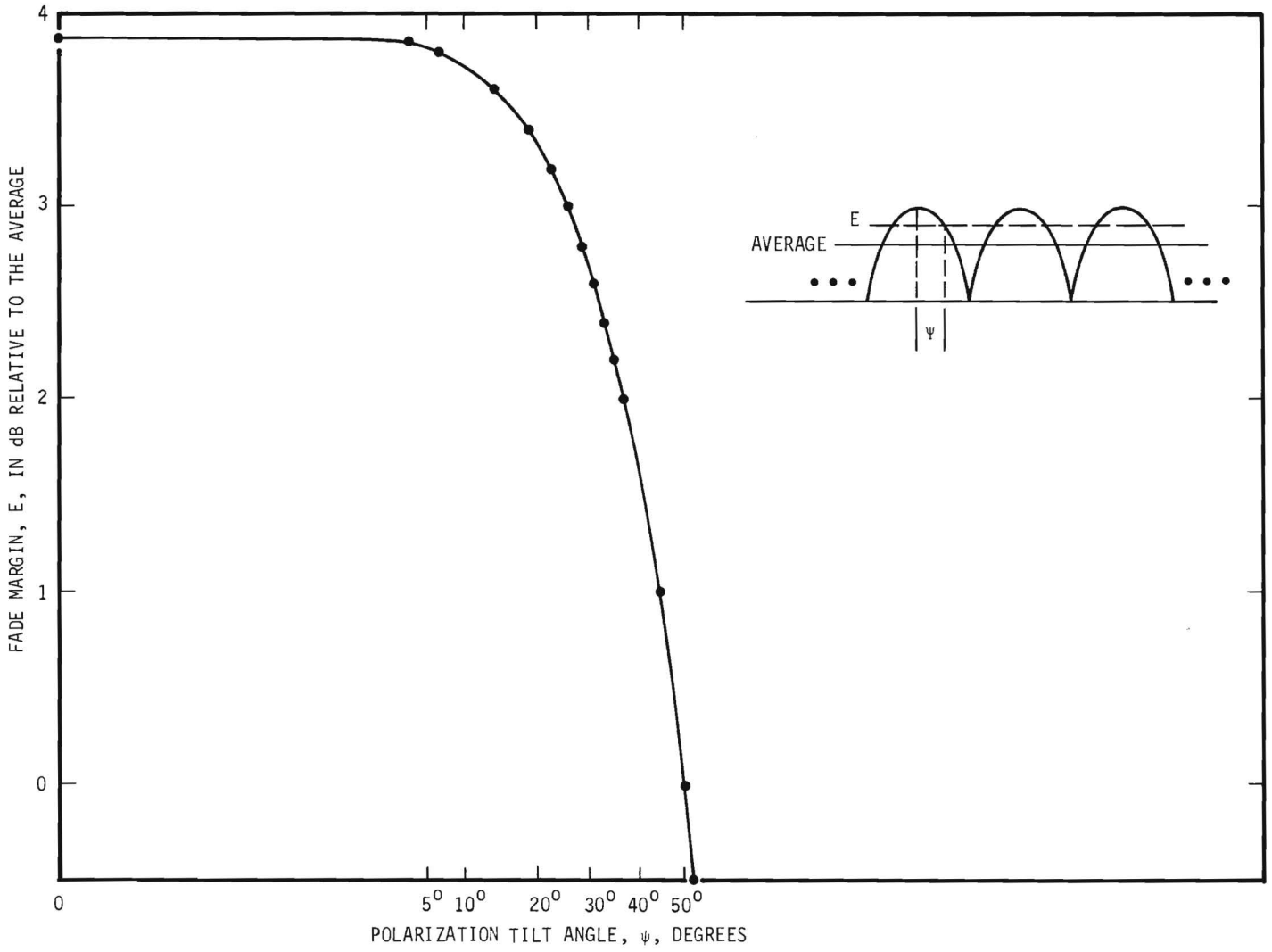

Figure 12. Fade Margin, E, Versus Polarization Tilt Angle, ψ, for Polarization Fading.

is about 20°. Assume that Φ is known or estimated to be about 45°. Hence, when a 3 dB fade margin is used, crest unblanking will begin when the bearing is about 15° from the GCB and continue until the bearing swings through the GCB to 15° on the other side. Hence, a 3 dB fade margin with $\Phi = 45^{\circ}$ implies a bearing spread of 30° about the GCB.

Figures 13 and 14 illustrate operation with 0 and 5 dB fade margins, respectively. (The 5 dB was later changed to 3 dB).

The major advantage of this mode is its ability to (1) accomodate a wide range of fade rates, and (2) allow for a study of the effects of fade margin on bearing accuracy and spread. Limitations are: (1) a good SNR is needed to insure that the average value is not affected by noise and/or interference; and (2) a reasonably periodic fade is desirable in order to establish a steady average level.

2.3.3.4 Mode 3 - Peak Sample and Hold With Slow Discharge

This mode (figure 15) operates on the signal peaks directly and does not depend upon the average value. This mode operates in the following manner. When the input is applied, the hold capacitor charges to the peak value of the first fade cycle and is allowed to slowly discharge. When the next peak arrives and exceeds the level on the holding capacitor, the differential amplifier changes states until the hold capacitor recharges to the peak of the fade cycle. The sequence is repeated for succeeding fade peaks. Figure 17 depicts the operation (the time base is 1 sec/cm).

The 27 second discharge time constant was chosen to be several times larger than a fade cycle time of 10 seconds, which is considered to be a typical lower limit for multipath fading.

A major attribute of this mode is its ability to operate (1) at high fade rates, and (2) avoid unblanking on low-level fade peaks and/or interference that produces inaccurate bearings. It is especially useful when the desired signal is occasionally peaking-up out of the interference or noise.

2.3.3.5 Mode 4 - Peak Sample and Hold With Slow Discharge and Differentiation

Mode 4 (figure 16) is very similar to mode 3 with two basic differences: it unblanks more rapidly (due to a slower discharge time and the differentiator action) and only over the leading edge of a fade crest. The more rapid unblanking reduces spurious indication. The concept of unblanking before the fade crest maxima on the positive-

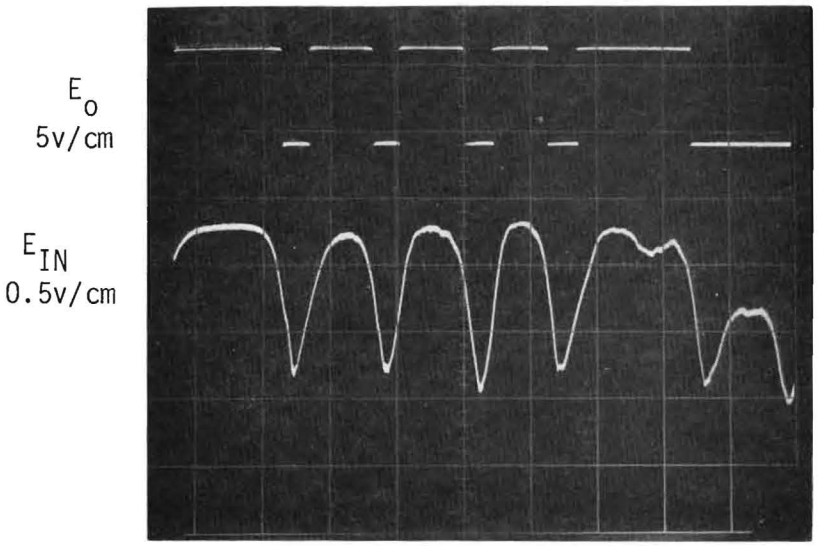

Figure 13. E_o and E_{IN} for the Averaging and Comparison Technique with a 0 dB Fade Margin. Time Base: 2 sec/cm.

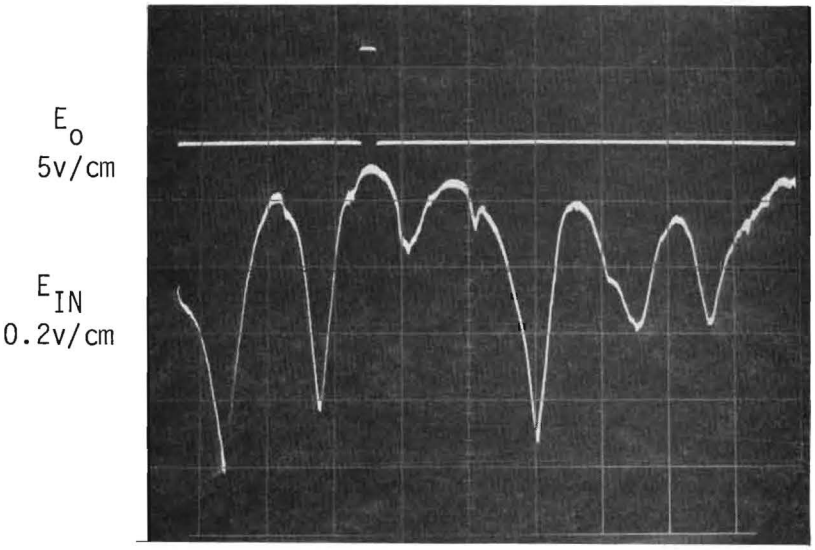

Figure 14. E_o and E_{IN} for the Averaging and Comparison Technique with a 5 dB Fade Margin. Time Base: 2 sec/cm.

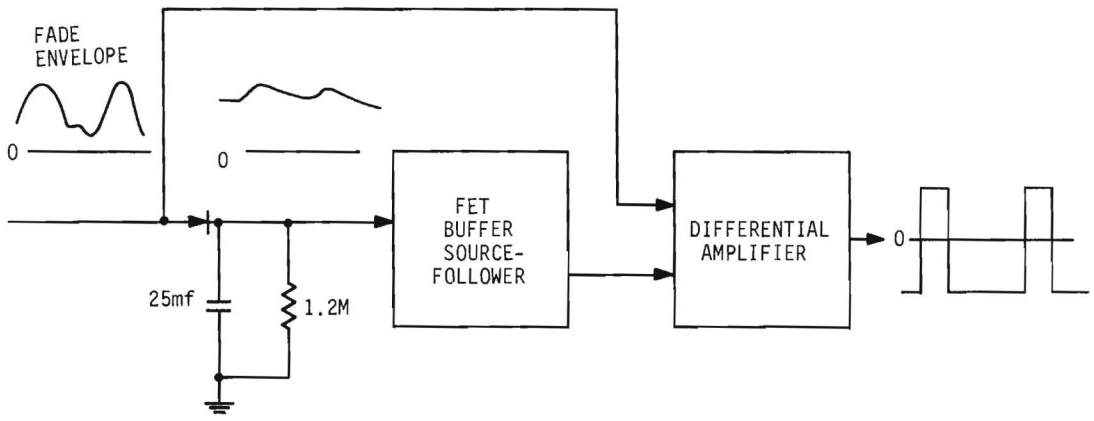

Figure 15. Fade Detector - Peak Sample and Hold with Slow Discharge.

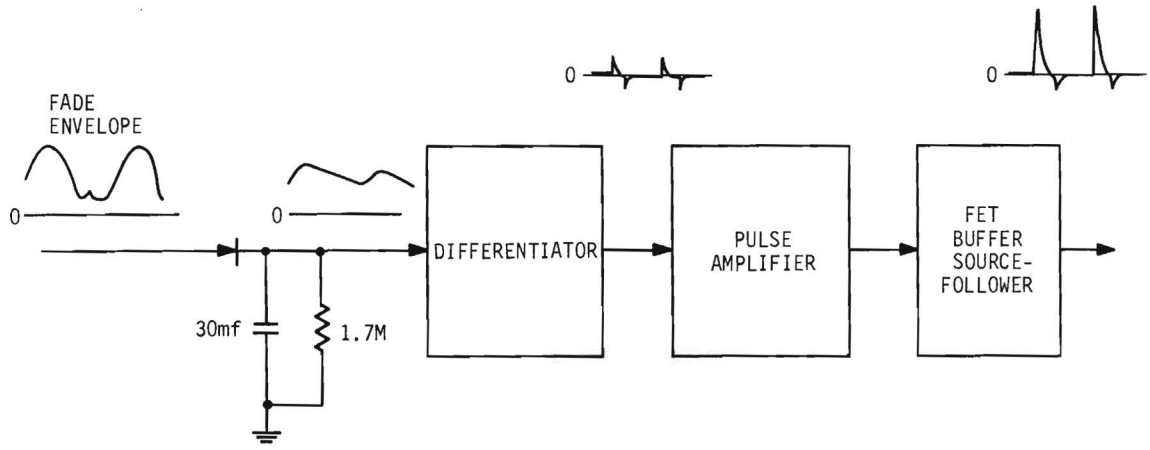

Figure 16. Fade Detector - Peak Sample and Hold with Slow Discharge and Differentiation.

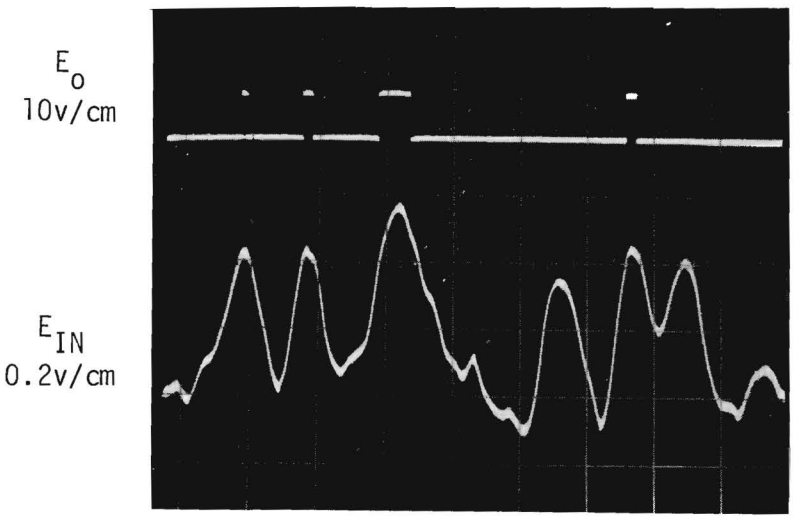

Figure 17. E_o and E_{IN} for the Peak Sample and Hold Technique.

going portion of the fade cycle resulted from observing a correlation between bearing swing rates and multipath fade characteristics during the first phase. This correlation indicates that bearing swings are more rapid immediately after the crest than immediately before the crest. Mode 4 also eliminates unblanking on the negative-going portions of the fade cycle when the SNR is decreasing.

Operation is depicted by figure 18. It may be noted that the trailing edge of the unblanking pulses coincide with the approximate peak of the fade. It may be noted that for both modes 3 and 4 the unblanking time is proportional to the magnitude of the fade crest amplitude. The larger the fade crest level, the longer unblanking occurs. This provides automatic amplitude weighting for the unblanking technique. It has been postulated that this weighting should reduce bearing errors.

2.3.4 Operational Evaluation Methods - Second Phase

2.3.4.1 Description of Test Site

All field tests during the second phase were conducted in a semi-rural area eighteen miles east of the Georgia Tech campus. Appendix C depicts the test site facility and environs. No significant major reradiators are present within a radius of several hundred feet from the equipment trailer. The closest possible reradiators are (1) an AC power line, which is viewed "end on" from the trailer site and supplies power to the area, and (2) a tree-line (consisting primarily of large, mature oak and poplar trees) running SE to NW with the closest approach to the trailer being about 150 feet at 20° azimuth. A target transmitter, using a vertical whip and eleven frequencies in the 5-20 MHz range, was positioned at various azimuths around the trailer to search for areas of reradiators as manifested by bearing deviation and display distortion (asymmetry and skew). It was found that a sector about 30° wide near the power line ($\approx 150^{\circ}$ azimuth) was a major source of reradiation. The pattern was badly distorted especially in the frequency range 6-10 MHz. The NE area also produced bearing off-sets with the average being 18° counter-clockwise. For comparison, the 70° - 123° and 180° - 235° sectors produced average off-sets of only 1.5° and 4.5° counter-clockwise, respectively. [The site calibration data were not incorporated in the data reduction because the calibration data were obtained for only a single polarization (vertical) and elevation angle (0°) whereas the actual data were obtained under a wide range of polarization conditions and angles of elevation].

The loop scan mechanism and auxiliary antenna were located on the roof of the trailer some 12 feet above ground. The loop and auxiliary antenna were separated by approximately 10 feet. The PRD-5 was located on the ground at a distance of approximately 12 feet from the trailer along the 315° azimuth.

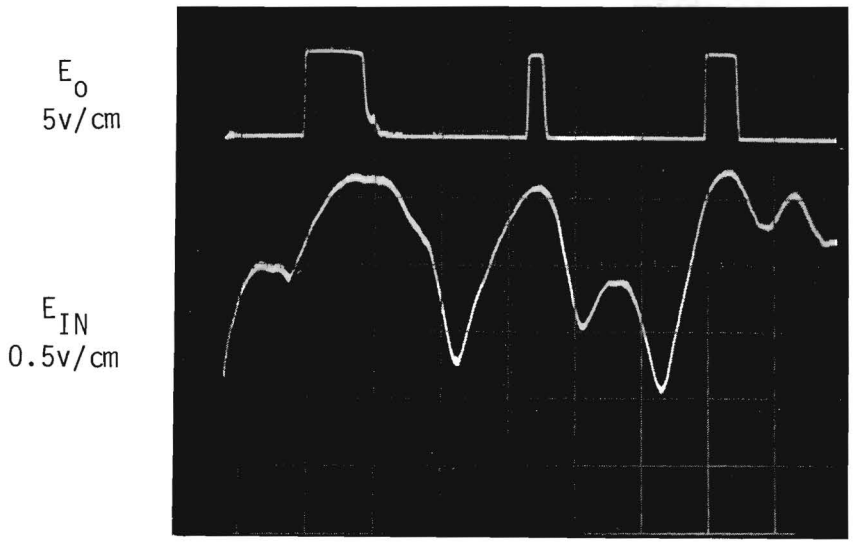

Figure 18. E_o and E_{IN} for the Peak Sample and Hold Technique with Differentiation.

2.3.4.2 Test Methods and Summary

All tests were performed on WWV or international short-wave broadcast stations of known bearing. Propagation path distances varied from about 600 km (Greenville, N. C.) to 8600 km (Moscow, U.S.S.R.). Essentially all the tests were taken on transmissions at or below the calculated F2MUF. A nominal test period of 5 minutes was chosen since the short-term statistical characteristics should be established in this time.

The general, preliminary procedures were to: (1) tune-in the test transmission and trim-up the antenna with the BFO, AGC, and limiter off; (2) reduce the RF gains to prevent overload on the fade peaks; (3) obtain the best display pattern possible (sharp and symmetrical) at the peak of a fade cycle by adjusting the main channel gain control; (4) adjust the null threshold level to provide for complete pattern intensification; and (5) select the auxiliary channel unblanking mode based on the predominant signal and fading characteristics.

Bearings were read either visually (to the closest 5° graticule) or printed-out automatically. On some tests, both were done simultaneously.

Visual bearings data were based entirely on the subjective evaluation of an operator who recorded a bearing when a symmetrical pattern was displayed. Displays asymmetrical in either azimuth or amplitude were not recorded. The storage scope was used to simultaneously display and store an entire series of bearings since it functions as a memory device when the variable persistence is adjusted to the maximum value of approximately one minute. It was found that if only a few (1-6) bearings were displayed at any one time, a "burst of bearings" occurring at the crest of a fade cycle could be stored and read during the period when no bearings were being displayed due to the absence of a fade crest. It is estimated that it was possible to take three-to-four more readings per-unit-time using the storage scope vis-a-vis a regular scope.

Listed below is a summary of the test phase.

Test Period : 12/17/66 - 4/1/67

No. of Test Days: 50

Total No. of Tests: 384

Tests from 1100 - 1500 GMT
(Morning Period): 62

Tests from 1500 - 2200 GMT
(Day Period): 138

Tests from 2200 - 0200 GMT
(Night Period): 174

Frequency Range: 5 - 20 MHz

No. of Frequencies: 67

No. of Locations: 23

2.3.4.3 Test Instrumentation

Instrumentation consisted of an automatic bearing print-out (APO) unit and a signal strength recorder.

The APO was used to provide direct print-out of the absolute bearings in time-sequence. The APO required no manipulation or decisions of the operator after initial adjustments were made. The APO unit used an events-per-unit-time meter (EPUT). A magnetic pick-up, which was located on the loop scan mechanism, generated a pulse for every 2^{o} of loop rotation. (Two degree resolution was the best that could be practicably implemented with the existing loop scan mechanism). The EPUT meter, operating in the $\frac{E}{B - A}$ mode, counted the number of pick-up pulses, E, that occurred in the time interval between a reference start pulse, B, and a stop pulse, A, occurring at the bearing null. The reference pulse was adjusted to occur when the normal to the loop plane passed through a reference azimuth. When the count was stopped, the digital recorder printed-out the reading in numeric form on paper and reset the count. (The total time from stop to re-set was approximately 1.1 second). If no bearing pulse occurred on a given scan, the count exceeded 180 and continued until a bearing pulse did occur. These high counts, which were ignored as valid bearings, indicated when a fade occurred; hence, they could be used to separate or group the bearing data in time-sequence by fade cycles. The magnitude of the high count provided a measure of the duration of the fade. The reference (start) pulse was obtained from a magnetic pick-up on the loop scan mechanism, which was aligned on some convenient landmark of known azimuth. The bearing pulses were obtained from the input to the storage scope Z-axis modulation, and, hence, were the result of processing by both the main and auxiliary channels.

The signal strength recording unit consisted of a 7 foot vertical whip, an R-391 receiver, and a strip chart recorder recording the R-391 diode load output. The recording was used to observe the real-time signal and fade characteristics.

2.3.4.4 Data Reduction Methods

The bearing data for each test were reduced to the following standard statistical parameters:

$\Delta\theta$: The average bearing deviation from the great circle bearing (GCB). This parameter is positive if the deviation is clockwise from the GCB; negative if it is counter-clockwise.

SP: The total range of the bearings, i.e., the total azimuthal separation between the two extreme bearings (one clockwise; the other counter-clockwise) relative to $\Delta\theta$.

SD: The standard deviation given by

$$\sqrt{\frac{\sum_{i=1}^{n}(\theta_i - \bar{\theta})^2}{n-1}}$$

where $\bar{\theta}$ = the average of the bearings,

θ_i = the individual bearings,

and n = the total number of bearings.

(The usage of standard deviation does not imply that the bearing data distribution is normal).

For analysis purposes, the reduced data from individual tests were grouped and further processed to obtain the following parameters:

$\overline{\Delta\theta}$: The average of the averaged bearing deviations, $\Delta\theta$.

$|\overline{\Delta\theta}|$: The average of the magnitudes of $\Delta\theta$, $|\Delta\theta|$.

$\overline{SP}$: The average of the spreads.

$\overline{SD}$: The average of the standard deviations.

$\overline{RMS}$ Error : Defined as

$$\sqrt{(\overline{SD})^2 + (\overline{\Delta\theta})^2}$$

The grouped, reduced data are presented in graphical form using convenient symbols for the above parameters. $\overline{\Delta\theta}$ is depicted as an open space in a rectangle. The rectangle represents the $\overline{SD}$ range. The length of line extending on either side of the $\overline{SD}$ rectangle defines the $\overline{SP}$ range. $|\overline{\Delta\theta}|$ and $\overline{RMS}$ error are noted directly above the individual plots.

Most of the test results are presented in graphical form with the above parameters plotted versus an absolute degree scale. This is proper since (1) the original bearing deviation values, $\Delta\theta$, are normalized relative to the individual GCB for each test to obtain absolute values, and (2) the other parameters (SP, SD and RMS error) are inherently absolute quantities.

The individual tests were grouped into various combinations based on particular areas of analysis. Appendix A defines the groupings that are cited in the text and on the figures.

2.3.5 Operational Evaluation Test Results - Second Phase

2.3.5.1 Evaluation of Fade Detector Effectiveness

The initial operational tests were concerned with determining the relative effectiveness of the four types of fade crest detectors. Comparisons were made by using all four modes in sequence on the same test transmission. Sixteen separate tests (group 1) were performed using all four modes. For mode 2, tests were performed for each fade margin except for the higher fade margins that provided no bearings.

Several characteristics were immediately evident. Mode 1 produced a relatively large number of spurious, isolated bearings considerably different from the GCB. These bearings, which usually occurred when the pattern was swinging and distorting, tended to clutter the display, obscure the more accurate bearing, and increase the difficulty in reading the display. Mode 2 operated poorly in the presence of a very low SNR especially for conditions when the signal peaked-up out of the noise; modes 3 and 4 operated best under these circumstances and when a high fade rate was present.

Table I presents data comparing the modes for fifteen of the sixteen test transmissions. On one test, only mode 4 was effective due to a very low SNR. For mode 2, the fade margins providing the smallest $\Delta\theta$ for each test were used for the cumulative averaging. The relative rating of the modes is 2, 4, 3, and 1 for each parameter listed and indicates the superiority of mode 2. The total number of bearings show that mode 2 produced the best performance with the smallest number of bearings. This is also an advantage.

TABLE I

COMPARISON OF ALL FADE DETECTOR MODES

Mode	Total No. of Bearings	$\lvert\overline{\Delta\theta}\rvert$ (deg.)	$\overline{SP}$ (deg.)	$\overline{SD}$ (deg.)
1	564	15	81	19
2*	456	9	33	9
3	711	14	64	18
4	635	11	44	13

*Results for fade margins providing smallest $\Delta\theta$

As a result of the initial tests, it was decided to conduct a second series of tests (group 2) comparing mode 2 and 4. Of 38 tests, mode 2 was unusable on 5 due to low SNR, but mode 4 could

be used. Table II shows the comparative results and again illustrates the better performance of mode 2 if a good SNR is present. It is also significant that mode 4 performance for a low SNR is essentially identical to that for a good SNR implying that mode 4 operates independently of the average value of the signal. Also, on the average, the performance of both modes is essentially the same for both the group 1 and group 2 series of tests even though different transmissions and times were used.

TABLE II

COMPARISON OF MODES 2 AND 4

Mode	Total No. of Bearings	$\lvert\overline{\Delta\theta}\rvert$ (deg.)	$\overline{SP}$ (deg.)	$\overline{SD}$ (deg.)
2*	1733	7	32	8
4	1813	12	42	10
4+	70	13	43	11

*Using optimum fade margin

+For the five tests with mode 2 unusable due to low SNR

2.3.5.2 Effectiveness of Mode 2 Fade Margins

The effects of fade margin (FM) on performance were measured. Tests were performed on thirty-six transmissions (group 3) using fade margins of 0, 3, 6, and 10 dB in sequence for each test. The reduced data are shown in figure 19. It appears that a 3 dB fade margin is about the largest value that should be used if reliable operation for a given condition is required. Bearings were obtained at 0 and 3 dB fade margins on all tests; however, five tests and twenty tests provided no bearings at fade margins of 6 and 10 dB, respectively.

The most noticeable characteristics of figure 19 are: (1) the monotonic decrease in the number of bearings, standard deviation, and RMS error with increasing fade margin; and (2) the consistency of the $\overline{\Delta\theta}$ and $\lvert\overline{\Delta\theta}\rvert$ values. This indicates that, in general, the more accurate bearings occur at the fade crests and the average across a fade crest with any fade margin is relatively constant due to symmetrical bearing swings.

The differences between 3 and 6 dB fade margins were further investigated by an additional series of twenty-two tests (group 4). Test results are given in figure 20, which also illustrates the decrease in reliability (four tests produced no bearings) for a 6 dB fade margin.

The overall results show that a 3 dB fade margin can be reliably used to restrict a large majority of the displayed bearings to within $\pm 15^{\circ}$ of the GCB; however, bearing deviations as large as about 25° can occur.

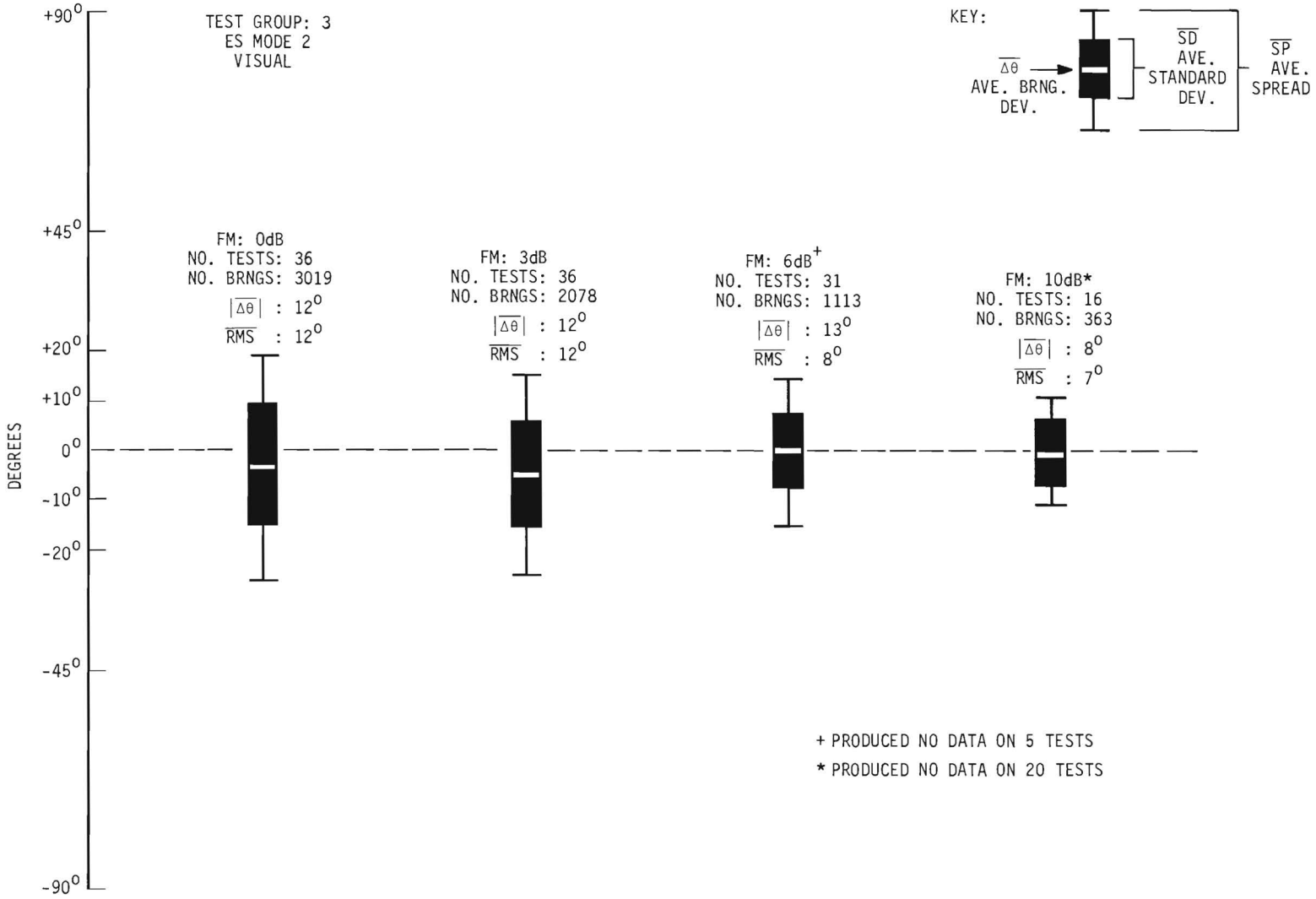

Figure 19. Test Results for Mode 2 Fade Margins of 0, 3, 6 and 10 dB.

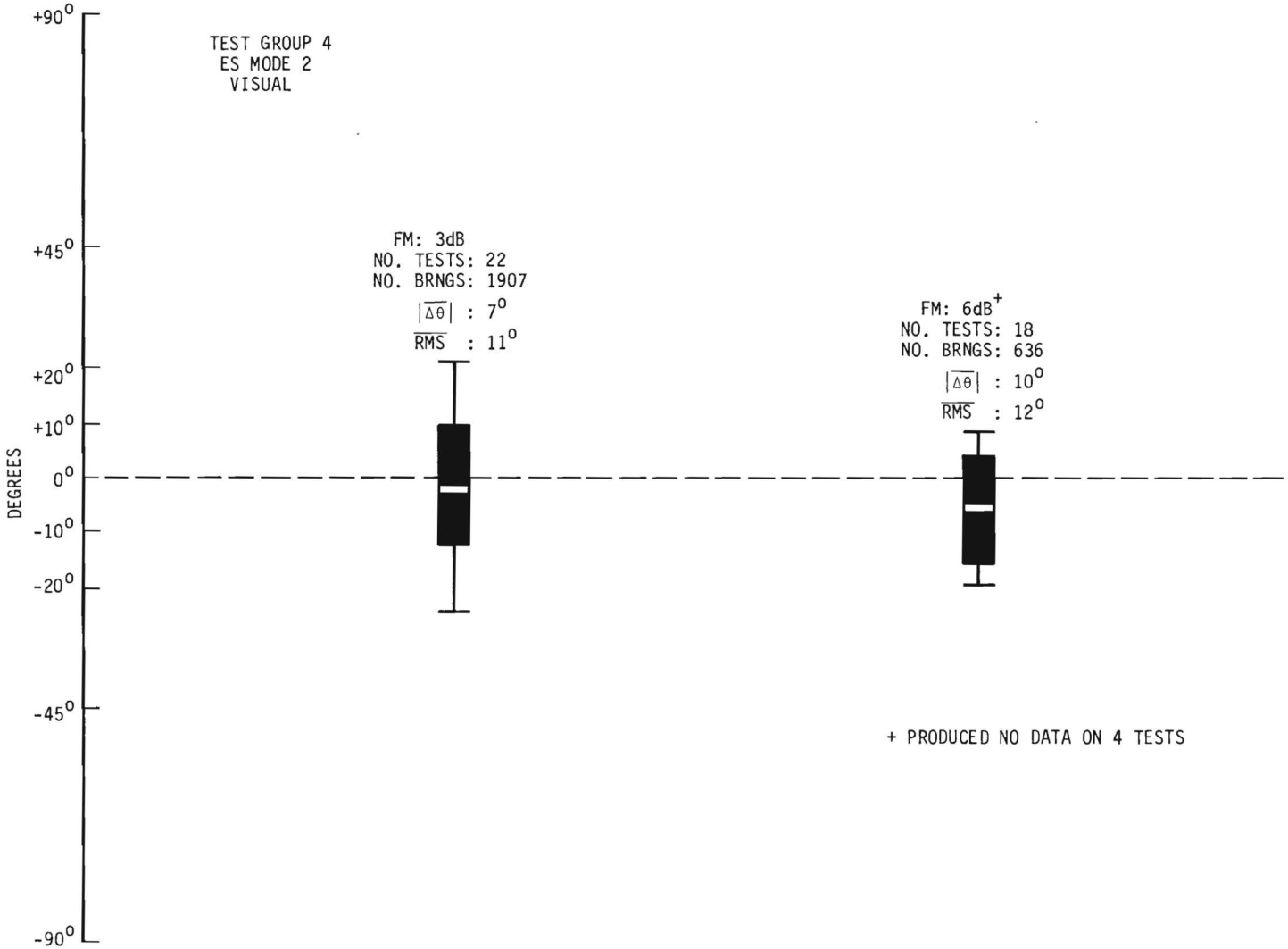

Figure 20. Test Results for Mode 2 Fade Margins of 3 and 6 dB.

2.3.5.3 Auxiliary Channel Antenna Investigations

Introduction

It was necessary to determine what type of antenna is best for use with the auxiliary channel. The first phase tests indicated that a horizontal dipole should not be used. The theory connected with wave interference and polarization error suggested that either a vertical loop or whip could possibly be used.

The anticipated advantages of the loop over the whip were azimuth directivity and increased sensitivity. It was thought that the loop azimuth directivity could be very useful in reducing interference arriving from azimuths perpendicular to the GCB after the sense of the GCB was determined. A major disadvantage of a loop is its sensitivity to all polarizations. This proved to be a major factor in the eventual rejection of the loop as an auxiliary antenna and is discussed in the next section.

The major advantage of a whip is its absence of response to horizontal polarization; therefore, using a whip, the auxiliary channel would not cause unblanking on a fade crest due entirely to a horizontal component. A secondary advantage of a vertical whip is that it could also serve as a sense antenna (or the sense antenna could be used as the auxiliary channel antenna).

Evaluation of the Loop During Polarization Rotation

It was determined that a loop antenna is unsatisfactory as an auxiliary channel antenna when polarization rotation (fading) is predominant. This is due to the fact that a loop is sensitive to all polarizations and, if the plane of the loop is perpendicular to the azimuth angle-of-arrival, unblanking will occur when the incident signal is primarily horizontally polarized. The unblanked displayed bearings will be highly erroneous. Theoretically, the error is 90°. Conversely, if the plane of the loop is parallel to the azimuth angle-of-arrival, unblanking will occur when the incident signal is primarily vertically polarized, and relatively accurate bearings will be displayed. Hence, in order to properly use the loop as an auxiliary channel antenna on polarization fading the azimuth angle-of-arrival must be known, i.e., the unknown parameter must be known in order to properly perform a test to define the same unknown parameter.

Data were obtained on thirteen tests to measure the above effects. All tests were on VOA (Greenville, N. C.) at frequencies of 6.2, 9.5, 9.7, and 11.9 MHz and Radio Havana at 6.1 MHz during periods of consistent polarization fading. The auxiliary channel used a loop with its plane positioned, first, north-south and then east-west for each test. The GCB for Greenville, N. C., is 71° approximately on an east-west azimuth. For Greenville, with the loop plane east-west, a

majority of the displayed bearings were in the 40° - 100° sector; however, with the loop plane north-south the sector changed considerably to the 330° - 50° region and the displayed bearings were shifted to a sector almost orthogonal to the GCB. The detailed data for GRE are shown in Table III. On one test, the north-south orientation gave no usable data whereas the east-west position produced a satisfactory set of bearings. Table III shows that the north-south orientation gave a larger absolute mean bearing deviation as well as increased spread and standard deviation. The mean bearing deviation is larger by a factor of about twelve and the spread and standard deviation are increased by about one-third. The tests on Radio Havana exhibited an even more significant difference between the east-west and north-south orientations. (Note that for Radio Havana the north-south loop plane orientation is practically on the GCB).

The major conclusion is that a loop should not be used as an auxiliary channel antenna if polarization fading is predominant.

TABLE III

EFFECT OF AUXILIARY CHANNEL LOOP ORIENTATION ON BEARING PARAMETERS DURING POLARIZATION ROTATION

Test Transmission	Loop Plane Orientation	No. Bearings	$\overline{\Delta\theta}$ (deg.)	$\overline{SP}$ (deg.)	$\overline{SD}$ (deg.)
GRE	EW	400	5	60	18
GCB: 71°	NS	323	59	79	25
HAV	EW	61	75	140	43
GCB: 171°	NS	95	3	50	15

Comparison of Vertical Loop and Whip

Even though the loop proved useless (if not harmful) as an auxiliary channel antenna during polarization fading, it was still desirable to compare the 1 foot diameter loop and 5 foot vertical whip in the presence of multipath fading and low SNR and/or RFI. Therefore, a series of 133 tests (group 5) with the loop and 87 tests (group 6) with the vertical whip were performed using test transmissions having multipath fading and, in most cases, low SNR and/or RFI. Mode 4 was used for all tests. The vertical loop was positioned with its plane along the north-south line. This was an arbitrary orientation, but typical of what would have to be done in an operational situation without a priori knowledge of the bearing sense.

Test results are depicted in figure 21 and indicate a slightly better overall performance for the whip. The whip was used for the remainder of the operational evaluation phase.

2.3.5.4 Exploratory System (ES) Test Results Using Vertical Whip with Modes 2, 3 and 4

The purpose of this section is to present a complete set of test results for the ES using the vertical whip. These results define the basic performance characteristics of the ES for a wide variety of conditions.

The mode 2 data (visual and APO) shown in figure 22 were obtained primarily on test transmissions (group 7 and 8) with polarization fading. Eight separate transmitter locations are represented. North-south and east-west propagation paths were present during dawn, dusk, and daytime conditions. However, a large number of the tests were on VOA (Greenville, N. C.) transmissions. The visual and APO data are very similar for all parameters with the visual data slightly better. Spreads over a significant portion of a quadrant were obtained; however, a large majority of the bearings were within a 30° sector with a mean absolute deviation of approximately 10°.

The mode 4, visual data taken on transmissions (group 6) exhibiting multipath fading is essentially identical to that for mode 2 (polarization fading) except for a slightly larger mean bearing deviation (3°). This similarity of results is somewhat surprising considering the dissimilar nature of the fade and bearing variations. The results for seven tests with heavy RFI and/or very low SNR are shown also under the mode 4 visual data. As expected, the parameters exhibit larger dispersion and less accuracy than the tests with better signal conditions; however, the data show that it is possible to obtain fairly reliable bearing data even for very poor signal conditions using mode 4.

Relatively little mode 4 and mode 3 APO data (groups 9 and 10) were obtained because the APO operation was not fast enough to optimally respond to the mode 3 and mode 4 operation. Even for visual readout bearings had to be stored prior to a reading since they occurred rapidly and for only a short time period. Therefore, the APO data given in figure 22 is included to simply illustrate the type of results that can be obtained even with non-optimum APO instrumentation. The operation could be significantly improved with the use of an instrument with faster print-out and re-set capability.

Considering all the results obtained for the ES using a vertical whip with the auxiliary channel operating in either mode 2 or 4, it appears that a standard deviation of 15° and a mean absolute bearing deviation of 10° or less can be cited as typical performance parameters for essentially all types of signal and fading conditions.

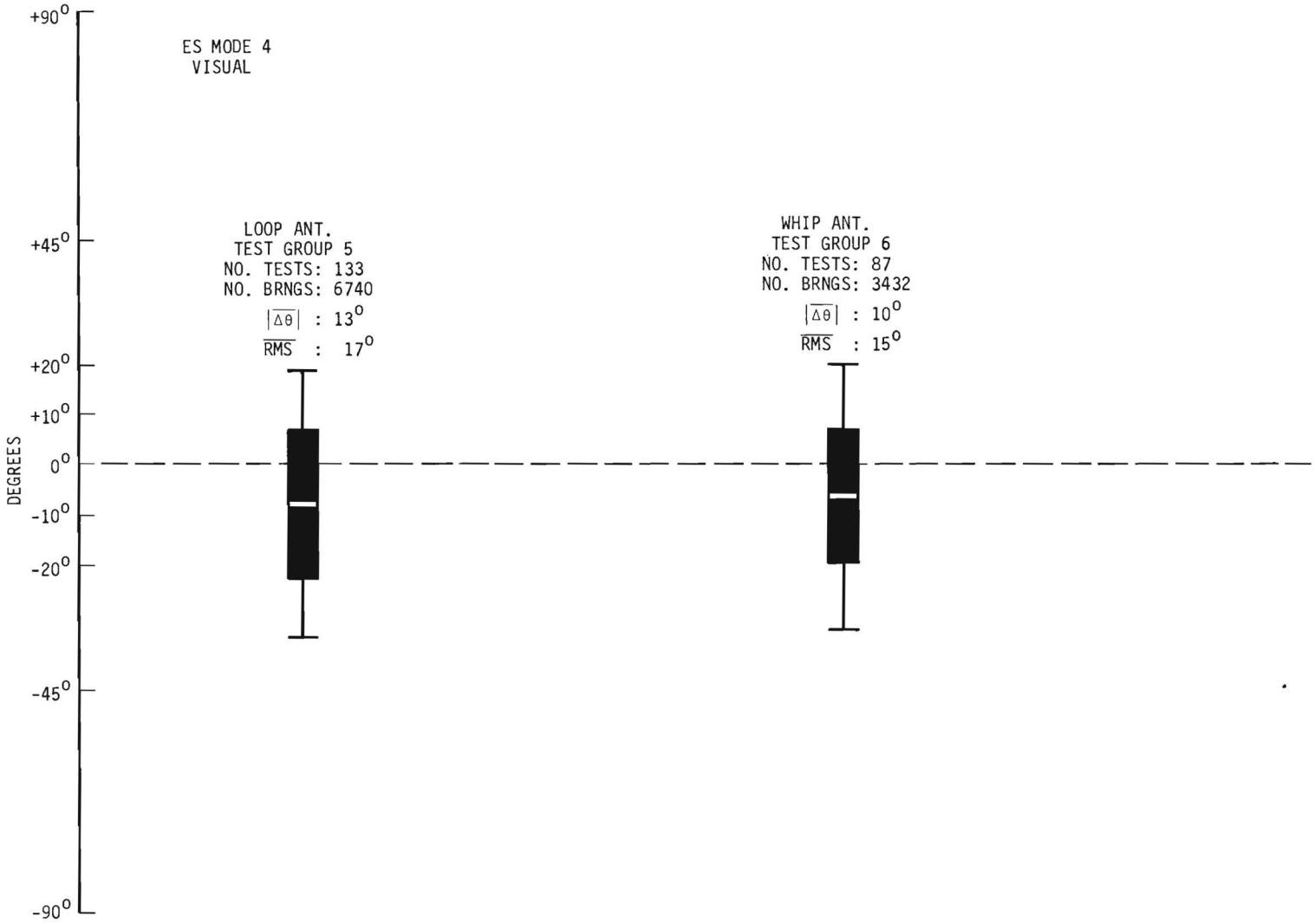

Figure 21. Comparison of Whip and Loop as Auxiliary Channel Antennas.

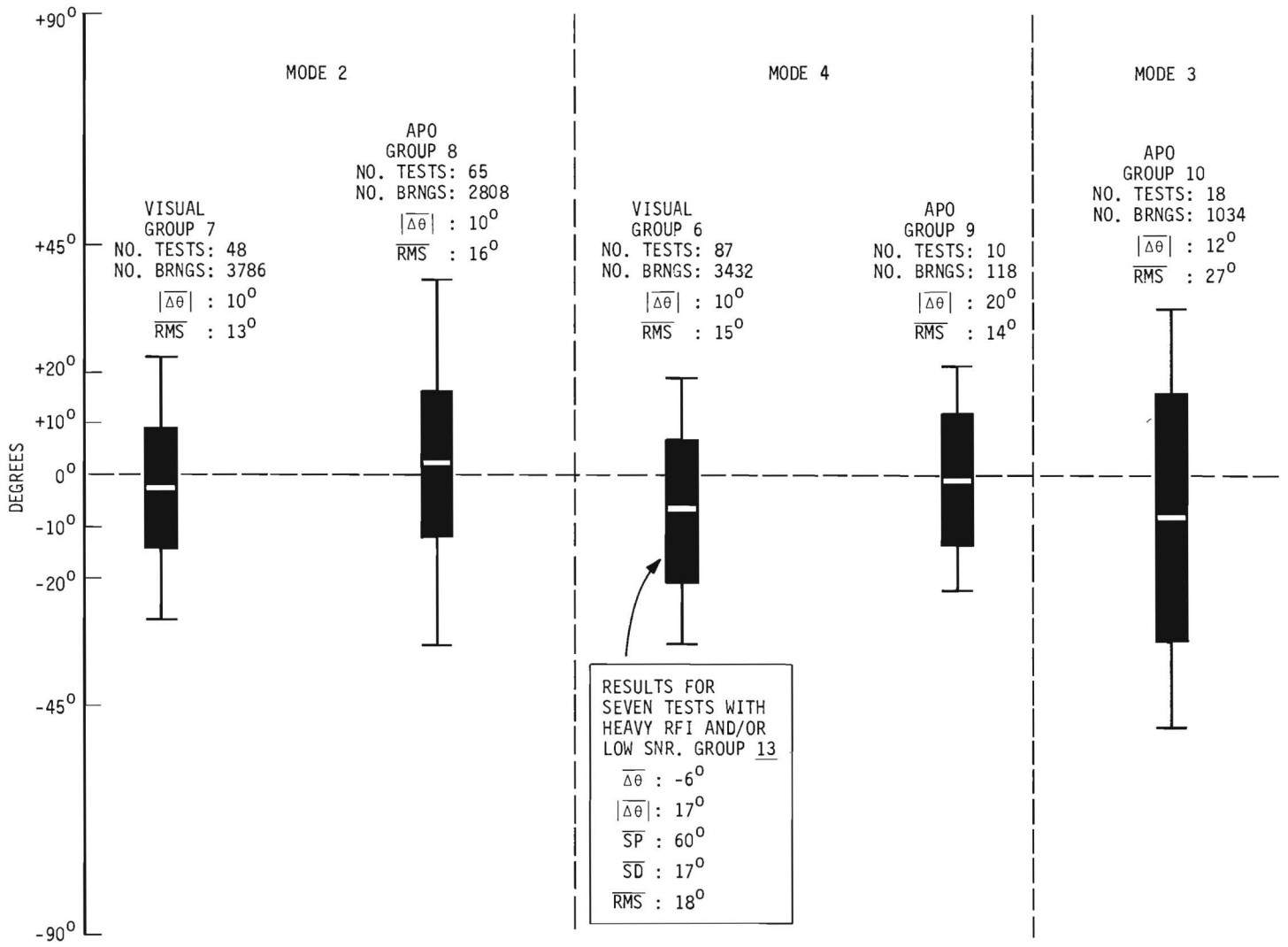

Figure 22. Test Results Summary- ES with Vertical Whip.

2.3.5.5 Operational Comparison of Exploratory System With The AN/PRD-5 HF/DF System

Introduction

A most significant and meaningful part of the field test phase was an operational comparison of the exploratory system with the AN/PRD-5 HF/DF system. The AN/PRD-5 operates from 0.5 - 20 MHz and uses a two-foot loop rotating continuously at 1 rps. The display unit is a 3 inch CRT with P7 phospher that displays a completely symmetrical two-lobe propeller pattern for each detected null of the rotating loop (i.e., two displays are generated for a single 360^{o} scan).

There are several significant differences between the exploratory system and the AN/PRD-5 in addition to the use of the auxiliary channel and the mode selectivity of the exploratory system: (1) the exploratory system uses a storage scope and 3:1 higher scan rate which produces a larger number of bearings per unit time in a more usable manner; and (2) each null of the exploratory system loop antenna produces only one-half of a propeller pattern which more clearly indicates the presence of accurate bearings through pattern symmetry.

Test Methods

The AN/PRD-5 was located on the ground some twelve feet away from the equipment trailer. It was located near the trailer in order to avoid (1) pick-up on the unbalanced lead-in and (2) spatial decorrelation between the signals at the PRD-5 and the exploratory system.

Two separate PRD-5 test methods were used. For the first method, bearings were taken as rapidly as the operator could subjectively judge the display steadiness and sharpness and record the bearing. This method was used primarily on test transmissions with multipath fading. For the second method, the single, best bearing in 15 second intervals were recorded. This provided for a more detailed evaluation of the bearing characteristics and a form of time-averaging. PRD-5 and ES data were obtained simultaneously by separate operators for tests using the second method. For the first method, the same operator evaluated the ES and then the PRD-5 using adjacent five minute time intervals.

The PRD-5 data were reduced in the same manner as the ES data.

Test Results

The test results, presented in figures 23 through 27, compare performance based on the test method, ES mode or operation (mode 2, 3, or 4) and ES method of data read-out (visual or APO).

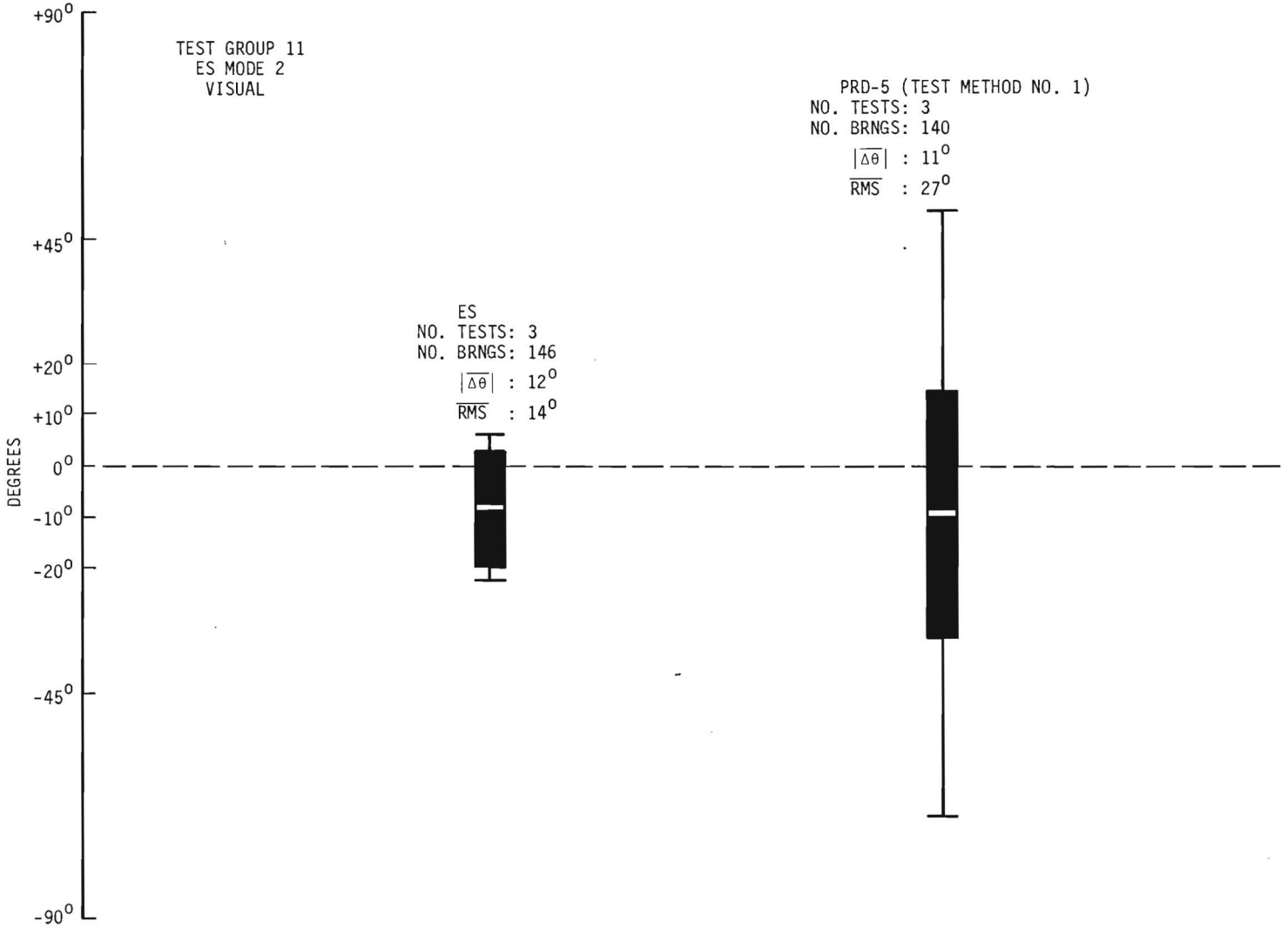

Figure 23. Comparison of ES and PRD-5 ES Operating in Mode 2, Visual Read-Out.

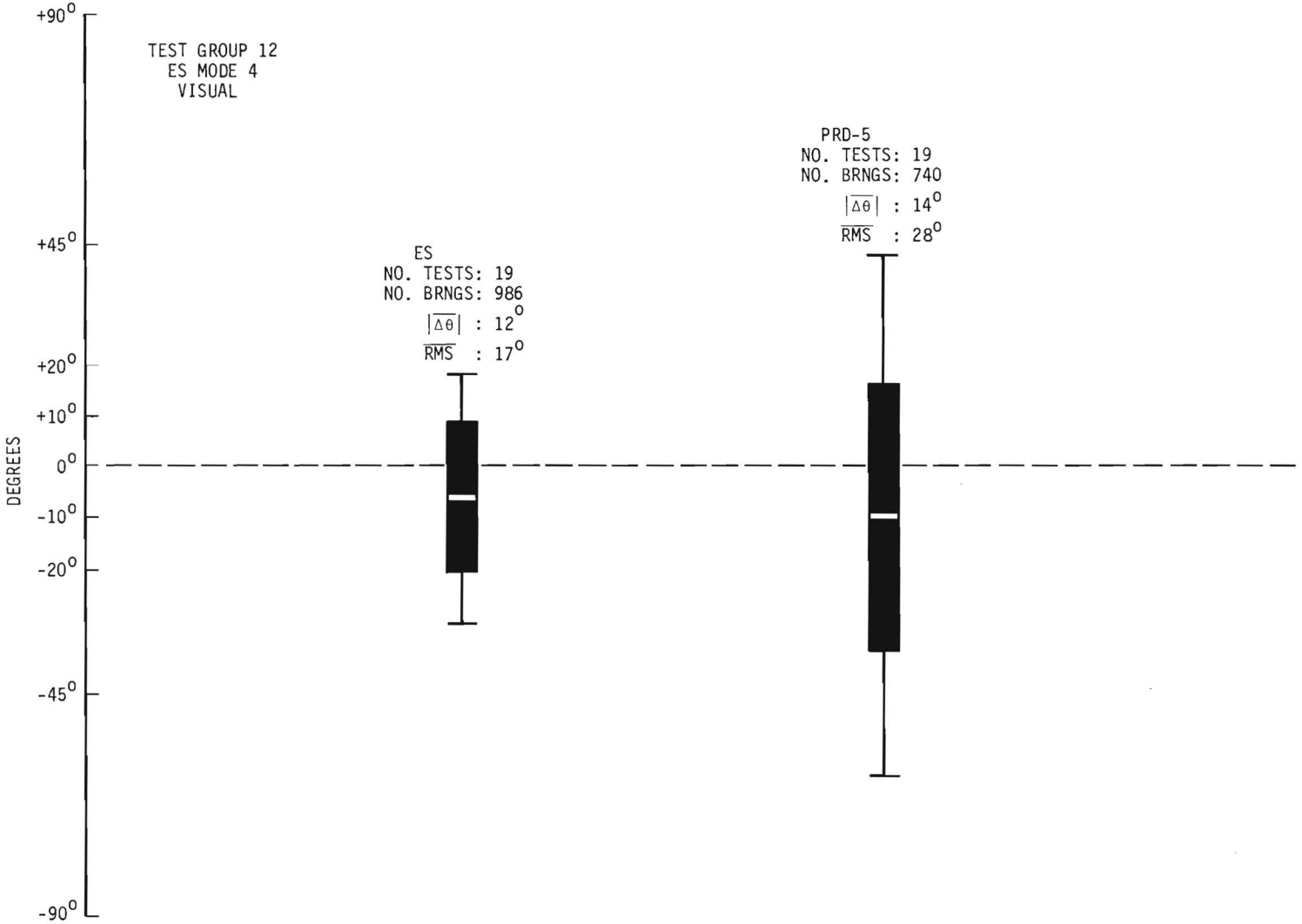

Figure 24. Comparison of ES and PRD-5 ES Operating in Mode 4, Visual Read-Out.

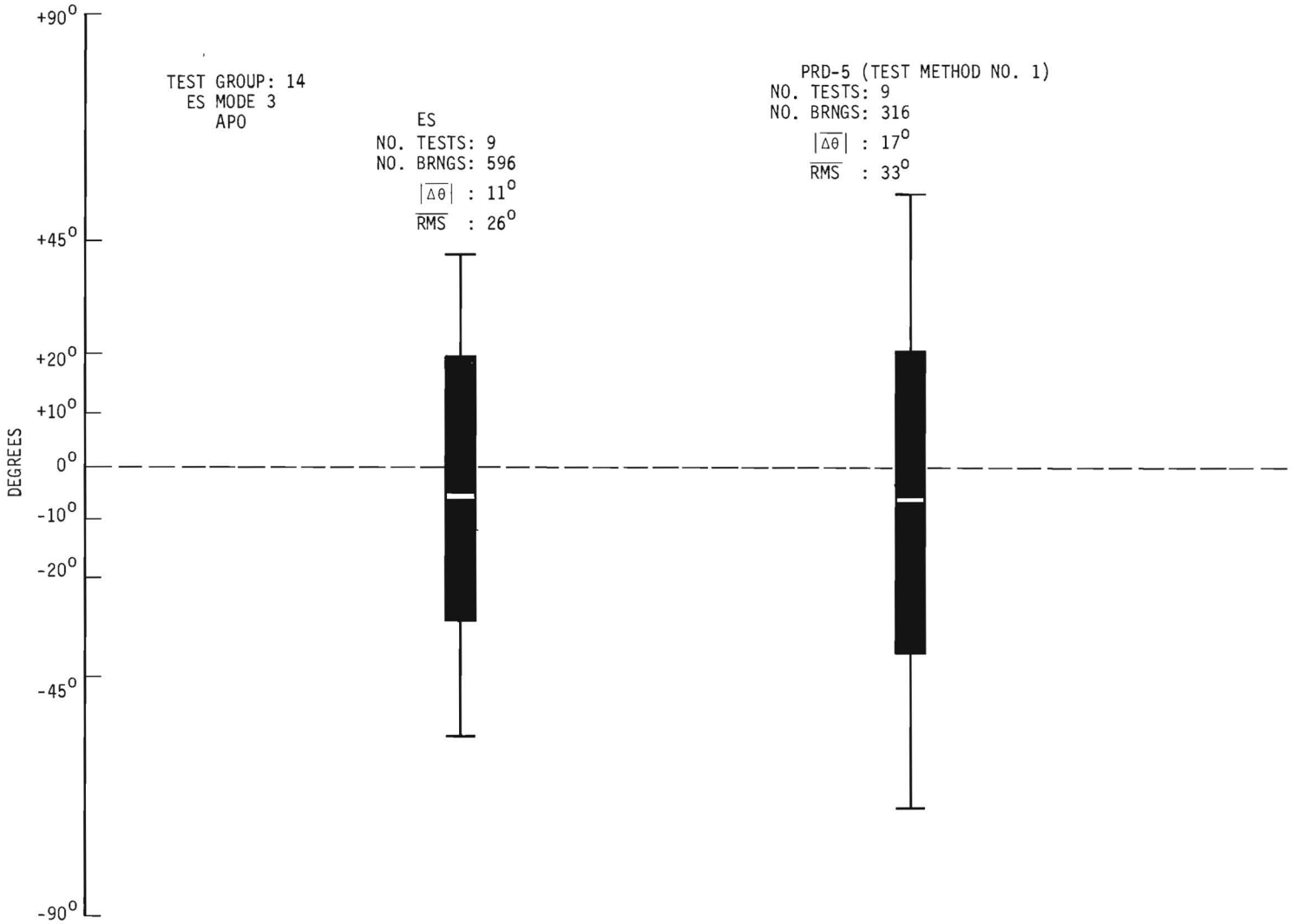

Figure 25. Comparison of ES and PRD-5 ES Operating in Mode 3, Automatic Print-Out.

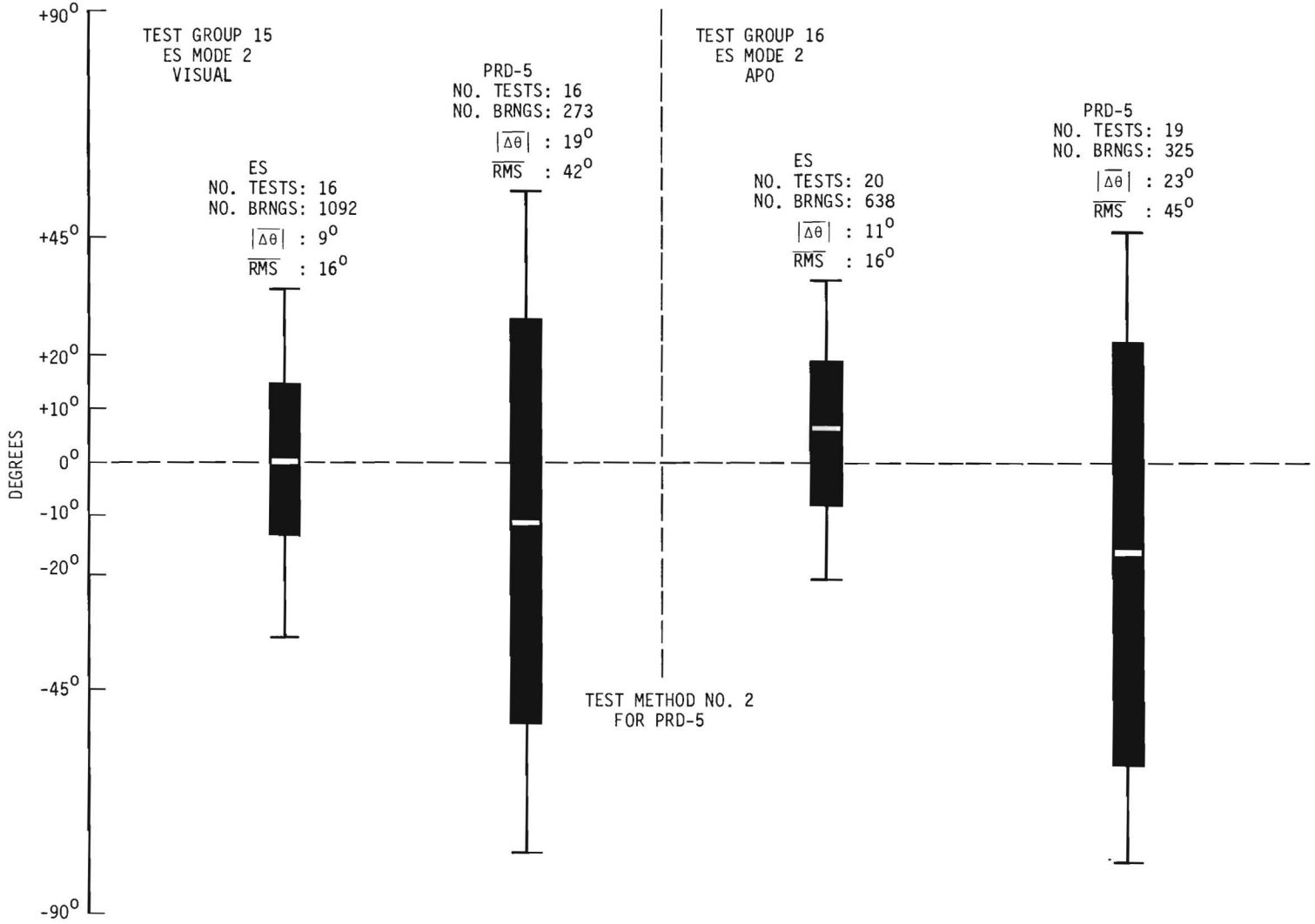

Figure 26. Comparison of ES and PRD-5 ES Operating in Mode 2, Visual and APO.

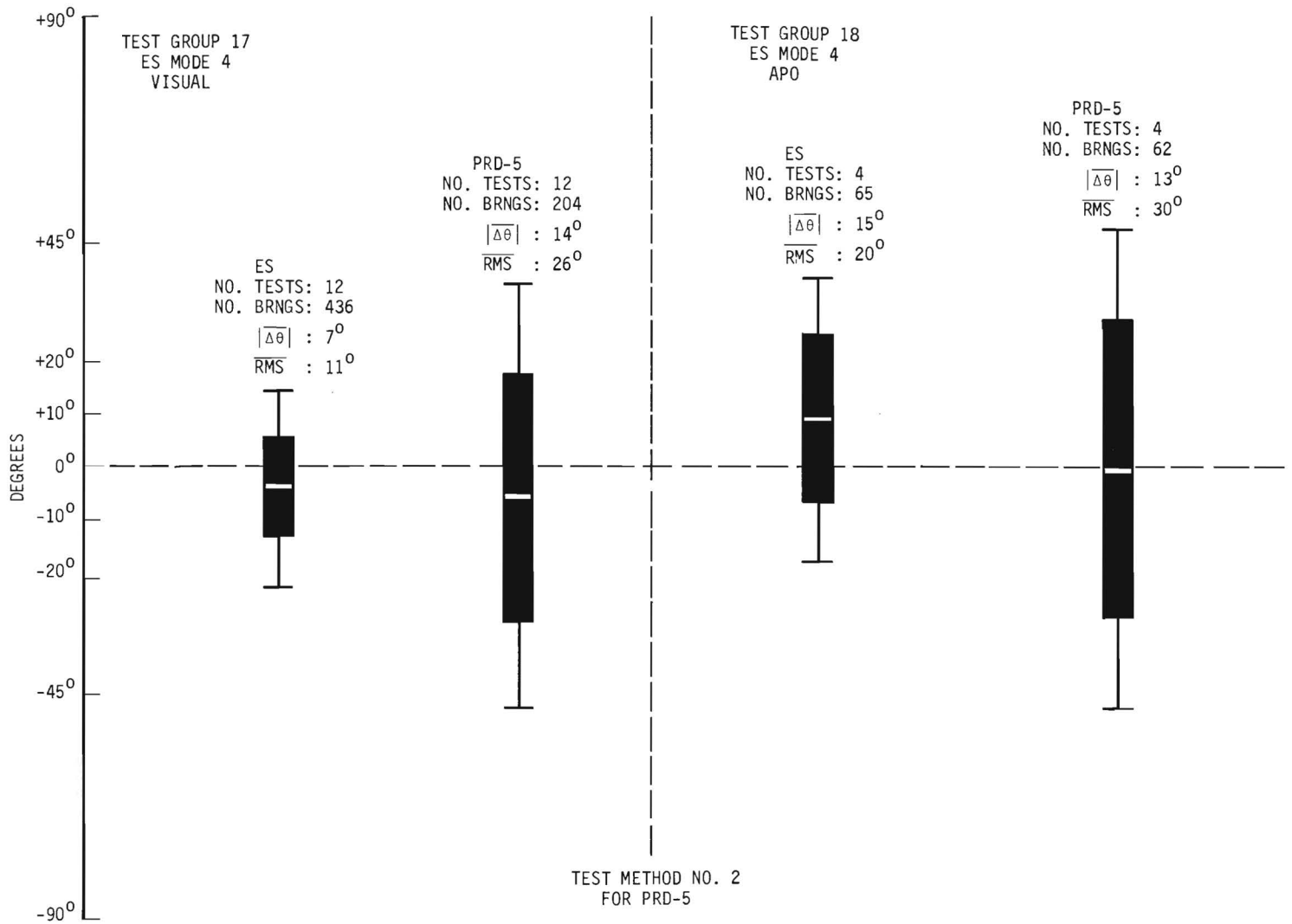

Figure 27. Comparison of ES and PRD-5 ES Operating in Mode 4, Visual and APO.

The major characteristics of figures 23 through 25 are that, in all cases for all parameters, the ES performance is better than the PRD-5 with spreads, standard deviations, and RMS error reduced by about one-half. The most significant improvement was with visual operation of the ES. (The APO makes no distinction between bearings based on pattern characteristics such as null asymmetry and skew. However, an operator can reduce the spread and, hence, standard deviation by rejecting displays with obvious asymmetry in null position or amplitude. It may be noted that the APO data has practically the same average values as the ES visual data but larger spreads and standard deviation).

Second Method - PRD-5 Operation

Tests using the first method included very little polarization fading; tests on polarization fading required a change in the method of reading the PRD-5 display. With polarization rotation, the bearing display can rotate 360° without any noticeable change in pattern or swing rate. (The relatively slow scan of the PRD-5 loop means fewer displays per unit time which increases the difficulty of judging the accuracy of bearings based on swing rates). This means that PRD-5 sensing must be performed before bearing data is recorded, because data recorded without an initial sense will provide a uniform distribution of bearings over 360°. This type of distribution has no meaningful average. (Using the ES operating principles, sensing can be performed at any time for polarization fading. Initial sensing is advisable in order to obtain bearings around the true GCB rather than its reciprocal; however, if conditions demand, no error should result if reciprocal bearings are obtained first and then converted after sensing. The ES type of operation is far more flexible in regards to using sensing with polarization fading). Also, a continuous recording of PRD-5 bearings as fast as possible is not optimum for polarization fading. It was decided that a better method would be to record the "best" bearing over a fixed time interval. Fifteen seconds was chosen as the time interval. This time period allows for an unhurried cycle of operator activities including display evaluation, reading, and recording. A longer time interval would not allow for a valid sample based on nominal polarization fade rates of about one per minute.

PRD-5 sensing with polarization fading was performed in the following manner. The sense switch was depressed and the display was observed over one or more complete bearing rotations. At some azimuths the typical cardioid sense pattern gradually degenerated into a crude form of a propeller pattern that existed for a relatively short period of time as the polarization rotated through the horizontal. The azimuth sector (a sector 20° wide was typical) where the propeller pattern occurred was assumed to be approximately 90° from the true azimuth angle of arrival for the following reason. The ideal

cardioid pattern degenerates as the vertical component of the incident signal decreases. Under polarization fading, when the horizontal component is near a maxima, the vertical component is essentially zero and no sense occurs. With no sense the effective loop antenna pattern is again double-nulled. At this time, the detected loop antenna pattern with no sense is operating in a primarily horizontally polarized field and the null locations are 90° from the true azimuth of arrival. Hence, it was possible to ascertain the 180° sector containing the GCB and record bearings that led to a meaningful distribution.

The above procedure appears to be simple; however, in practice, it is difficult and somewhat inaccurate because the patterns are never ideal and it requires a considerable amount of subjective interpretation by the operator. A trained operator is also an asset. (The PRD-5 operator during these tests had previous military service DF experience. An attempt to determine if an operator with little experience could successfully accomplish the sensing procedure was unsatisfactory due to the lack of optimum polarization fading during the particular test).

The test results are illustrated in two figures that compare the PRD-5 and ES performance, both visual and APO, for modes 2 (figure 26) and mode 4 (figure 27). Essentially all of the mode 4 data were obtained on multihop transmissions with a low SNR; in most cases, the signal was peaking-up out of the noise. Mode 2 was used mostly during polarization fading on single-hop transmissions at or near the F2MUF. The fade margin was either 1 or 3 dB. 3 dB was used on a large majority of the tests.

Figures 26 and 27 illustrate the better performance of the ES. PRD-5 spread, RMS error, and standard deviation values are 2 to 3 times greater than those for the ES. For polarization fading tests (mode 2), the PRD-5 bearing deviations are larger by, at least, a 2 to 1 factor. For multipath fading (mode 4), the overall ES performance is better but PRD-5 results are improved over that for polarization fading. This tends to confirm that polarization fading is indeed a serious problem for conventional loop DF systems.

2.3.5.6 Results from Tests on the Same Transmission During Polarization Fading

Transmissions from VOA at Greenville, N. C., provided an excellent set of test transmissions for both dawn and dusk transitional ionospheric conditions. The 9.5 and 11.7 MHz frequencies during dawn and dusk were essentially at the F2MUF for the Atlanta-Greenville path and created excellent polarization fading. The 9.5 MHz frequency was used in the dawn and dusk period; 11.7 MHz was used during the dusk period.

Data from these tests were reduced separately and are given in figures 28 and 29. The figures represent data comparing the PRD-5 and ES systems during conditions of excellent polarization fading.

The ES was operated in mode 2 with a 1 or 3 dB fade margin (a majority were at 3 dB) for all the tests.

Several factors are evident from the data for both frequencies. The ES data show about a 2 to 1 reduction in spread and standard deviation relative to the PRD-5. In some cases, the reduction is closer to 3 to 1. Also, the mean bearing deviations for the ES are less by factors greater than 2 to 1. The RMS errors for the PRD-5 range from about 36° to 58°. The RMS error for the ES range from about 13° to 20° showing a 2 to 1 reduction in RMS error. The PRD-5 spreads are over two quadrants which is to be expected for polarization fading. This spread is reduced to less than a quadrant using the ES.

A comparison of the visual and APO data shows similar spread, standard deviation, and RMS error values. However, the APO mean bearing deviation is off-set clockwise. This is due to the fact that, for most tests, the bearing swing was counterclockwise, i.e., the bearings rotated into the GCB (71°) from the 90° - 180° quadrant; hence, the first bearing print-outs on each fade crest were clockwise from the GCB. In general, these bearings had poor patterns. Visual interpretation lead to a rejection of these bearings; however, the APO accepted all bearings providing an unblanking pulse. This created a slightly larger number of APO bearings to the SE quadrant and a clockwise off-set of the mean bearing deviations.

A comparison of the 9.5 and 11.7 MHz data is also interesting because two different fading characteristics occurred. The 9.5 MHz tests had deeper polarization fading than the 11.7 MHz tests. The 11.7 MHz fades were shallow with almost a sinusoidal variation and the bearing rotation was not over a complete 360° range. This smaller rotation range resulted in smaller spreads, standard deviations, and RMS errors for the 11.7 MHz tests. The implication is that the character of the polarization fading has a direct effect on the bearing accuracy.

The calculated vertical angle of incidence, Φ, from Greenville, N. C., is in the 45° - 60° range. Using a 3 dB fade margin ($\psi \doteq 20°$) and the theoretical model for polarization fading, figures 2 and 12 predict bearing spreads from about ± 8° to ± 12° for a Φ range of 45° to 60°. The ES measured spreads were larger than this; however, the standard deviation and RMS values are fairly close to the predicted bearing spread implying that the model is possibly a better estimate of dispersion rather than spread. Also, the model seems to predict best-case rather than worst-case conditions.

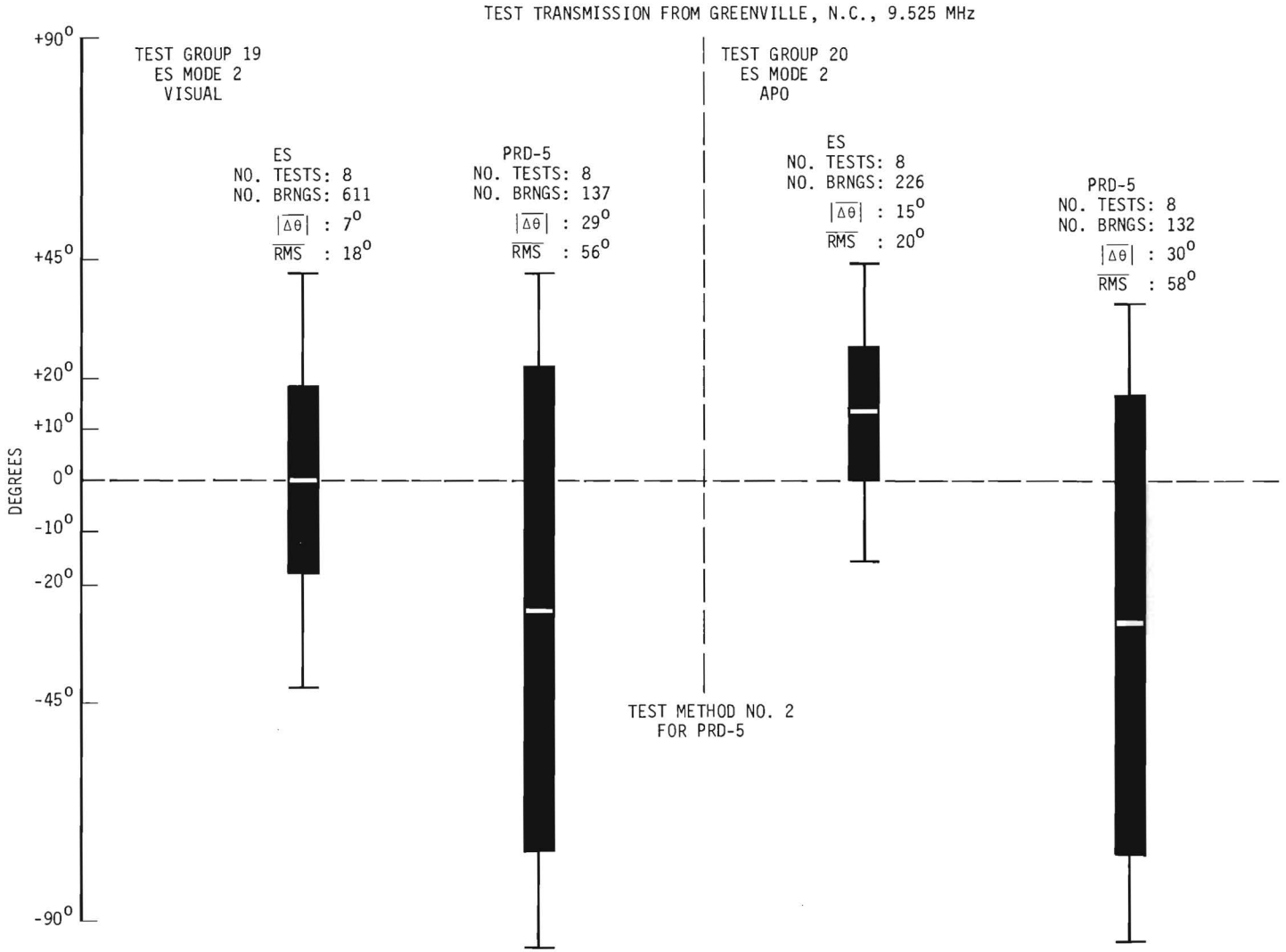

Figure 28. Comparison of ES and PRD-5 for GRE 9.525 MHz with Polarization Fading.

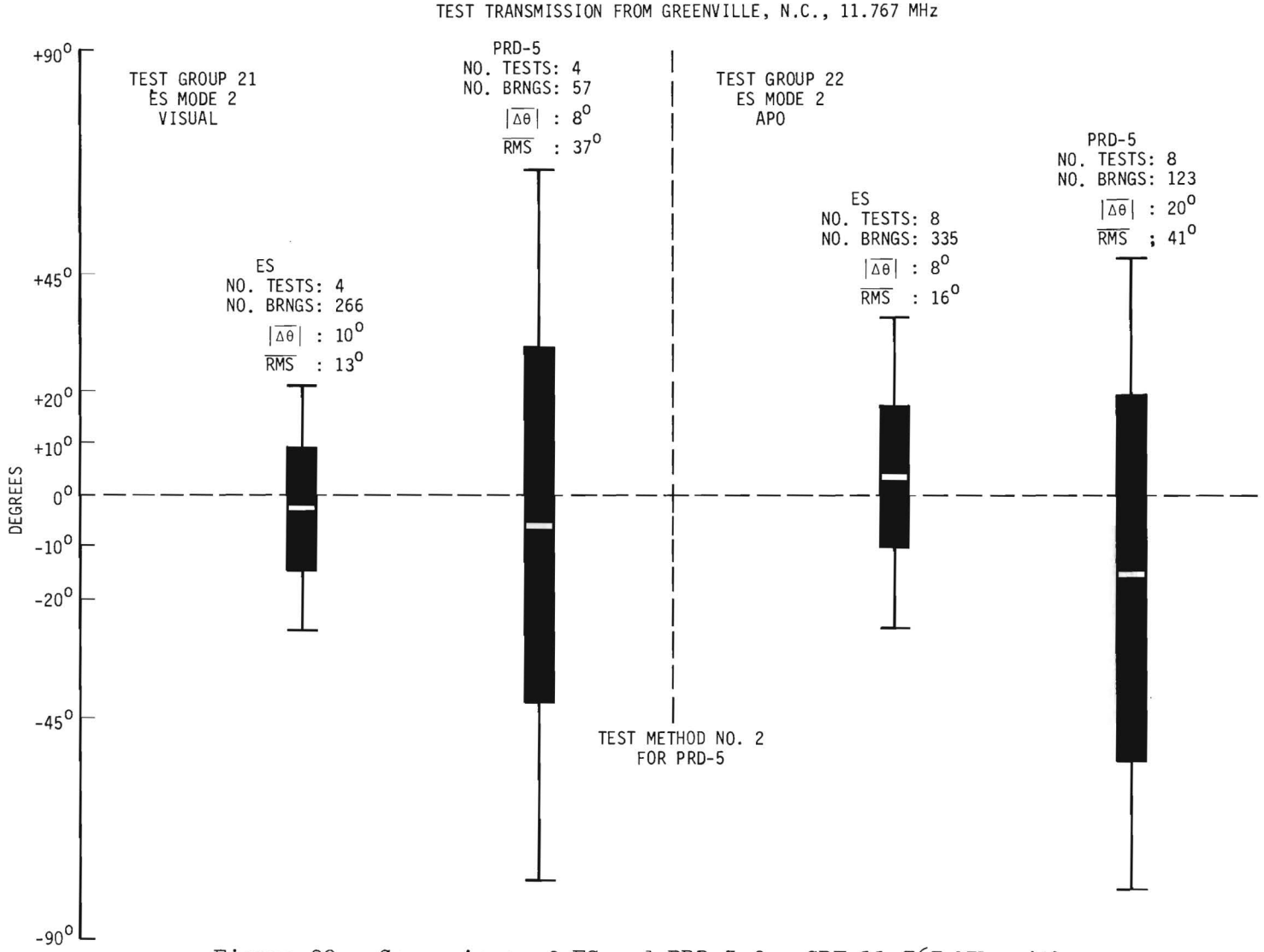

Figure 29. Comparison of ES and PRD-5 for GRE 11.767 MHz with Polarization Fading.

2.3.5.7 Comparison of ES (with APO) and PRD-5 on Ground-Wave Signals

One minute tests on seven local broadcast stations were performed using the ES operating in the APO mode without the auxiliary channel and the PRD-5 operating in the normal manner with the operator recording a single bearing at the end of each test. For the ES, about thirty bearing print-outs were obtained on each station. These data were averaged for each test. Table IV shows the average bearing errors. A slightly better overall performance for the ES is indicated. However, the major advantages of the ES with APO are that (1) no operator decisions are required after initial adjustments are made, and (2) a permanent record of the test is provided for either future processing or, perhaps, transmission to a central DF control site.

TABLE IV

COMPARISON OF ES (WITH APO) AND PRD-5 PERFORMANCE ON GROUND-WAVE SIGNALS

Station	ES $\Delta\theta$ (deg.)	PRD-5 $\Delta\theta$ (deg.)
WSB	-1°	-2°
WPLO	-2°	-3°
WQXI	-1°	-2°
WGST	0°	-1°
WGUN	0°	0°
WGKA	0°	0°
WTJH (low SNR)	-3°	-6°

2.3.5.8 Storage Scope - Bearing Processor

Under certain conditions, the storage scope acting alone could be used to reduce bearing uncertainty. One condition occurred when the bearing swung symmetrically about a center azimuth over a portion of a quadrant e.g., 20°. It was difficult to observe and average the swings and estimate the center of the fluctuations using a regular scope; however, this became simplier using the storage scope with maximum persistence. As more and more bearings were painted on the scope, a slit or eye effect began to form and became more pronounced as time in-

creased with the centerline of the slit indicating the center of the bearing swings. The storage scope essentially averaged the fluctuations. Table V summarizes the results for several tests. $\Delta\theta$ is the difference in degrees between the centerline of the slit on the storage scope and the GCB. In all tests, the bearings were fluctuating over tens of degrees (one-half of a quadrant); however, the storage scope could be used to obtain an average value to within ten degrees of the GCB on 26 of the 35 tests.

The storage scope could also be used to estimate the bearing location even though the pattern was rotating over 360° without any discernible change in shape. A method was devised that used the variable persistence of the storage scope and intensity modulation only on the tips of the propeller display. The null detector threshold was lowered until only a small portion of the display was consistently intensity modulated by the sharpest nulls near the GCB. But some spurious intensity modulation at other bearings also occurred. These spurious indications could be reduced by simultaneously adjusting the scope intensity level and variable persistence. This left only a small (e.g., 20°) portion of the scope intensity modulated. Four tests on GRE, HAV, NY, and CAN were performed. In all cases, it was virtually impossible to estimate the quadrant containing the GCB due to pattern rotation. However, using the technique above, it was possible to restrict the intensity modulation to azimuth sectors of approximately 20° or less which contained the GCB.

TABLE V

BEARING AVERAGING USING STORAGE SCOPE

Station	Freq (MHz)	Mode and Fade Margin	Observation Time (Mins)	$\Delta\theta$ (deg.)
BON	11.7	2; 6dB	1	- 6
"	"	2; 10dB	1	-21
QUI	17.8	2; 0dB	1	-10
"	"	" "	1	-10
"	"	" "	1	-10
NY	9.8	4	0.5	+ 7
"	15.4	2; 0dB	1	- 8
"	"	3	1	-13
"	"	2; 3dB	3	- 8
"	"	4	0.5	+ 2
HAV	15.2	3	1	- 5
WWV	15.0	3	1	+ 6
"	"	3	1	+ 1
"	"	3	1	+ 1

TABLE V (Continued)

BEARING AVERAGING USING STORAGE SCOPE

Station	Freq (MHz)	Mode and Fade Margin	Observation Time (Mins)	Δθ (deg.)
WWV	15.0	2; 0dB	1	- 4
"	"	4	1	+ 1
"	"	"	1	- 5
"	"	"	1	+ 1
"	20*	NONE	0.5	-24
"	"	"	0.5	-19
"	"	"	0.5	- 9
"	"	"	0.5	- 4
"	"	4	1	- 9
"	"	"	1	-14
"	20	2; 0dB	0.5	- 4
"	"	"	0.5	- 9
"	"	"	0.5	- 9
"	"	NONE	0.5	- 4
"	"	"	0.5	- 4
"	"	"	0.5	- 4
"	"	"	0.5	- 9
"	"	"	0.5	- 1
"	"	"	0.5	- 9
"	"	"	0.5	- 4

*Low SNR on WWV 20 MHz

To summarize, the storage scope can be used to reduce bearing uncertainty under conditions of either symmetrical fluctuations or complete pattern rotation. However, the effectiveness of the methods are a function of the capability of the operator to judiciously adjust controls such as the intensity, persistence, and null detector threshold.

2.3.5.9 Effect of Fade Crest Amplitude on Bearing Accuracy During Polarization Fading

Tests on transmissions experiencing polarization fading indicated that bearing accuracy increased as the fade crest amplitude increased, i.e., the fade crests producing the most bearings provided the most accurate bearings.

Several tests were performed to check-out this effect. Transmissions from VOA, Greenville, N. C., were used at times when exceptionally constant polarization fading occurred over a number of fade cycles. The APO was used

to separate the recorded bearings by fade cycles. The number of bearings per fade crest was related to the average absolute bearing deviation from the GCB for each fade crest. Table VI shows the result for the two tests on GRE 9.5 MHz with the data grouped by the number of bearings per fade cycle and the individual absolute bearing deviations averaged for each grouping. Both tests definitely show that fade crests producing the most bearings provided the most accurate bearings.

A similar test was performed using GRE 11.7 MHz. Nine fade crests were obtained with essentially the same number of bearings per crest (the range was 6-9). The average bearing deviation per fade crest varied from 1° to 11°; however, five of the fades produced average deviations in a small 3° to 7° range indicating constant bearing error for constant fade crest magnitude.

To summarize, it appears that if the polarization rotation characteristics are uniform, the statistical parameter of the bearing distribution will be constant. However, if the fade crest amplitudes are varying, the most accurate bearings apparently occur on the crests with the largest amplitudes.

TABLE VI

BEARING DEVIATIONS AS A FUNCTION OF FADE CYCLE MAGNITUDE

Test	No. of Fade Cycles	No. of Bearings Per Fade Cycle	$\lvert\overline{\Delta\theta}\rvert$ (deg.)
No. 1	5	0-2	26°
GRE 9.5 MHZ	5	3-4	18°
	4	5-6	14°
	1	7-8	13°
	3	9-10	4°
No. 2	4	0-16	9°
GRE 9.5 MHz	1	32	2°

2.3.5.10 Effect of Fade Moding During Polarization Rotation

When polarization fading is predominant, the best conditions for bearing unblanking is with a constant fade (rotation) rate and equi-amplitude vertical component fade crests. Whenever the fade rate

and/or fade crest amplitudes vary, the mean deviation, spread, and distribution will also change. In some cases, the polarization rotation will cease and a steady-state amplitude (moding) occurs. (For example, see figure 44). The bearing parameters are a direct function of the position on the polarization fade cycle where moding occurs. If it occurs at the null or on the skirt of the polarization fade cycle, erroneous steady bearings are displayed. Null and skirt moding are especially harmful, because the bearings are reasonably steady and appear to be accurate to an operator lacking knowledge of the previous fade characteristics.

Some form of moding was observed on essentially every test where polarization fading was dominant. Moding was usually preceeded by a decrease in the fade rate and change in amplitude. In general, moding was of relatively short-duration and usually followed by a gradual increase and stabilization of fade rate and amplitude. The direction of bearing display rotation usually reversed after a mode occurred. This was possibly due to a change in polarization rotation direction.

The effect of skirt moding is best illustrated by the results of a test conducted on GRE 9.5 MHz with polarization fading dominant. Consistent polarization rotation was observed over a five minute test using mode 2 (1 dB fade margin) that produced values of + 10°, 64° and 16° for $\Delta\theta$, SP, and SD, respectively. Immediately after the test, a skirt mode occurred with the signal maintaining a constant value slightly above the fade null level for about one minute. During this time, excellent, relatively steady bearings were observed in the 20° azimuth sector. After a short-period of time, the mode 2 circuitry began unblanking (due to the low fade margin) and produced results of -51°, 30°, and 10° for $\Delta\theta$, SP, and SD, respectively. The spread and standard deviation from the skirt mode are less than those obtained during consistent polarization fading implying that a more acceptable display existed during the skirt mode; however, the bearing is highly erroneous. This same type of result was evident on many other tests. Crest moding occurred also but less frequently. On one test (also GRE on 9.5 MHz) polarization rotation stopped at the crest of a fade cycle and held fairly steady for approximately four minutes. During this time, the bearing display scintillated in the 40° - 90° region. The statistical parameters were + 9°, 55°, and 5° for $\Delta\theta$, SP, and SD, respectively, for one-hundred and five recorded bearings obtained using the APO.

The major conclusions are that: (1) "snap" bearings taken during polarization fade moding can be highly inaccurate; and (2) an operator needs a knowledge of the previous fade pattern in order to avoid taking bearings during skirt or null moding unless he restricts his bearing readings to the periods when the fade rate is relatively constant and non-zero.

2.3.5.11 Deviated Bearing Groupings on Fade Crests

A small number of tests produced sets of deviated bearing groups on individual fade crests. This effect was observed only in the presence of a strong ionosphere (daytime) on frequencies above 15 MHz.

The fading was characterized by very slow rates (less than one per minute) and shallow nulls. It is believed that slow multipath (multi-mode) fading with mode switching was dominant because the fade crests were essentially the same amplitude. (Polarization rotation moding would produce different amplitudes). A fade null possibly represented a rearrangement of the propagation (multipath) structure with a particular mode dominating the fade crest immediately after the fade null. The deviated bearing groupings could be due to the fact that each propagation mode had a different azimuth angle-of-arrival.

This action is illustrated in Table VII which was prepared from a forty minute (2050-2130 GMT) set of automatic print-out data obtained on NY (GCB: 48°) on 15.4 MHz. The data, which were separated by fade cycles (blocks), were acquired using mode 2 with a 0 dB fade margin. The blocks are in time-sequence.

The calculated F2MUF was about 15 MHz. Hence, conditions were proper for a relatively small number of propagation modes of about the same strength.

The major factors that may be noted from Table VII are: (1) a definite grouping of bearings for each fade crest; (2) a definite clock-wise progression in the average bearing between blocks 1, 2, and 3; blocks 4, 5, and 6; blocks 7, 8, 9, 10, and 11; (3) the fade crests (blocks) with the larger number of bearings (e.g., blocks 12, 13, 14, and 16) have a larger spread but the average is more accurate. The first and second factors indicate a definite mode structure with switching; the third factor implies that the modes of longer duration are more accurate. The overall results support the well-known principle that the longer the averaging time the better the overall bearing. The overall average is 40° for the total deviation of -8°, however, prior to block 11. the cumulative average was less than 35°. Blocks 11, 12, 13, 14, and 16 improved the overall average.

The implication from an operational aspect is that "quick-look" bearings taken during blocks 1-10 and 15 could have provided inaccurate data even though acceptable bearings were evident. It should be stressed that this type of moding effect occurred infrequently and was not evident during a transitional or weak ionospheric period.

TABLE VII

DATA ILLUSTRATING DEVIATED BEARING GROUPINGS ON FADE CRESTS

Block No.	Bearings		
	No.	Spread (deg.)	Average (deg.)
1	26	15 -27	22
2	37	27 -36	32
3	10	31 -52	36
4	6	3 -15	8
5	14	17 -53	22
6	2	34	34
7	1	19	19
8	8	21 -29	24
9	22	27 -53	30
10	8	32 -39	35
11	17	35 -45	40
12	49	23 -96	45
13	37	23 -78	42
14	64	24 -67	39
15	3	77	77
16	45	41 -79	53
		Overall Average:	40° ($\overline{\Delta\theta}$ = -8°)

2.3.5.12 Second Phase Test Results - Summary

The second phase test results may be summarized as follows:

(1) The optimum auxiliary channel antenna is a vertical whip rather than a horizontal dipole or vertical loop.

(2) The optimum fade crest detector modes are mode 2, with a 1 or 3 dB fade margin, for polarization fading and mode 4 for multipath fading.

(3) Using mode 2, an increasing fade margin results in a monotonic decrease in standard deviation, spread, and RMS error with the

average bearing error remaining approximately the same. This indicates that more accurate bearings occur at the fade crests and bearing swings are symmetrical across the crest. Unblanking reliability decreases for fade margins greater than 3 dB, hence, a maximum fade margin of 3 dB is indicated.

(4) Mode 2 performs best when the SNR is greater than one and the fading is reasonable periodic with well-defined nulls and crests (e.g., polarization fading). Mode 4, which operates on the signal peaks independently of the average value, performs best in the presence of multipath fading especially if there is a low SNR and/or interference.

(5) The overall test results for the ES using the whip and the optimum fade crest detector for the prevalent conditions show that a large majority of the unblanked bearings occurred within ± 15° of the GCB for any signal or fade condition. Average bearings deviations of 10° or less are typical. (It may be noted from the graphs that a consistent negative [counterclockwise] deviation is present. It is believed that this is primarily a site effect since a major reradiator [a tree line] was located to the NNE and a majority of the test transmissions arrived from the NE and ENE. The effect of the tree line would be to create counterclockwise deviations as indicated by the site calibration).

(6) Operational comparison of the ES and PRD-5 showed ES performance is better with spreads, standard deviations, and RMS errors reduced by about one-half. ES improvement for polarization fading is most significant showing about three-to-one reductions in spread, standard deviation, and RMS error. The mean bearing deviations for the ES are less by factors of about 2 to 1.

(7) The storage scope was useful in storing and displaying groups of bearings. The storage scope was particularly useful with mode 4 when a "burst of bearings" occurred rapidly at the crest of a fade cycle. The storage scope could also be used to obtain the approximate center of bearings fluctuating over a small (e.g., 20°) azimuth sector.

(8) Tests on transmissions experiencing polarization fading indicated that the bearing accuracy increased as the fade crest amplitude increased. Also, if the polarization rotation characteristics are uniform, the statistical parameters describing the bearing distribution are also uniform. However, if the fade crest amplitudes are varying, the most accurate bearings apparently occur on the crests with the largest amplitudes. If polarization rotation ceases, the accuracy of the resultant steady bearing is a direct function of the position on the polarization rotation cycle where rotation ceased. If rotation ceases at the null or skirt of a vertical component fade cycle, an appreciable horizontal component is present and erroneous bearings occur even though the display is steady and appears to be accurate.

2.3.6 Reduction of Bearing Errors Caused By Polarization Rotation

2.3.6.1 Background

It has been shown that the polarization bearing error in a simple loop antenna DF system can be expressed as

$$\theta = \tan^{-1}(\cos \Phi \tan \psi) \quad , \qquad (2)$$

where,

θ = bearing error in degrees,
Φ = vertical angle of arrival in degrees measured with respect to the vertical,

and

ψ = polarization tilt angle in degrees.

Figure 1 illustrates the relationship between these units and the loop antenna position. Under the ideal conditions of uniform polarization rotation, Φ is constant and ψ changes with time at a uniform rate. Under practical conditions for polarization rotation, Φ is approximately constant and ψ varies approximately uniformly with time for some time interval. Field observations indicate that the polarization vector may rotate in one direction for one time interval and then reverse directions for another time interval. Although Φ is in general, a time varying quantity which depends on the mode of propagation and the ionospheric conditions existing at a given time[13], it is relatively constant for significant amounts of time. The bearing error, obtained from equation (2), versus the polarization tilt angle is shown in figure 2 for various angles of arrival. Note that the bearing error is zero only when the tilt angle is zero; however, note also that for values of Φ greater than zero, the bearing error is not a linear function of tilt angle. If ψ varies uniformly with time, as during polarization rotation, and Φ ranges from 0 to 90 degrees exclusively, figure 2 indicates that the time rate of change of θ is smallest when ψ is near 0 or 180 degrees. This fact is clearly demonstrated in figure 30 which shows the angular change in bearing error per angular change of tilt angle as a function of tilt angle and vertical angle of arrival. From figure 30 it may be concluded that if ψ rotates uniformly with time and Φ lies between 0 and 90 degrees, then the bearing indication rotates and the rate of rotation is lowest whenever the indicated bearing is near the true bearing. This conclusion has been partially substantiated by visual observations of the bearing rotation rate when polarization rotation was occuring.

From the theoretical results predicted from figures 2 and 30 and the results of field observations, it appeared that bearing errors

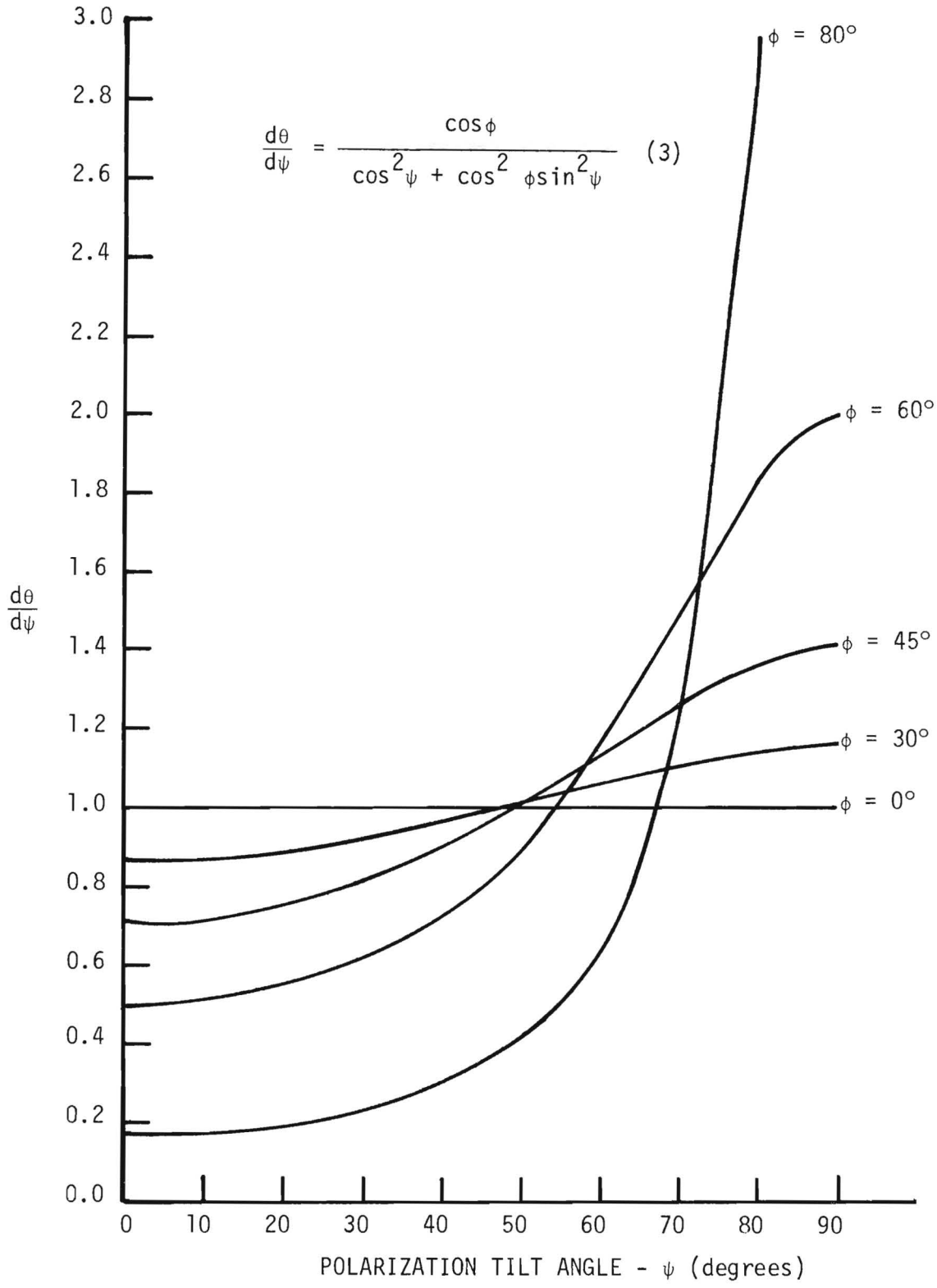

Figure 30. Derivative of Bearing Error with Respect to Tilt Angle.

could be reduced under polarization rotation if the bearing presentation was read at its lowest value of angular rate of change. In order to determine if this technique was indeed valid for error reduction, it was necessary to construct a device that would allow a bearing presentation only if the time rate of change of the indicated bearing was below some fixed value. Operationally, such a device would function as a swing rate discriminator.

The following sections outline the design techniques that were used to implement a swing rate discriminator. The results of data obtained using the swing rate discriminator are also discussed with primary emphasis on the use of the technique for bearing error reduction.

2.3.6.2 Design of Swing Rate Discriminator

The basic design objective for the swing rate discriminator (hereinafter referred to as SRD) was that it allow the bearing presentation to be read at its lowest value of angular rate of change. A suitable technique for accomplishing this objective is to compare a fixed number of successive bearings with an initial reference bearing. If the bearing samples differ from the reference sample by less than an allowable amount, the bearing display is unblanked for one loop scan. Otherwise, the bearing display remains blanked and no bearings are displayed. Note that this procedure provides swing rate discrimination in that a rapidly rotating bearing will give rise to bearing samples which differ from the reference sample by more than the allowable amount. Slow bearing rotation, however, give rise to bearing samples which differ little from the reference sample. Consequently, the bearing display is unblanked for slow angular rates of change. This sample and comparison technique is feasible only if the bearing samples are obtained at a uniform rate which is also much faster than the polarization rotation rate, and if the number of bearings compared with the reference bearing is small in relation to the total number of bearings per rotation period. Since the experimental DF system, developed during this study, provides bearing indications at a uniform rate of approximately three per second, and since polarization rotation periods are typically about thirty seconds, the sampling and comparison technique for swing rate discrimination was used in the SRD. The selection of the optimum number of sample bearings to be compared to the reference bearing is not straight-forward. If too many samples are selected for comparison, a large difference will always be generated and no bearing indications will be displayed. If too few samples are selected, the difference is always small and little swing rate discrimination is provided. Based on field observations of typical polarization rotation rates, and for reasons of circuit simplicity, the SRD was designed to compare eight bearings in succession. The SRD was designed for adjustable swing rate discrimination to allow for varying polarization rotation rates.

Since bearing position information was available in the form of pulses from other circuits of the experimental DF system (see figure 8),

the SRD was designed to accept these pulses as input bearing information. A fixed azimuth pulse from a magnetic pickup on the loop scan mechanism provided a convenient reference pulse for SRD operation. The time positions of the azimuth reference pulses, the loop null pattern, and the null detector pulses are shown in figure 31. The azimuth reference pulses occur at exactly the loop scan rate and two null pulses are produced for each loop scan (bearing and reciprocal). As explained earlier in this report, the null pulses are not produced during fade nulls; however, the null pulses rarely disappear during consistent polarization rotation. Note from figure 31 that the time position of the first null pulse relative to the azimuth pulse is directly related to the bearing position in degrees. This relationship is a consequence of rotating the loop antenna at a fixed rate. It should be emphasized that the reference azimuth pulse can be generated at any convenient azimuth position. Since swing rate information depends only on the relative time difference between the azimuth pulse and the first bearing null pulse, it is not necessary that the reference pulse occur at true noth. For similar reasons, it is also unnecessary that the leading edge of the bearing null pulse occur exactly at the loop null position. However, it may be observed from figure 31 that amplitude variations in the loop null pattern will cause the position of the leading edge of the bearing null pulse to vary. These variations produce an apparent swing insofar as the SRD is concerned and some amplitude discrimination is inherent in the SRD.

The bearing null pulses and the azimuth reference pulses of figure 31 were used to generate two analog voltages of bearing position. One of these voltages represented the instantaneous bearing position and could change from one loop scan to another. The other voltage represented the azimuth position of a single bearing pulse and was used as a reference sample bearing. To determine the swing rate, the analog voltage of instantaneous bearing position was compared to the analog reference sample voltage. If the absolute value of the difference between the two voltages was within tolerance for at least eight loop scans, the bearing display oscilloscope was unblanked for one loop scan. If the difference exceeded the tolerance before eight loop scans occurred, a new reference sample was obtained, but the display was not unblanked. (As shown in Appendix B, the tolerance is determined by the setting of the allowable swing control of the SRD.) Since polarization rotation periods and vertical angles of arrival are time variables, it was unnecessary to calibrate the allowable swing control precisely. This control was made continuously variable from approximately 0 to 20 degrees. Thus, the SRD will accept only those bearings whose rotation rates lie in the range 0 to 20 degrees per eight loop scans. Time-wise these rates lie in the range 0 to 7 degrees per second.

A complete description of the swing rate discriminator, along with a circuit schematic, is included in Appendix B of this report.

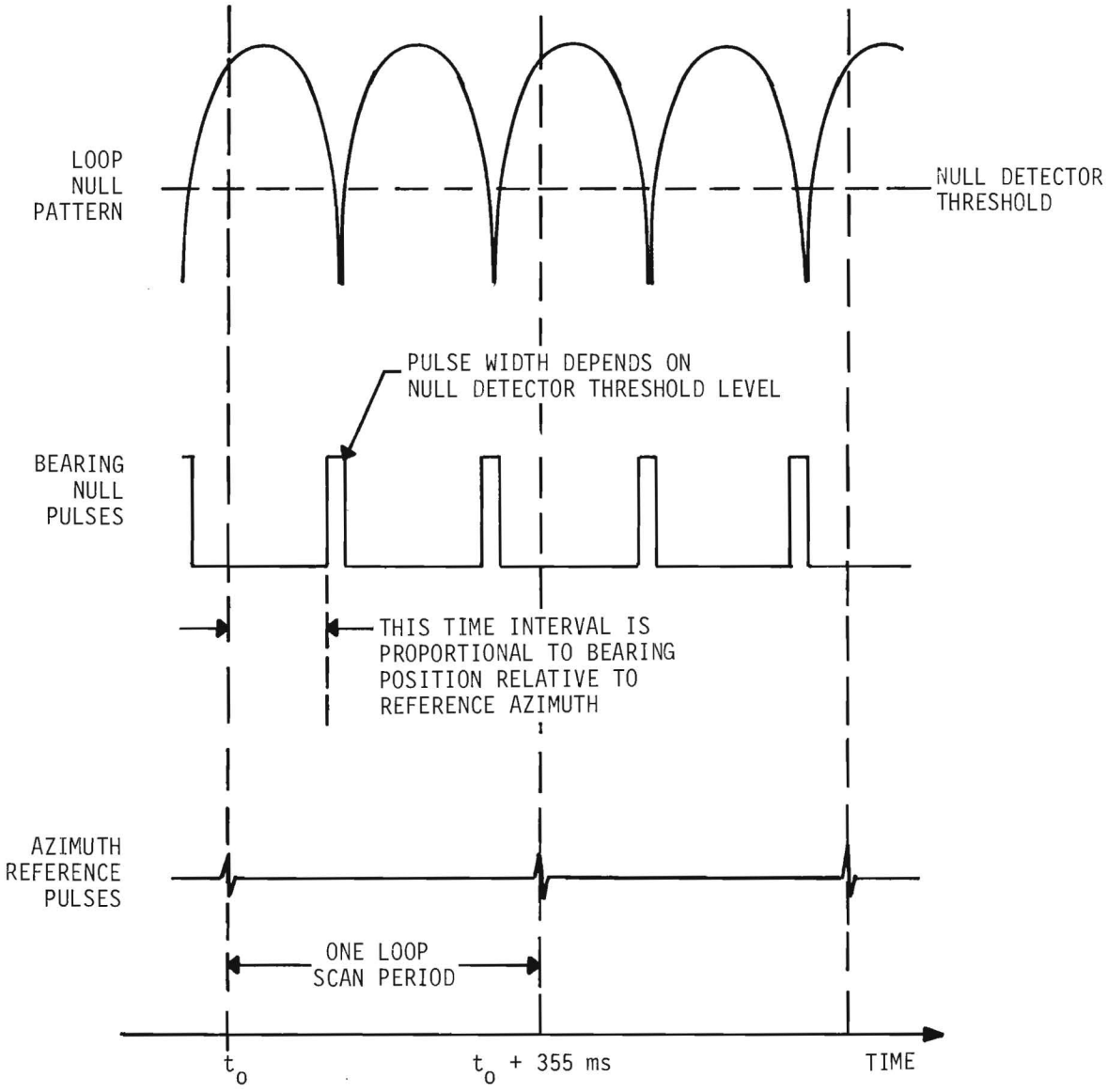

Figure 31. Time Relationship between Bearing Pulses and Azimuth Reference Pulses.

It should be emphasized that the SRD is a purely experimental device which was designed on the basis of preliminary field observations and from theoretical considerations. With the knowledge gained from the present SRD circuit, it might be possible to improve the overall technique of swing rate discrimination.

2.3.6.3 Effectiveness of Swing Rate Discriminator for Error Reduction

Introduction

To determine the effectiveness of the swing rate discriminator as an error reduction device, a large number of field tests were conducted. Most of the tests were conducted under worst case conditions, i.e., very little data was obtained for transmissions whose indicated bearing was essentially steady for long periods of time. Although some data were collected under a variety of conditions such as multi-path fading, most of the data were collected under the conditions of bearing swing due to polarization rotation. Since the SRD was intended primarily as an error reducing device for time-varying polarization errors, the evaluation of the SRD was based on its performance under these conditions. In some tests, the SRD was used in conjunction with other operating modes of the experimental DF system. The various other operating modes have been discussed in quarterly reports 5 and 6 and are summarized in section 2.3.3. of this report. In the following discussion, SRD operation is conveniently referred to as an additional mode of operation.

For comparison purposes, some tests were conducted using two complete DF systems. For these tests, data were obtained simultaneously from the experimental DF system using SRD mode (occasionally in conjunction with other modes) and the AN/PRD-5.

With few exceptions all data were obtained on A0 or A3 modulated signals of known location. Most of these signals were high frequency (HF) broadcast transmissions whose origination points ranged from approximately 600 kilometers to 9,000 kilometers from the receiving site location. Tests were conducted during daytime and nighttime hours, although worst case conditions for polarization rotation occurred typically during local sunrise and local sunset.

Before presenting the results of the aforementioned tests, some comments are in order concerning methods of collecting and interpreting bearing data under the conditions of polarization rotation. It is clear from figure 2 that a rotating polarization vector will give rise to a rotating bearing indication on a continuous display type DF system such as the PRD-5. Under conditions such as these, if a bearing measure is obtained at all, it is usually obtained in either one of two ways. First, a "snap" bearing, i.e., a single bearing that is obtained at an arbitrary time, may be taken. Since the "snap" bearing

is taken without regard to the position of the polarization tilt angle, the curves of figure 2 show that the bearing error could be as much as ± 90 degrees. (Throughout the present discussion, it is assumed that sense information is available). A second method for obtaining a bearing indication is to average a number of selected bearings. The bearing error for such an averaging technique depends to a large extent on the observer's interpretation of the quality and number of bearings to be included in the average. Typically the bearing errors for an averaging process are smaller than "snap" bearing errors. It will be shown later in this report than an average bearing obtained under the conditions of polarization rotation can be accurate provided that certain conditions are met.

Since the SRD mode of operation does not provide a continuous display, neither of the above two methods for obtaining a bearing are directly applicable. A "snap" bearing may be obtained using the SRD; however, it should be noted that since the SRD allows the bearing display to be presented only at low angular rates of change, the bearing error, in general, should not be as great as ± 90 degrees. An average bearing is readily obtained from SRD mode of operation. In this case the bearing measure would be the average value of a number of bearings obtained at low swing rates.

Since bearing data may be obtained in a variety of ways, the question naturally arises as to which method provides the most meaningful data for evaluating the SRD. From the discussion above, it is apparent that comparisons on the basis of "snap" bearings would indicate that the SRD could never produce errors greater than those produced on a continuous display. It is also apparent that comparisons of averaged bearings may be subjective in character unless precautions are taken to assure that the sample bearings are objectively obtained. In order to properly evaluate the error reduction characteristics of the SRD, the test procedure for collecting data consisted of recording bearings over a relatively long time interval. In the SRD mode of operation, the indicated bearings were recorded whenever the display oscilloscope was unblanked. Whenever data was collected for the PRD-5, a bearing identification was recorded approximately every 15 seconds. Well-defined bearings were accepted regardless of their proximity to the geometric true bearing. Most tests were approximately 5 minutes in duration. With the recorded data from each test, several comparisons could be made. The spread, distribution and average value of a series of bearings could be compared to the true bearing and, when simultaneous data were available, these quantities could be used to compare the two DF systems.

Test Results

Figure 32 and figure 33 show typical data that were collected when polarization rotation was occurring. Figure 32(a) and figure 33(a) show bearing indications that were obtained using

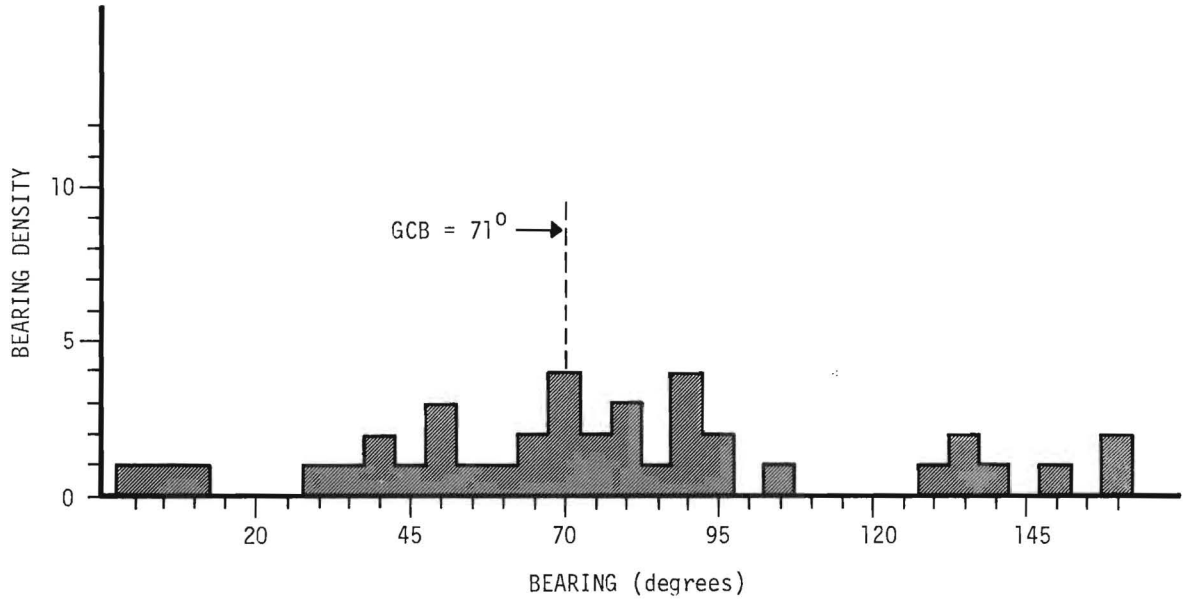

(a) SRD Mode with Allowable Swing Approximately 20°.

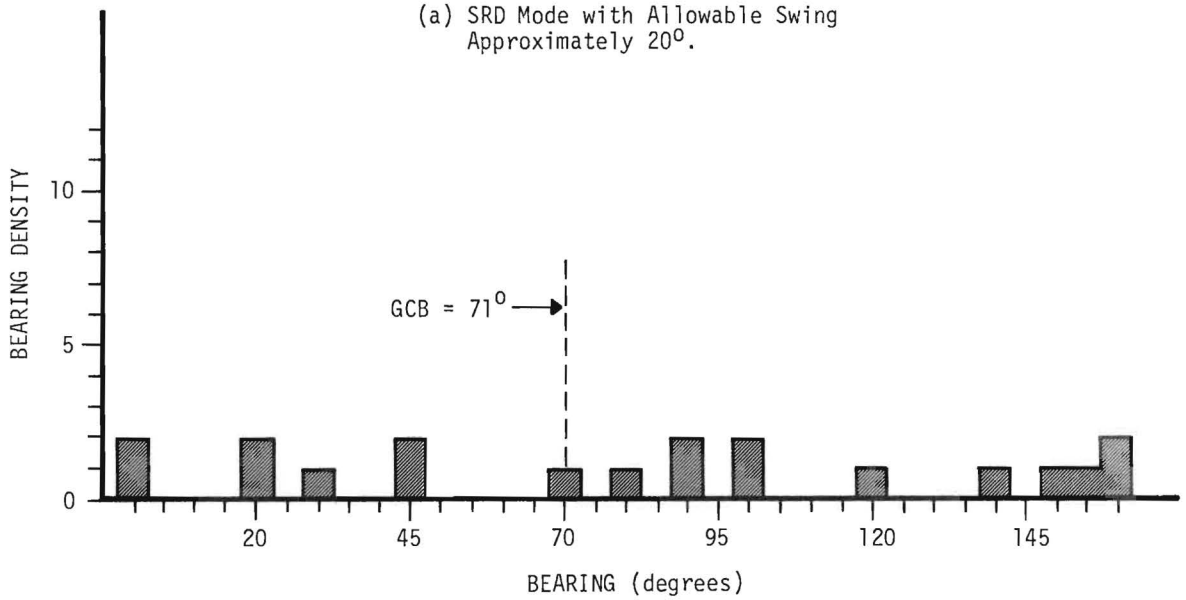

(b) PRD-5 Data Obtained Simultaneously with the Data of (a).

Figure 32. Comparison of SRD with PRD-5 with Allowable Swing Setting Too Large.

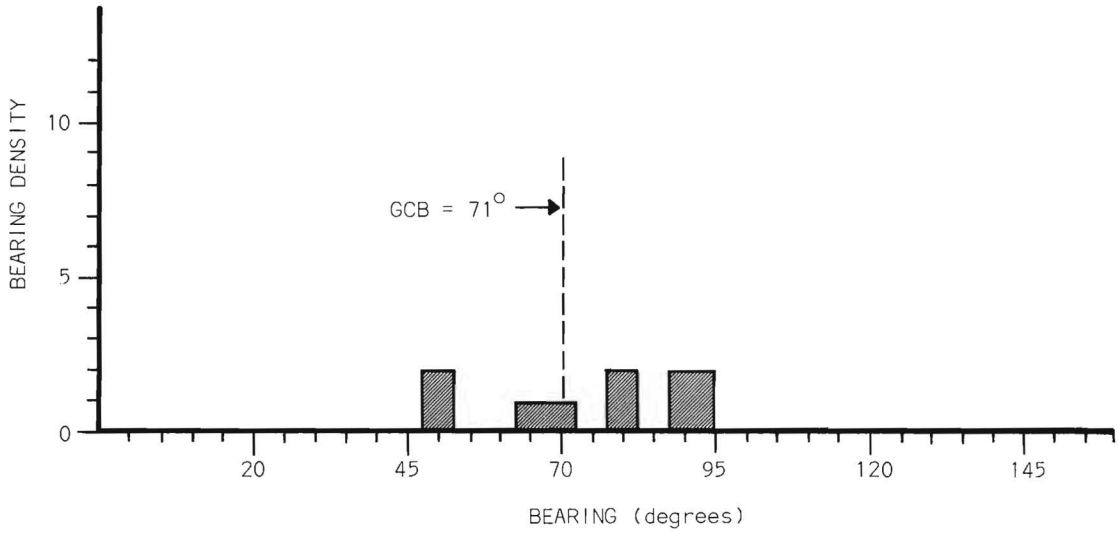

(a) SRD Mode with Allowable Swing Approximately 5°.

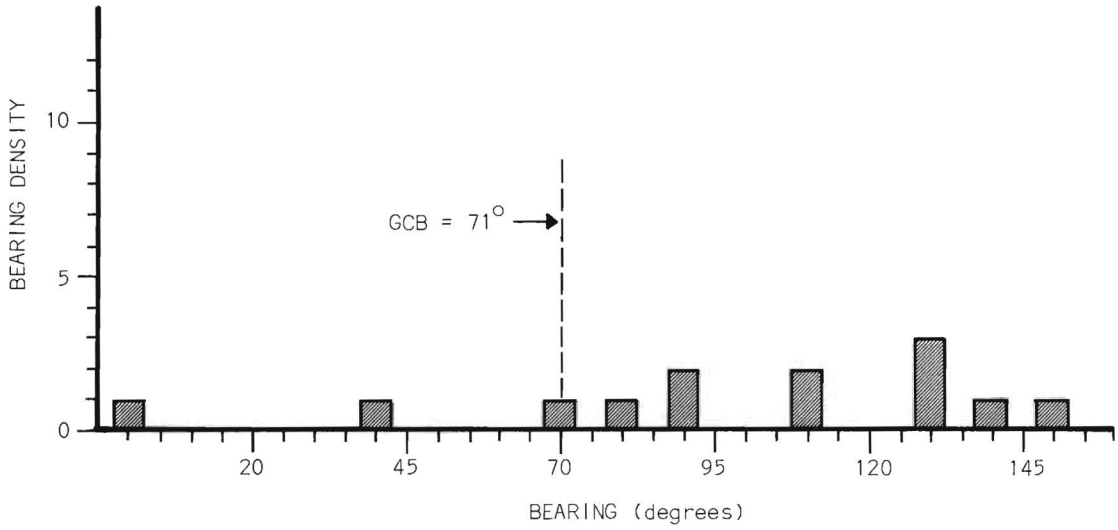

(b) PRD-5 Data Obtained Simultaneously with the Data of (a).

Figure 33. Comparison of SRD with PRD-5 with Allowable Swing Setting About Optimum.

SRD mode with allowable swing settings of 20 degrees and 5 degrees, respectively. Note that the magnitude of bearing errors is significantly smaller for the data of figure 33(a) than for the data of figure 32(a). These two histograms indicate that the SRD will provide a reduction of bearing errors if a sufficient amount of swing rate discrimination is provided. Observe that the spread of bearing indications is smallest for an allowable swing setting of 5 degrees. This result is not unexpected since a greater amount of swing rate discrimination is provided at lower allowable swing settings. The data of figure 32(a) indicate that bearing errors as large as ± 90 degrees can occur unless the SRD allowable swing setting is properly adjusted. It should be emphasized that the optimum allowable swing setting for a given condition depends on the elevation angle of arrival and the polarization rotation rate. Since these parameters are not usually known, the optimum allowable swing setting is established under field conditions by adjusting the amount of swing discrimination until the display oscilloscope is unblanked only for a small percentage of time. In general, the allowable swing setting should be large for rapid polarization rotation and should be small for slow rotation. Field observations have indicated that in most cases an intermediate allowable swing setting of approximately 10 degrees is close to the optimum value. It should be noted that some swing rate discrimination is provided by the SRD regardless of the allowable swing setting. For example, the data of figure 32(a) are grouped about the great circle bearing even though the allowable swing setting was too large. Figure 33(a) shows bearing data that were obtained with the SRD when the allowable swing setting was about optimum for the test conditions. If a smaller allowable swing setting had been used, few if any bearings would have been obtained.

Figure 32(b) and figure 33(b) show data that were obtained on the PRD-5 DF system simultaneously with the data of figure 32(a) and figure 33(a), respectively. Note that in both curves of PRD-5 data, the bearing indications are almost randomly distributed about the GCB. Again, this result is not unexpected, since figure 2 indicates that an instantaneous bearing obtained without consideration of the polarization tilt angle will produce an error with no particular relationship to the GCB. The PRD-5 data of figures 32(b) and 33(b) are typical of data obtained on a conventional simple loop antenna DF system under the conditions of polarization rotation. It should be noted that the bearing errors for the PRD-5 system are confined to approximately ± 90 degrees. This result is a consequence of the observer's ability to determine the approximate 180 degree sector which contained the GCB as a midpoint. This determination was based on observation of the visually displayed null pattern when the sense feature of the PRD-5 was being utilized. In general, errors in excess of ± 90 degrees may be experienced with the PRD-5.

The data of figure 33 provide a preliminary indication of the error reduction capability of the SRD. The SRD errors are limited to

about ± 25 degrees while PRD-5 errors may be as great as ± 90 degrees. Since the experimental DF system did not provide sense determination, all bearings obtained using SRD mode are subject to an ambiguity of 180 degrees. This ambiguity is, of course, based on the assumption that the transmission site is unknown. Since the location of all signals were known for the data obtained during this study, no ambiguity is present insofar as the test data are concerned.

Typical bearing data obtained under the conditions of multi-path fading are shown in figure 34. Note that the use of the SRD for conditions such as these does not provide a significant amount of error reduction. The magnitudes of bearing errors are approximately equal for both the experimental system using SRD mode and the PRD-5 DF system. As indicated earlier in this report, the SRD was not expected to reduce errors under the conditions of multi-path signals. The data of figure 34 show primarily that the SRD mode of operation does not increase bearing errors relative to the bearing errors produced by a conventional simple loop antenna DF system. It should be noted, however, that the SRD is useful for detecting such conditions as directive moding. This source of DF error was discussed earlier in this report and has been observed by other investigators[2]. If a particular directive mode is stable for several seconds, the SRD will unblank the display oscilloscope and allow the bearing to be presented.

As indicated above, some data were collected for the experimental DF system when the SRD mode was used in conjunction with other operating modes. A series of field tests were conducted in which the SRD mode was used along with each of the other operating modes. These tests indicated that a significant error reduction was realized when the SRD was operated in conjunction with mode 2. Modes 3 and 4 did not significantly enhance the error reducing capability of the SRD. Figure 35 illustrates the combined effectiveness of the SRD mode along with mode 2. Observe that the main advantage of mode 2 is that it reduces the number of bearings that deviate widely from the GCB. Since mode 2 blanks the display oscilloscope whenever the vertical signal level is below a weighted average of the vertical signal level, and since the vertical signal level is below the average for large polarization tilt angles, mode 2 provides some additional discrimination against polarization errors. Thus, mode 2 and SRD mode together place two restraints on the bearing display. The display is unblanked only if the swing rate is low and the vertical signal level is above a weighted average signal level.

The typical test data of figure 32 through 35 have been used to illustrate various operating characteristics of the SRD. The performance of the SRD as an error reduction device is more easily established by inspection of the cumulative test data of figures 36, 37, and 38. These data represent the results of several tests on a single transmitting station. The data were obtained on different frequencies and

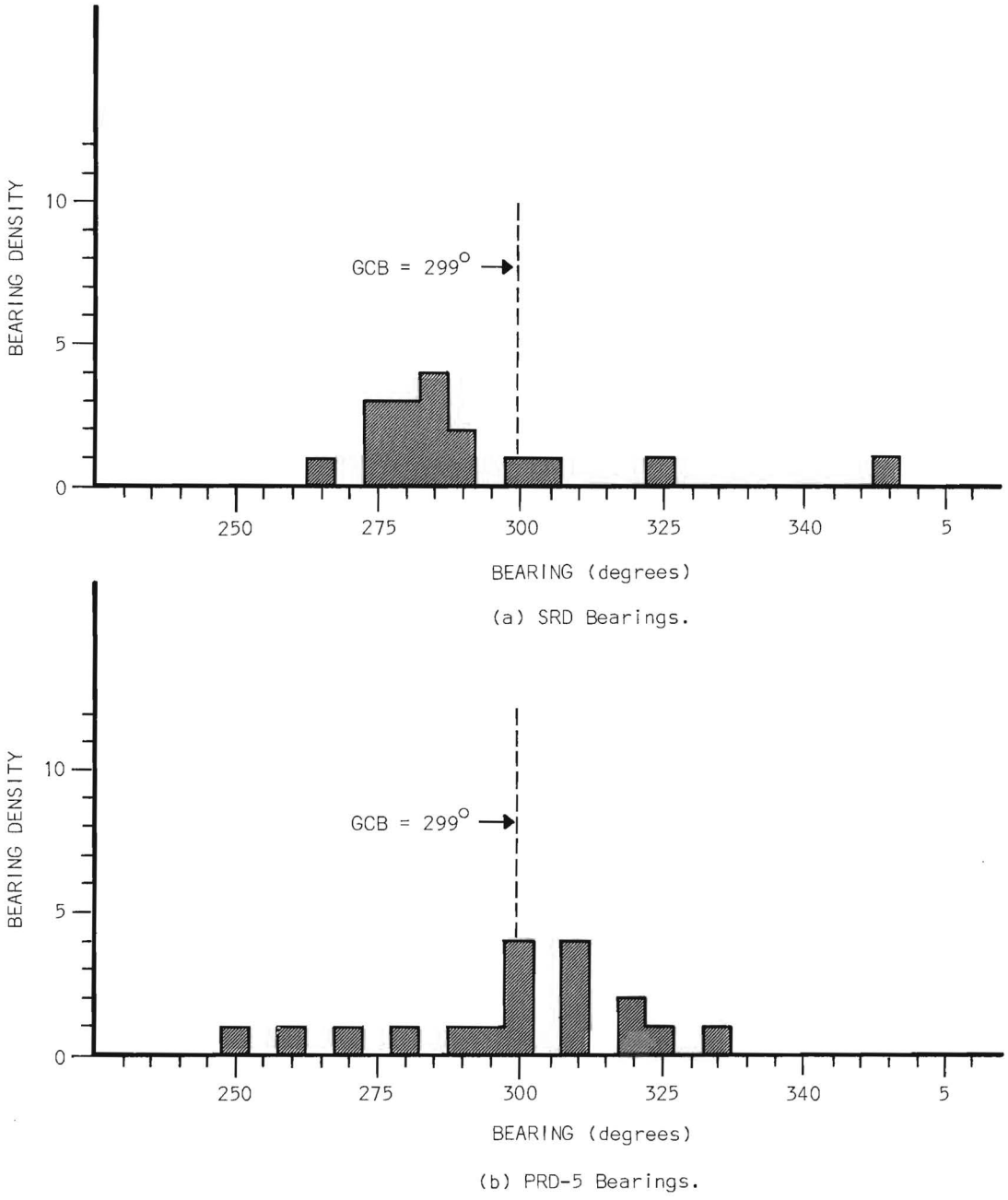

Figure 34. Comparison of SRD with PRD-5 Under the Conditions of Multipath Fading.

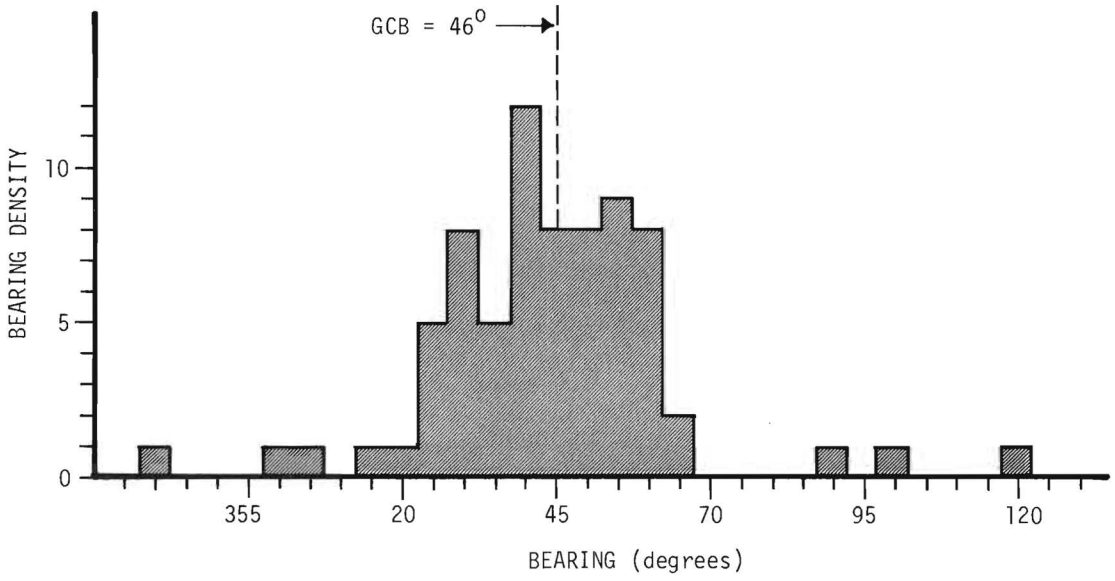

(a) SRD Mode

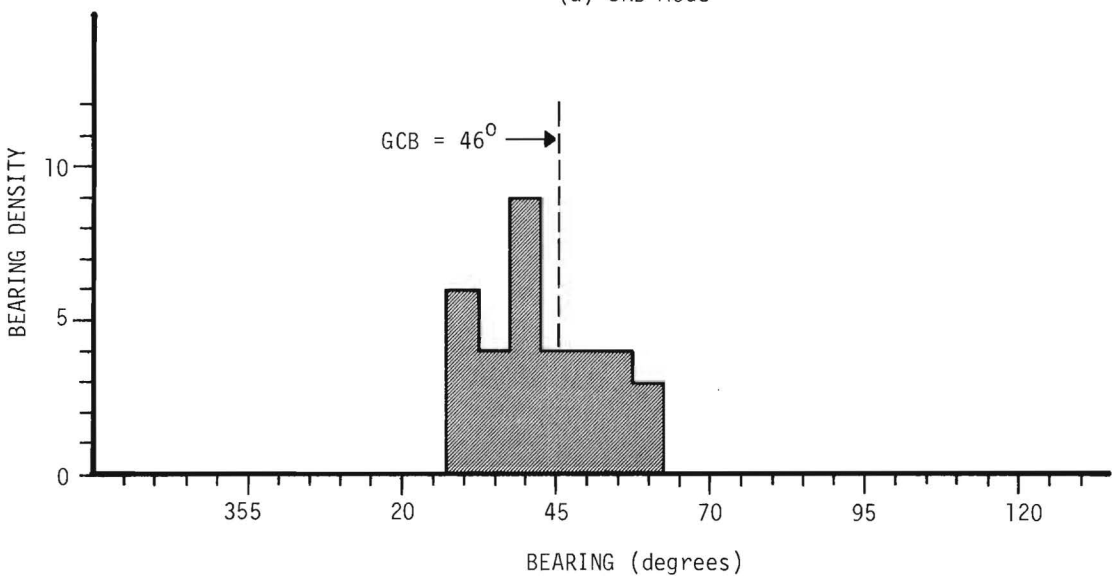

(b) SRD in Conjunction with Mode 2, 0 dB Fade Margin

Figure 35. Comparison of SRD Mode and SRD Mode with Mode 2.

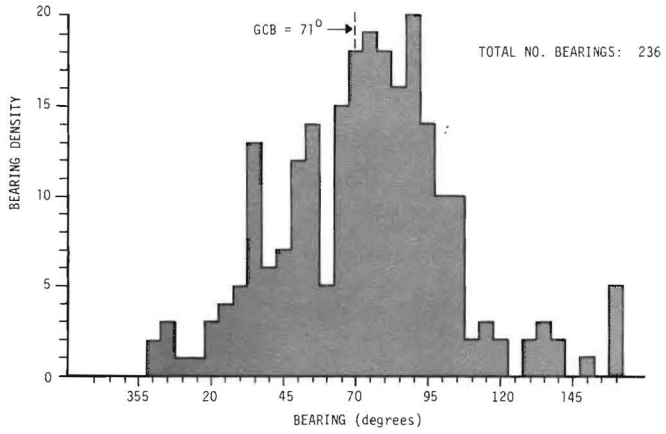

Figure 36. Bearing Density Versus Bearing Indication for SRD Mode - Cumulative Data.

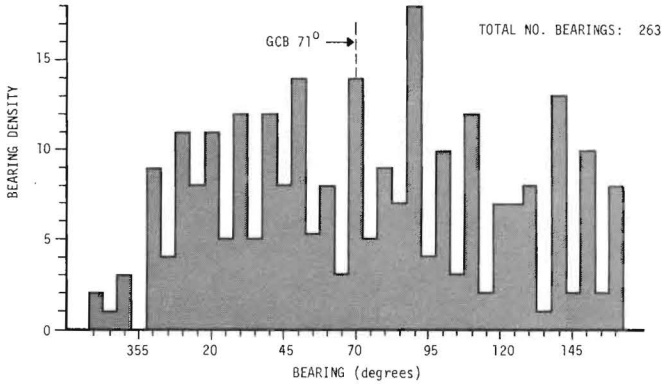

Figure 37. Bearing Density Versus Bearing Indication for PRD-5 - Cumulative Data.

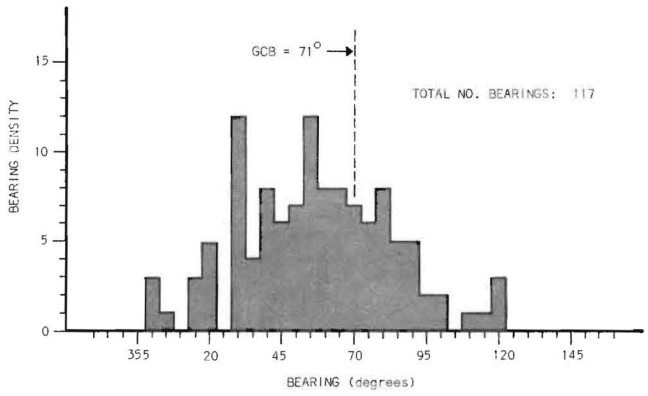

Figure 38. Bearing Density Versus Bearing Indication for SRD Mode and Mode 2 - Cumulative Data.

at different times; however, polarization rotation was the predominant cause of bearing errors for all of the test data. During some tests, polarization rotation ceased, but data were collected until termination of the test. It may be observed from figure 36 and figure 37 that the SRD reduces the number of bearings which differ appreciably from the GCB. Note that the SRD data of figure 36 are not as widely dispersed as the PRD-5 data of figure 37. Although appreciable errors are apparent in the SRD data, it is felt that most of these errors were produced when the allowable swing setting was too large and/or the polarization rotation period changed. The majority of the SRD bearing indications are grouped about the GCB. While there is some inclination for the PRD-5 data of figure 37 to be grouped about the GCB, most of the data are distributed approximately uniformly over the range ± 90 degrees of the GCB. Figure 38 illustrates the combined action of the SRD mode and mode 2. Note that the data of figure 38 show fewer extreme errors than the data of figure 36.

Test results from sixty-five separate tests, with approximately five minutes of observation time for each test, are tabulated in Table VIII. These results which were obtained from tests conducted at different times, on several different frequencies, and on several different transmitting stations, represent typical results which might be encountered during field operation. As before, the underlying data were collected when polarization rotation was the predominant cause of bearing errors. As shown in Table VIII, the statistical parameters are based on bearing indications that were obtained with the PRD-5 system and the exploratory system.

Several significant trends are apparent from the data of Table VIII. It is evident from the parameters $\overline{\Delta\theta}$ and $|\overline{\Delta\theta}|$ that the average bearing for any one of the three modes of operation differs little from the great circle bearing. Note that the value of $|\overline{\Delta\theta}|$ is approximately the same for all three test setups. Since $|\overline{\Delta\theta}|$ is a measure of the deviation of the average bearing from the GCB, the PRD-5 and the ES give approximately the same results with respect to average bearings. This equivalance of performance for average bearings is also apparent in the data of figure 33. Note, however, that the two systems do not give equivalent performance with respect to the average standard deviation. The PRD-5 produced an $\overline{SD}$ of 43° while the ES produced values of $\overline{25}^{\circ}$ and 13° for, respectively, SRD mode and SRD mode with mode 2. Since $\overline{SD}$ in an indication of the dispersiveness, or variability, of the bearing errors, it is clear that the ES produced errors of smaller magnitude than those produced by the PRD-5. Moreover, of the three test configurations, SRD mode with mode 2 produced the minimum average standard deviation. It is also apparent from Table VIII that the average RMS error was smaller for the ES than for the PRD-5. Note that there was approximately a three-to-one reduction of the average RMS error when the ES was operated with SRD mode plus mode 2.

TABLE VIII

TEST RESULTS OBTAINED UNDER
CONDITIONS OF POLARIZATION ROTATION

	PRD-5**	Exploratory System** SRD Mode	Exploratory System** SRD Mode with Mode 2
$\overline{\Delta\theta}$	- 7°	0°	- 3°
$\lvert\overline{\Delta\theta}\rvert$	11°	9°	9°
$\overline{SD}$	43°	25°	13°
RMS Error	44°	25°	13°
No. of Bearings	857	365	653
Test Group*	23	24	25

* See Appendix for tabulation of test transmissions.
** All values rounded to nearest whole degree.

It should be clearly emphasized that the data of Table VIII is based on average values obtained from a relatively small number of samples. A single bearing or even a single test might not yield results indicative of those in Table VIII. It is felt, however, that the data of Table VIII provide a realistic basis for evaluating the technique of swing rate discrimination.

Conclusions

On the basis of the data presented in figures 32 through 38 and in Table VIII, several significant conclusions can be drawn, as follows. (1) The ES with SRD mode and the PRD-5 gave approximately equivalent results with respect to average bearings. It is important to recognize that this conclusion is valid only if two important conditions are met. First, the sense determination feature of the PRD-5 must be properly utilized to establish the approximate 180° sector which contains the GCB. If this condition is not met, PRD-5 errors may be expected to be even more widely dispersed. Note that this restriction does not apply to the SRD mode. Second, PRD-5 bearings must be collected over at least one complete polarization rotation period. Realistically, PRD-5 bearings must be observed over several rotation periods before the average bearing becomes meaningful. Again,

this restriction does not apply to the SRD mode. (2) The average RMS bearing error for the ES is significantly smaller than the average RMS bearing error for the PRD-5. Moreoever, the average RMS error for the SRD mode in conjunction with mode 2 is smaller than the average RMS error for the SRD alone. This conclusion is particularly significant when a degree of confidence must be attached to a single bearing or a small number of bearings. For example, a "snap" bearing obtained using SRD mode (or SRD mode with mode 2) can be given a much higher degree of confidence than a "snap" bearing obtained with a conventional simple loop antenna DF system. (3) Swing rate discriminator appears to be a valid technique for reducing bearing errors caused by polarization rotation.

There are several possibilities for improving the overall technique of swing rate discrimination. Field observations of the SRD performance indicated that the analog voltage of bearing position was not completely independent of such factors as signal modulation and net signal strength. Since these factors are not generally related to bearing position, their net effect was to degrade the performance of the SRD circuit. Ideally, swing rate information should be developed independently of all other parameters. If a satisfactory method of obtaining an exact analog bearing position could be developed, even greater error reduction might be realized. Another possibility for improving the swing rate discrimination technique would be to unblank the bearing display at the point of maximum swing rate. It is clear from figure 30 that the region of maximum swing is narrower and more pronounced than the region of minimum swing. Hence, maximum swing rates would be more easily detected than minimum swing rates. Since the maximum swing rate occurs 90° away from the GCB, a correction factor would have to be applied to the unblanked bearing.

2.3.7 Additional Parameters Related to Polarization Bearing Errors

2.3.7.1 Introduction

It has already been indicated by equation (1) of section 2.3.6.1 that the time variation of bearing errors produced by polarization rotation are a function of elevation angle of arrival and the polarization rotation rate. With the tilt angle replaced by a linear time variation, equation (2) becomes

$$\theta(t) = \tan^{-1}(\cos \Phi \tan Kt) \qquad (4)$$

where t is time in seconds, K is the time rate of change of tilt angle, and the other parameters are as defined in figure 1. Since equation (4) and its related parameters form a basis for investigating bearing errors caused by polarization rotation, an attempt was made to verify the applicability of this equation to polarization bearing errors. It may be noted from figure B2 of Appendix B that the SRD circuit provided a continuous voltage analog of bearing position versus time. This capability of the SRD was used to collect substantial amounts of analog data related to bearing errors caused by polarization rotation. Bearing null position as a function of time was obtained by recording the bearing sampler output on a dual-channel chart recorder. For reasons which will become clear later, the second channel of the chart recorder was used to record the signal amplitude of an auxiliary receiver with a vertical antenna. The purpose of this section of this report is to relate the empirical data obtained to the data which might be expected on the basis of equation (4). The probable causes for some of the extreme errors that were evident in the SRD mode of operation will be discussed, and some interesting uses of the SRD analog data will be presented.

Figure 39 shows a typical section of a chart recording of bearing indication versus time which was recorded under the conditions of polarization rotation. This figure is shown primarily to illustrate the type of data that could be recorded and should be considered as typical of the data that is discussed subsequently in this report. Several salient features are immediately apparent in the record of figure 39. First, it should be noted that due to the operational characteristics of the SRD circuit, the vertical indication covers a range of 180°. The minimum value of bearing indication occurs at the reference azimuth position and the maximum value occurs 180° away from the reference position. The reference azimuth was 133° with respect to north so that the recorded bearing indications lie in the range -47° to + 133°. Since the SRD circuit could not distinguish the actual null from the reciprocal null, the recorded data are continuous and represent bearing indications that might be obtained on a visual display with no sense provision. Second, since the bearing sampler circuit of the SRD acts as a sample and hold circuit for one loop scan period, the bearing data of figure 39 are in the form of discrete steps. It should be emphasized that the minor perturbations from step-to-step of the recorded data do not indicate corresponding bearing changes. These perturbations were produced by noise, signal modulation, and field strength changes (fading). This characteristic of the SRD circuit was explained in section 2.3.6.2 with reference to figure 31. The bearing position data is contained in the general trend, or the running average of neighboring steps, of the curves of figure 39. Third, the most pronounced feature of the data of figure 39 is its resemblance to a periodic waveform. Since uniform polarization rotation will cause the bearing error to be periodic, the curve of figure 39 is characteristic of bearing swings due to polarization rotation. For the particular

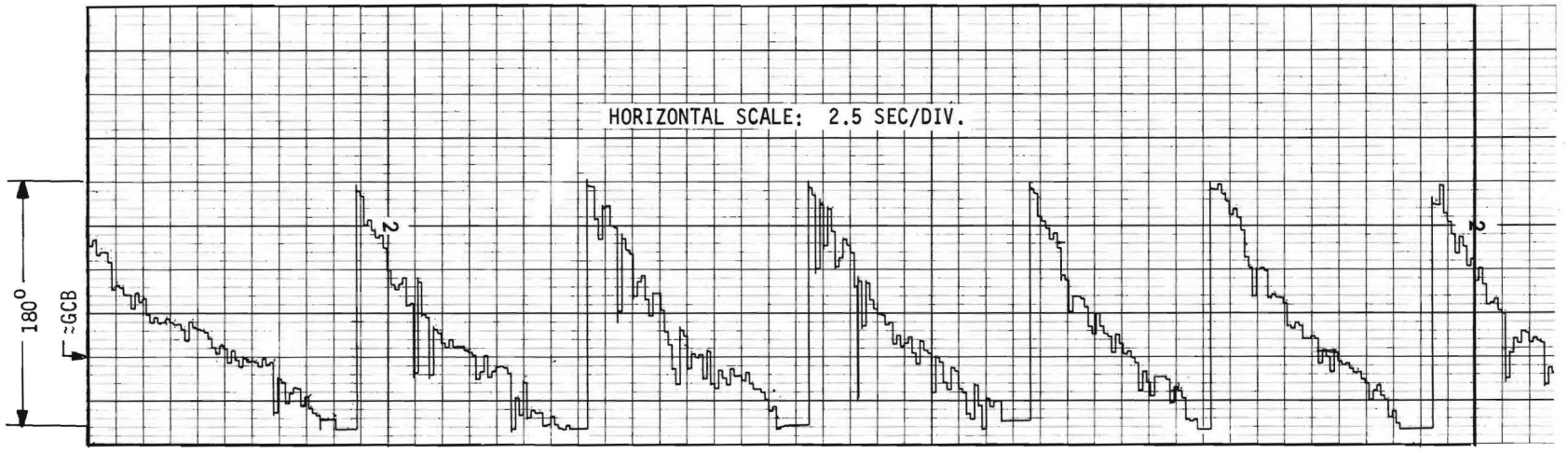

Figure 39. Typical Bearing Indications Versus Time Recorded from SRD Circuit.

sample record of figure 39, the instantaneous bearing display was rotating clockwise, and the period of rotation was approximtaely 45 seconds. Note that two cycles of the waveform correspond to a complete revolution of the polarization vector. Whereas a rotating bearing will produce data similar to that of figure 39, a steady bearing would appear as a straight line.

2.3.7.2 Bearing Distribution

With data such as that of figure 39, the number of bearings that fall in a particular azimuth sector can be determined for a number of complete polarization rotation periods and for azimuth intervals that cover the complete spread of bearing indications. With this procedure, a relative frequency histogram can be developed. Figure 40 shows a relative frequency histogram for bearings that were obtained on a particular signal under the conditions of polarization rotation. The horizontal scale of figure 40 has been normalized to a 0° - 180° range, and the azimuth intervals are 20° in width. Smaller azimuth intervals were not used since the recorded bearing data were not of sufficient resolution. The relative frequency histogram of figure 40 shows a distinct maxima occurs in the interval containing the GCB. Note also that a distinct minima occurs in the interval which differs from the GCB by 90°. Since the largest number of bearings occurred in the interval containing the GCB, the data of figure 40 show that the angular rate of bearing swing is lowest near the GCB. The data of figure 40 substantiate the error reducing capability of the SRD.

If uniform polarization rotation is assumed ($\psi = Kt$) and the elevation angle of arrival is known, equation (4) may be used to determine an ideal relative frequency histogram for bearing observations. Such a histogram is shown in figure 41 where an elevation angle of 57° has been assumed. (The choice of an elevation angle of 57° was not arbitrary. It will be shown later in this report that the elevation angle can be estimated from recorded data). The horizontal scale of figure 41 has been normalized to a 0° - 180° range and the azimuth intervals are 20° in width. Moreover, the histogram of figure 41 was determined on the basis of a GCB corresponding to the approximate GCB of figure 40. Note that the histogram of figure 41 shows a maximum in the interval which contains the GCB and shows a minimum in the interval which differs from the GCB by 90°. These characteristics of figure 41 agree with the characteristics of figure 40. Note also from these two figures that the measured relative frequency for a given azimuth interval correlates closely with the expected relative frequency for the same azimuth interval. The greatest difference between the two histograms occurs near the end intervals. It is felt that these differences were the result of inadequate bearing resolution near the end points of the recorded data. The close similarities between the two histograms of figure 40

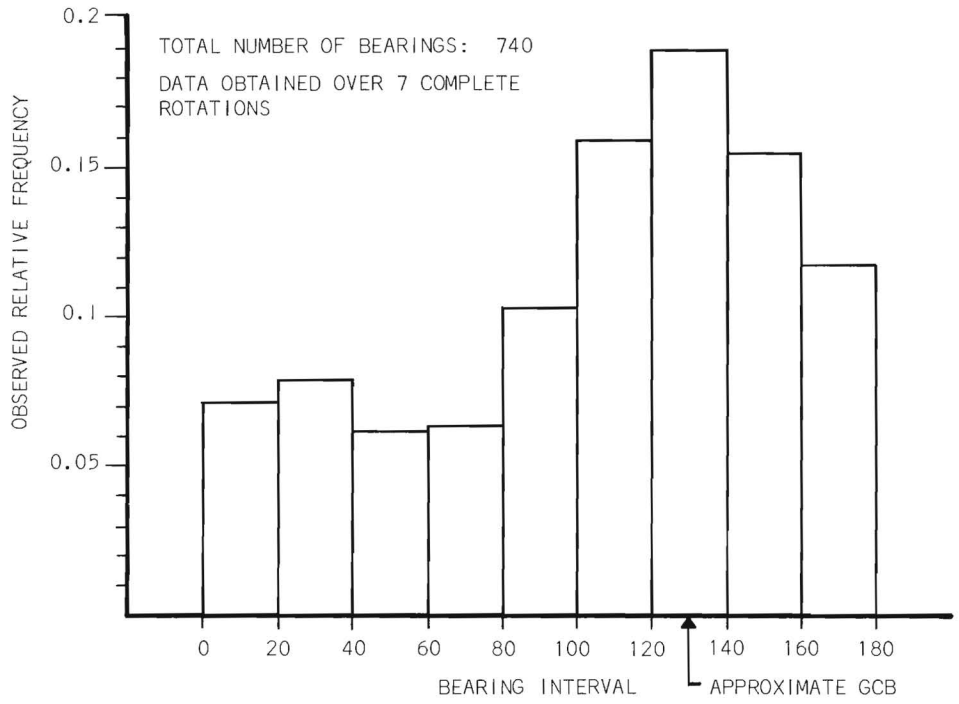

Figure 40. Observed Relative Frequency of Occurrence of Bearings.

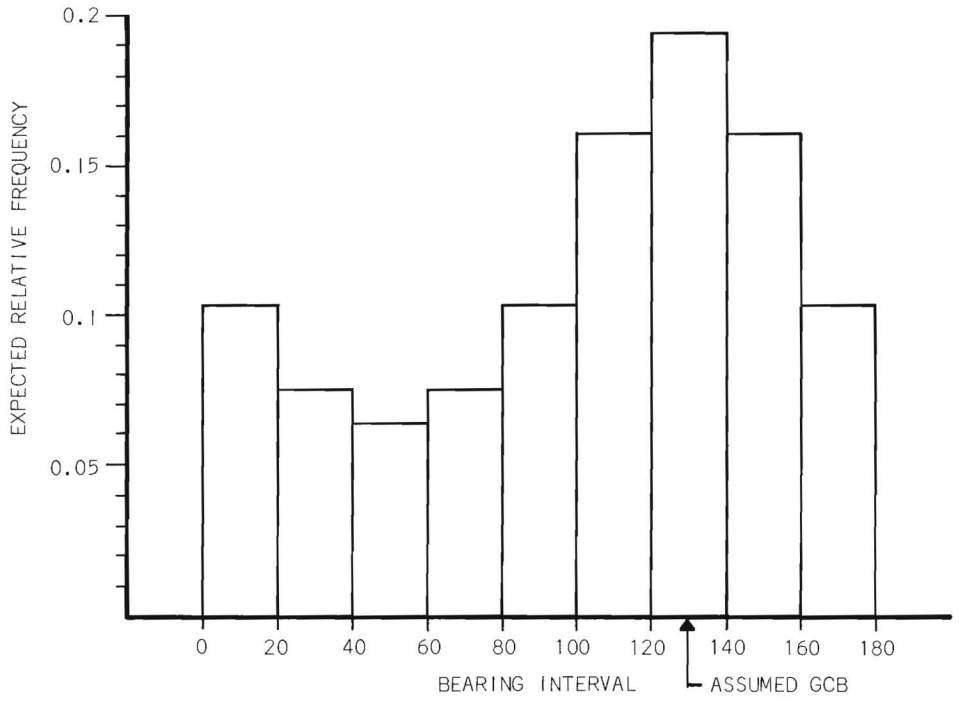

Figure 41. Theoretical Relative Frequency of Occurrence of Bearings.

and figure 41 substantiate the validity of equation (4) as a model for describing bearing errors caused by polarization rotation. It should be emphasized that the data of figure 40 are based entirely on recorded bearing indications, while the data of figure 41 are based entirely on theoretical calculations.

The fact that equation (4) appears to be valid for describing polarization bearing errors suggests the interesting possibility of a probability approach to polarization errors. If the elevation angle of arrival is known or can be estimated and the time of bearing observation is treated as a random variable, a probability density function can be calculated. From the density function so obtained, a probability measure or confidence level may be attached to a single bearing or to a number of bearings. This technique is, of course, valid only if polarization rotation is the cause of bearing error. As an example, it may be deduced from figure 41 that a single random bearing will lie within ± 30° of the GCB with a probability of approximately 0.5. This value applies only if the elevation angle is 57°. The probability for the same range would be higher if the elevation angle (measured with respect to the vertical) were larger.

2.3.7.3 Elevation Angle

It has been shown above that equation (4) describes the variation of polarization bearing errors. Since the elevation angle of arrival is a parameter in equation (4), it should be possible to estimate the elevation angle from recorded data of bearing position as a function of time. The time derivative of equation (4) reduces to

$$\frac{d\theta}{d\tau} = K\left[\frac{\cos\Phi}{\cos^2 K\tau + \cos^2\Phi \sin^2 K\tau}\right] \quad , \tag{5}$$

where the function in brackets with $K\tau = \psi$ has been plotted in figure 30. At the maximum rate of bearing swing, $K\tau$ is some odd multiple of 90° and equation (5) becomes

$$\left(\frac{d\theta}{d\tau}\right)_{max} = \frac{K}{\cos\Phi} \quad , \tag{6}$$

where the subscript indicates that the derivative is evaluated at the maximum angular rate of bearing swing. At the minimum rate of bearing swing, $K\tau = 0°$ or an even multiple of 90° and equation (5) becomes

$$\left(\frac{d\theta}{d\tau}\right)_{min} = K \cos \Phi \quad , \tag{7}$$

where the subscript indicates that the derivative is evaluated at the minimum rate of bearing swing. Thus, the elevation angle may be determined from either of the two expressions,

$$\Phi = \cos^{-1}\left[\frac{K}{\left(\frac{d\theta}{d\tau}\right)_{max}}\right] \quad , \tag{8}$$

or

$$\Phi = \cos^{-1}\left[\frac{\left(\frac{d\theta}{d\tau}\right)_{min}}{K}\right] \quad . \tag{9}$$

Since $\frac{d\theta}{d\tau}$ and K may be graphically determined from chart recordings provided by the SRD circuit, the elevation angle of arrival may be estimated. It should be noted that the minimum value of the time derivative occurs when the bearing error is zero and the maximum value occurs when the bearing error is 90°.

Figure 42 shows a section of chart recording where superimposed lines have been drawn to emphasize the three distinct slopes. The data of figure 42 are a portion of the data that were used to determine the histogram of figure 40. Note that each half revolution of the polarization vector provides two measures of the elevation angle. For the particular example shown in figure 42, the average elevation angle computed from equations (8) and (9) was 57°. Although the accuracy of this value could not be verified without the benefit of extensive ionospheric data, it is felt that the computed value did not deviate greatly from the true elevation angle. The agreement between the empirical histogram of figure 40 and the calculated histogram of figure 41 indicates that the calculated value was essentially correct.

The technique for estimating elevation angle described above and illustrated in figure 42 provides the possibility of ray-tracing on unknown signals. Note that all of the data required to estimate the elevation angle is obtained from a DF system with a simple loop antenna. It should be emphasized that the technique is useable only if the signal is observed at the time polarization rotation is occurring. There is some indication that polarization rotation is more likely to occur for high angle signals. The limiting accuracy of a ray-tracing technique

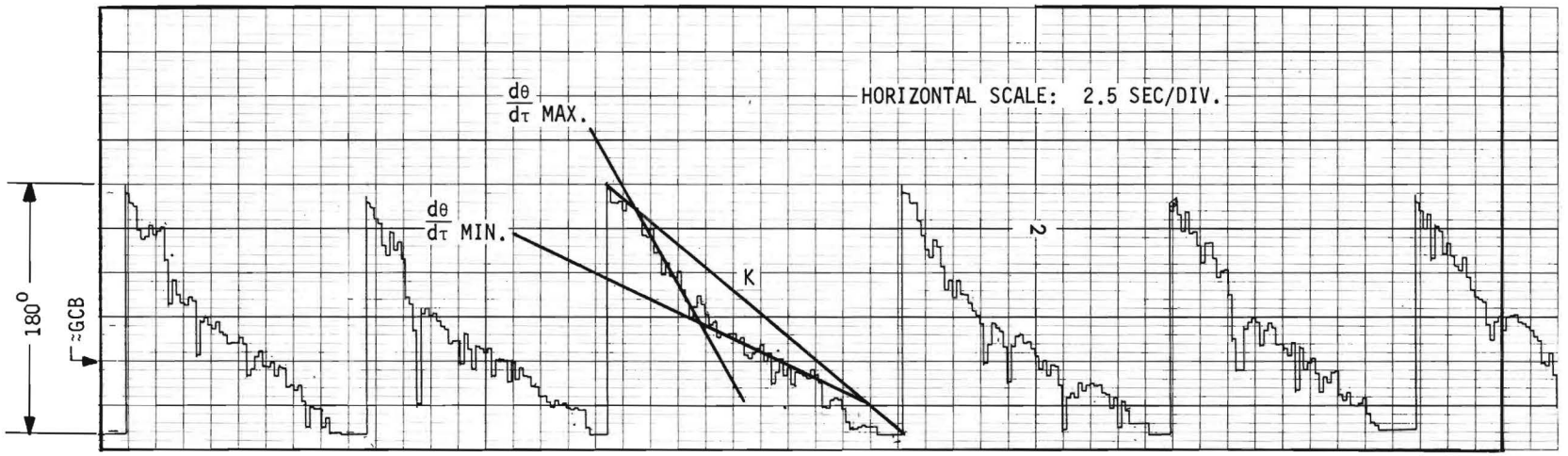

Figure 42. Estimating Elevation Angle from Bearing Versus Time Data.

would probably depend on the accuracy with which ionospheric conditions could be established rather than the accuracy of elevation angle.

2.3.7.4 Correlation Between Vertical Signal and Bearing Position

It is apparent from figure 1 that if the polarization tilt angle varies uniformly with time, the magnitude of the vertical component can be expressed as

$$E_V = |A \cos K\tau| \quad , \tag{10}$$

where A is the magnitude of the polarization vector and K expresses the linear time variation of the tilt angle. E_V is the ideal signal level that would be received on a vertical antenna if pure polarization rotation was occurring. Since both E_V and the time varying polarization error are related to the polarization tilt angle through equation (4), the time variation of these two quantities should be closely correlated. In order to determine the degree of correlation between the vertical signal level and the bearing position, these two quantities were plotted simultaneously on the dual-channel chart recorder. The vertical signal was obtained from the diode load voltage of an auxiliary receiver which was connected to a vertical whip antenna. In addition to correlation observations, the data obtained in this manner was useful for determining the consistency of polarization rotation and likely causes for some of the bearing errors that were evident in SRD mode of operation. Throughout previous discussions, the implication has been that the polarization vector rotates approximately uniformly in a given direction. From figure 39 it is obvious that this implication is correct for a time interval; however, it will be shown below that the polarization vector can change direction of rotation from one time interval to another.

Figure 43 shows a portion of a typical recording of bearing position and vertical signal amplitude as a function of time. Each division along the horizontal time axis corresponds to a time interval of 2.5 seconds. The small rapid variations in the upper trace of figure 43 were caused by signal modulation, while the slow variations represent the vertical signal strength. The upward trend of the bearing position data in the lower trace of figure 43 show that the instantaneous bearing display was rotating counter-clockwise. It is clear from figure 43 that the vertical signal amplitude and the

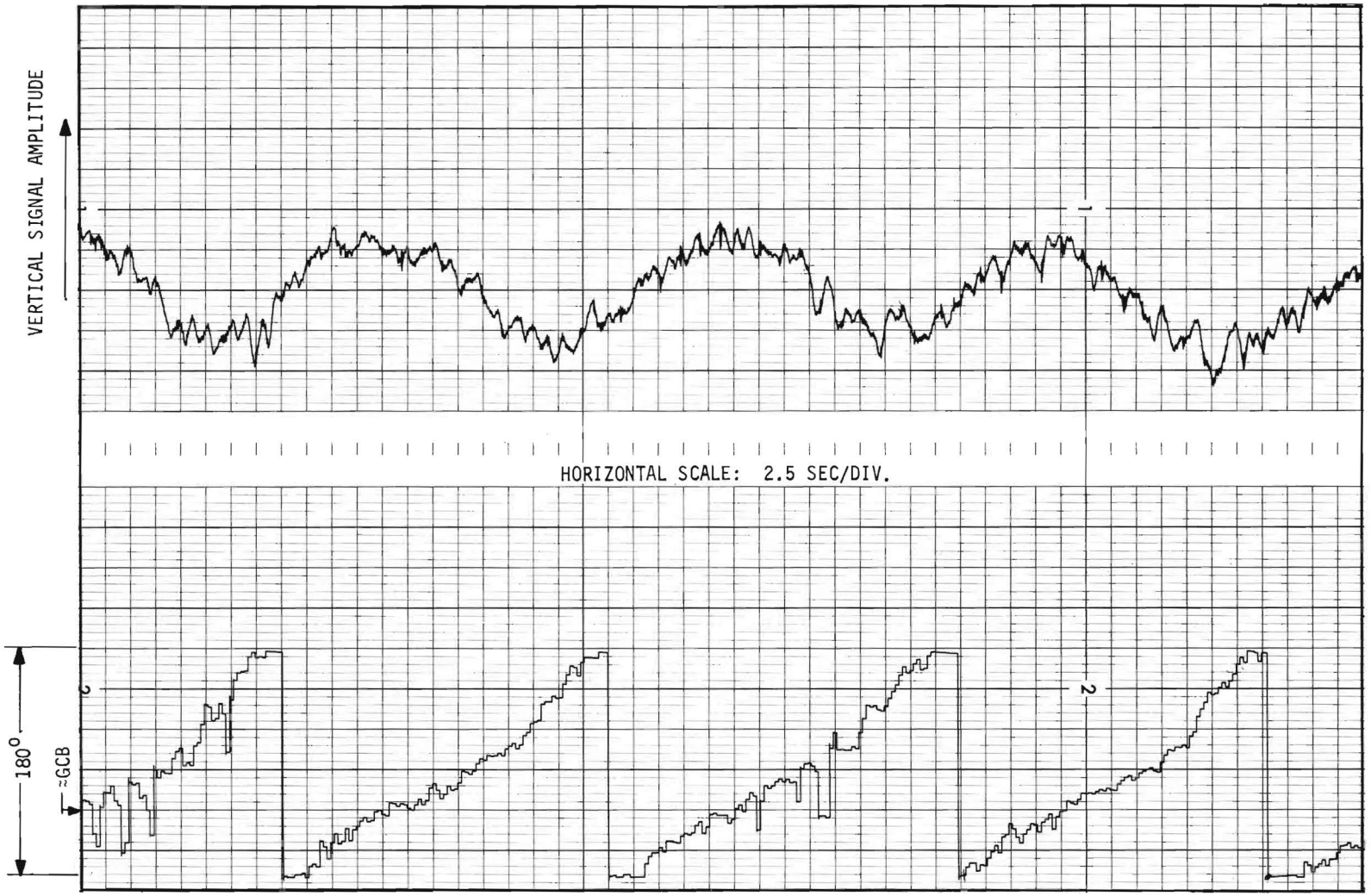

Figure 43. Correlation of Vertical Signal Level with Bearing Swing.

bearing position are closely correlated for polarization rotation. Note that the period of vertical signal variation corresponds almost exactly with the period of bearing rotation. This result is as anticipated since the time variation of the tilt angle controls both bearing position and vertical signal amplitude. The most significant feature of figure 43 is the correlation between the maxima and minima of the vertical signal level and the bearing position. Note that the maximum vertical signal amplitude occurs when the bearing position is at the GCB and the minimum signal amplitude occurs when the bearing position differs from the GCB by 90°. This result is easily predicted from equations (4) and (10). The data of figure 43 substantiate the operational characteristics of mode 2 of the experimental DF system. Since mode 2 allows the bearing display to be unblanked whenever the vertical signal level is near the maximum, the bearing errors are reduced.

Figure 44 shows a particular time interval in which the polarization vector reversed its direction of rotation. Note that the bearing display changed from clockwise to counter-clockwise rotation. It is evident that the angular rate of bearing swing decreased to zero during the transition interval. At the time of low swing rate, the indicated bearing did not coincide with the GCB. Since the SRD unblanks the bearing display at low swing rates, an incorrect bearing may be obtained when the polarization vector reverses rotation direction. This source of bearing error for the experimental model with SRD mode probably accounts for some of the large bearing errors that are evident in figure 36 and Table VIII. It may be observed from figure 44 that during the change in rotation direction, the vertical signal amplitude remained correlated with the bearing position. If the direction of rotation reverses when the polarization vector is horizontal and mode 2 is used with SRD mode, the bearing display remains blanked even through the swing rate is low and no large bearing errors are likely to occur. This observation is evident in the data of figure 38 of section 2.3.6.3. It should be emphasized that the direction of rotation can reverse when the polarization vector is vertical. However, in this case, the indicated bearing is near the GCB and extreme errors are not produced.

In clear contrast to the curves of figure 43 and figure 44, figure 45 shows the bearing position and vertical amplitude versus time when multipath signals were the main cause of bearing errors. Note that the bearing swing as a function of time exhibits no periodic characteristic as is evident in the polarization rotations of figure 43. Note also that the vertical signal variations are not as closely correlated with the bearing position. As noted earlier in this report, there is definite evidence that the vertical signal peaks are correlated with the bearing position; however, for the particular data of figure 45 extensive tests for correlation were not pursued. Figure 45 is shown primarily to illustrate the distinct differences between bearing errors caused by polarization rotation and bearing errors caused by multipath signals.

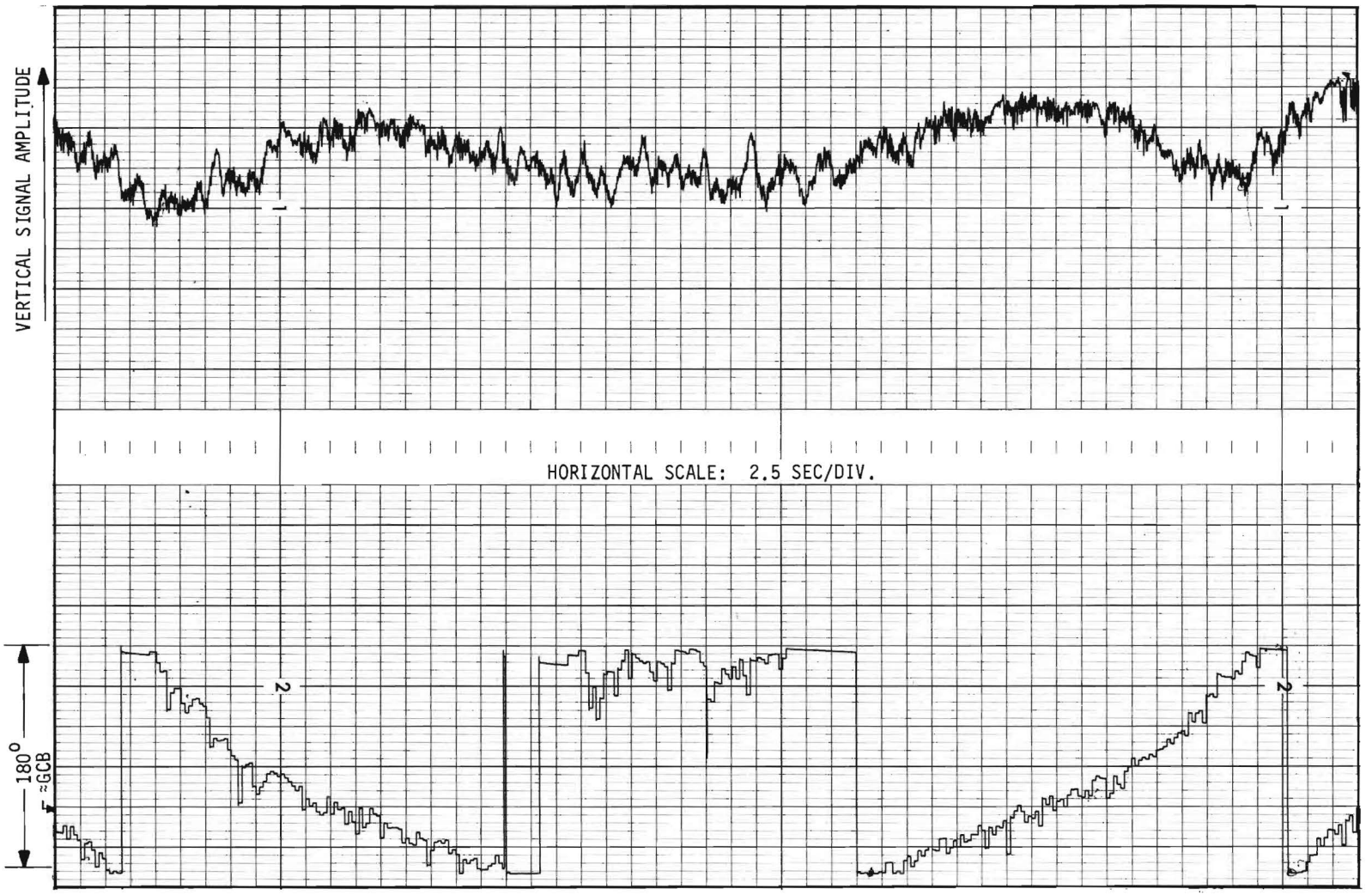

Figure 44. Reversal in Polarization Rotation Direction.

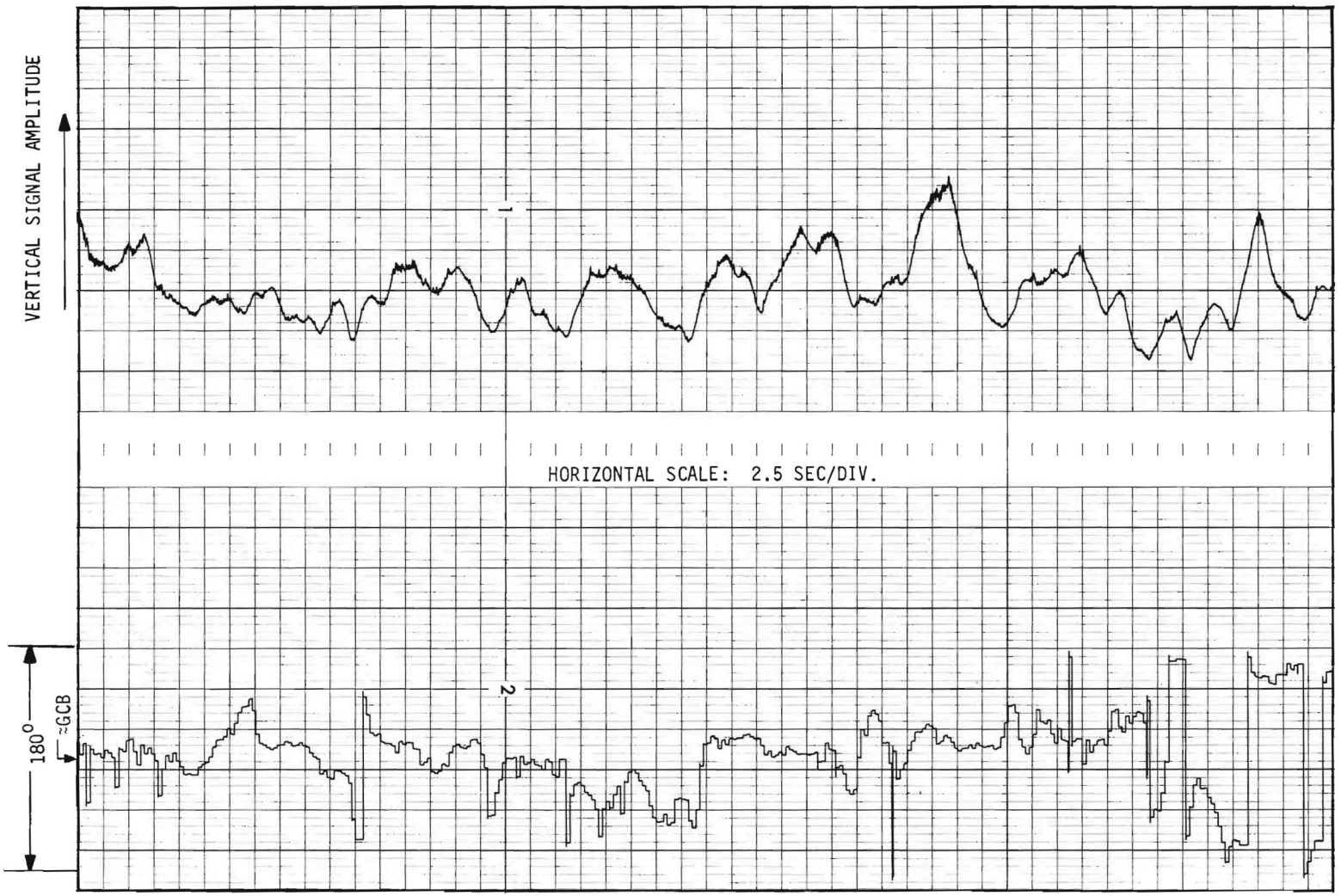

Figure 45. Vertical Level and Bearing Position Versus Time for Multipath Fading.

2.3.7.5 Conclusions

On the basis of the data presented in figures 39 through 45, several significant conclusions may be drawn as follows. (A) Bearing swings due to polarization rotation are in many instances describable by equation (4). This conclusion is not meant to imply that bearing errors under all conditions of polarization rotation are directly predictable; however, it is felt that equation (4) is a reliable model for describing bearing swings if the polarization vector rotates approximately linearly with time for a significant time interval. (B) The elevation angle of arrival may be estimated directly from data that are obtained from a simple loop antenna DF system, if the data are obtained under the conditions of uniform polarization rotation. This conclusion is a direct consequence of the validity of equation (4). (C) Under the condition of polarization rotation, the time variations of vertical signal amplitude are closely correlated with the time variations of indicated bearing position. Again, this conclusion is a direct consequence of equation (4). (D) The SRD of the experimental model can produce large errors if the direction of polarization rotation reverses when the polarization vector is horizontal. As a corollary to this conclusion, the SRD may produce large errors if the polarization rotation rate decreases appreciably. It should be noted that many of these errors can be removed if SRD mode is used in conjunction with mode 2. (E) The condition of polarization rotation is easily distinguished from the condition of multipath signals by observation of the bearing swing. In many instances, the condition of polarization rotation can be established by observation of the vertical amplitude time variations. This conclusion is of prime significance since polarization rotation must be recognized before appropriate error reducing techniques can be applied.

2.4 Additional Investigation

2.4.1. Introduction

Additional investigations were conducted on: (1) specially-wound and doubly-loaded loops; (2) direct, indicated, and inverse loop compensation techniques; (3) low-impedance loading of a loop; and (4) a null width discriminator designed with the purpose of providing for operation on ICW signals.

2.4.2 Specially-Wound Loop

This 1 foot square loop was constructed and tested to determine if a special winding of the horizontal members could reduce the effects of abnormal polarization incident on the loop. The special-winding consisted of winding the horizontal elements such that alternate turns were wound in opposite directions. Detailed

construction procedures are in quarterly report no. 5.

The sensitivities or pick-up factor were compared with a standard 1-foot loop using standard HF fields of normal polarization established by a transmission line in an 8' x 8' x 8' shielded room. These tests showed that the design of the specially-wound loop did not adversely affect the pick-up factor and horizontal plane response pattern when compared with a regular loop. The effects of abnormal polarization were determined by positioning the specially-wound and regular loop at various locations in the near-field of a short dipole and measuring the pick-up factor at four frequencies between 2.5 and 9.5 MHz. The field near a short dipole is elliptically polarized and simulates the type of condition that exists when an ionospherically propagated signal is incident on a loop. A comparison of the regular and specially-wound loops at the same frequency and location showed no significant difference; hence, it was concluded that the special-winding was ineffective in reducing the effects of abnormal polarization.

2.4.3 Doubly-Loaded Loop

This antenna was built to determine if the E and H fields incident on a loop can be obtained as separate output signals.

The doubly-loaded loop (figure 46) had broad-band transformers located in the upper and lower horizontal members. The balanced outputs from the transformers were connected through baluns to the input of a sum and difference network.

Whiteside and King[21] have stated that with an arrangement of this type the sum output is a measure of the H-field incident on the loop whereas the difference output is a measure of the E-field incident on the loop. A loop sustains not only the usual (desired) circulating current which is proportional to the normal H-field, but also other currents which are functions of the incident E-fields. The total circulating currents are broken down into zero and first phase currents proportional to the incident H-and E-fields, respectively. It is shown that for an arrangement such as that shown in figure 46, the zero phase currents are in-phase through the transformers and the first phase currents are out-of-phase. It is further shown that vertical E-fields in the plane of a vertical loop can be ignored in detecting the first phase currents. Hence, the first phase currents are a function only of the incident horizontal E-field. If the upper and lower members of a square loop are loaded with transformers, the sum, Σ, of the outputs will be proportional to the zero-order currents produced by the H-field whereas the difference, Δ, will be proportional to the first-order currents produced by the horizontal E-field.

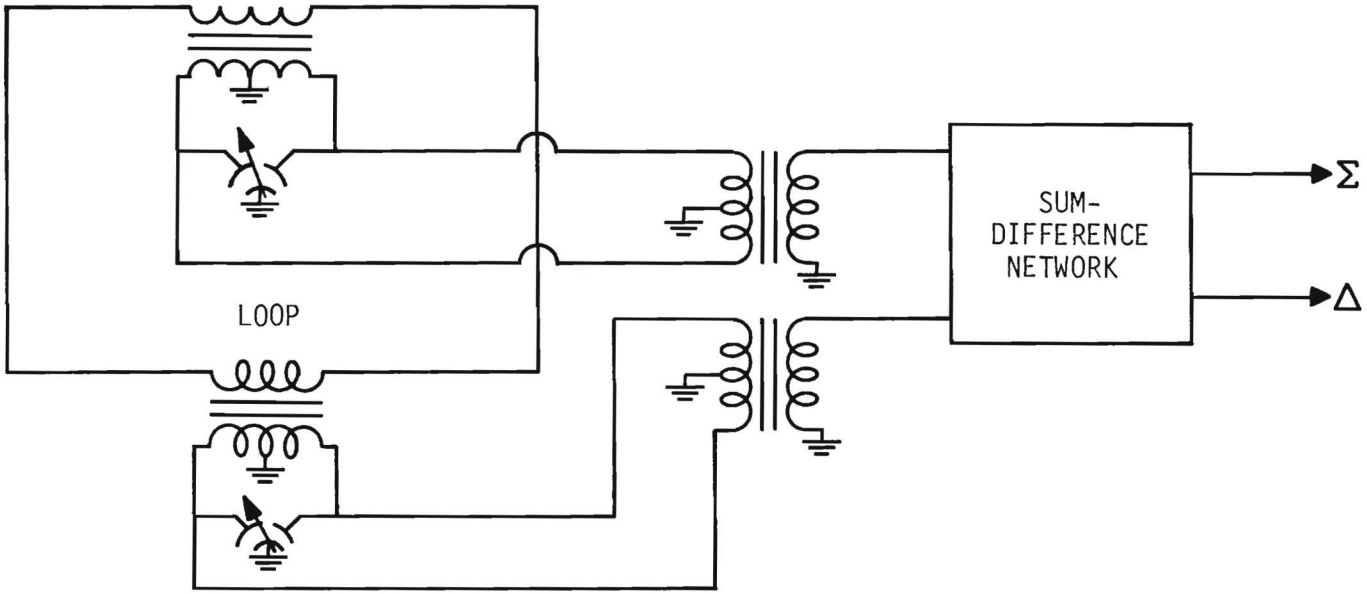

Figure 46. Schematic of Doubly-Loaded Loop.

The Σ port essentially sees the antenna operating in a loop-mode whereas the Δ port sees the antenna operating in a dipole-mode. In the dipole-mode the antenna may be viewed as functioning as double-dipoles separated by the vertical height of the antenna.

The above suggests the use of a doubly-loaded loop as a method to indicate the presence of erroneous bearings caused by abnormal horizontal polarizations. Abnormal horizontal polarization creates a non-zero Δ value when the Σ value is zero. The lack of abnormal horizontal polarization leads to a zero Δ value when the Σ level is zero. Unfortunately, when the incident E-field contains no vertical component, the Δ and Σ levels are simultaneously zero at the null position implying no bearing error when actually a large error could exist especially if the angle-of-incidence is large. Therefore, successful operation on signals with a high angle-of-incidence is questionable. This is a major disadvantage of this technique.

Other disadvantages are that: (1) the E-field response is considerably less than that for the H-field; (2) H-field response is limited by the fact that only one-turn can be used; and (3) the technique is more useful when polarization fading dominates over multipath fading. In regard to item (3), multipath fading is characterized by synchronous fading of the vertical and horizontal components in an incident field; polarization fading creates asynchronous fading. Therefore, if multipath fading is the predominant fade pattern, the Δ and Σ ports will be at minimum levels simultaneously. This would indicate a reliable bearing; however, in fact, it has been shown that the bearings are probably highly erroneous at the minimas of multipath fade cycles. Also, it has been shown that, with multipath fading, bearing errors can occur even though there are no horizontal components in the incident fields. In this case, the Δ output would always be zero and indicate no bearing error.

The sum and difference pickup factors and horizontal plane response patterns were measured using standard HF fields in a 8' x 8' x 8' shielded room. Results show that (1) the pickup factors are less than those for a regular loop by about 10 dB and 20 dB for the sum and difference ports, respectively, and (2) the patterns are very similar to a regular loop. The antenna was used to receive both local (ground-wave) and remote (sky-wave) transmissions. The sum and difference outputs were monitored with R-391 receivers as the loop was rotated through 360°, and the detected outputs of the receivers were recorded on a strip-chart recorder.

Tests on nine local broadcast stations disclosed that the sum output is considerably larger than the difference output. In all cases, the difference output was not large enough to produce a readable output on the strip-chart recorder, which is as it should be for a plane-wave situation with a relatively small amount of abnormal polarization. It was anticipated that the difference outputs would be significantly

larger for sky-wave signals with abnormal polarization. However, the pick-up factor of the loop proved to be too small for the collection of meaningful data on sky-wave transmissions. A major conclusion that has resulted from all tests on the doubly-loaded loop is that the pick-up factor is considerably reduced (tens of decibels) by the transformer loading inserted in series with the loop turns. (It should be noted that only a single-turn can be used, thus the pick-up factor cannot be increased by increasing the number of turns). The experiments indicate the technique, as implemented, to be ineffective for sky-wave signals.

2.4.4 Direct, Indicated, and Inverse Compensated Loop Techniques

Attempts have been made by other investigators to reduce polarization error effects in loop antennas by directly inserting a cancellation signal between the loop and the DF receiver, but success has been limited. A critical analysis of directly compensated loops has been performed and is summarized below.

It has been suggested that, since direct compensation has not been useful, it may be possible to simply indicate a calculated bearing error based on measure of the horizontal polarization present and other pertinent parameters. This has been termed indicated compensation and is discussed below.

The basic concept of inverse compensation, which is discussed below is to use the presence of horizontal polarization to accentuate the distortion of the bearing display that occurs in the presence of abnormal polarization. Hence, an operator may more readily distinguish erroneous bearing conditions.

2.4.4.1 Directly Compensated Loop

The compensated loop DF system consists of a combination vertical loop antenna and one or two horizontal dipoles. Theoretically the outputs are combined in such a manner that the effects of abnormal horizontal polarization on the loop output are cancelled by the dipole(s) output.

An analysis of compensated loop techniques was performed with emphasis on the effects of practical, field conditions on performance. The analysis showed that accurate cancellation is a function of many time-and frequency-variable parameters such as ground reflection ratios and phase angles, elevation angle of arrival, dipole and loop loading networks, and dipole sensitivity. Major conclusions were that accuracy of cancellation is limited by: (1) the changing angles of incidence due to propagation mode shifting; and (2) the variations in loop and dipole(s) output amplitudes and phase do not track as a function of frequency leading to over

or under compensation. In regard to item (2), a review showed that most past efforts did not properly allow for the effects of the equivalent source impedance of electrically-small loop antennas and dipoles on the amplitude and phase shift of the loaded output voltage as a function of frequency. It appears that the undesirable effects of a frequency sensitive source impedance may be reduced by using a high-input, broadband impedance load at the loop and dipole outputs to obtain a proper measure of the open-circuit induced voltage.

2.4.4.2 Indicated Compensation

It has been suggested that, since it has proven difficult to properly combine the loop and dipole outputs in a compensated antenna system, it may be feasible to simply measure the dipole output level and, with proper calibration and processing, display the instantaneous calculated bearing error. This may be termed "indicated compensation" as opposed to actual compensation where the outputs are combined directly. Several formidable problems arise in implementing this concept. One problem concerns the position of the dipole relative to the loop. With the dipole axis parallel to the plane of the loop and rotating with the loop, the output level of the dipole is modulated by the dipole antenna pattern. Hence, if the dipole output were monitored directly it would be impossible to determine when to measure the level corresponding to that of the abnormal horizontal polarization unless there were a priori knowledge of the true bearing. If the dipole were not rotated with the loop, the output may possibly include the horizontal polarization levels that lie in the plane of propagation. Polarization of this type does not produce bearing errors.

In addition, the indication of a zero output level from either a rotating or stationary dipole is deceptive because it has been shown that bearing errors can exist due to multipath effects even though there are no horizontal components in the incident fields. Therefore, it does not necessarily follow that there are no bearing errors if the horizontal dipole output is zero.

Several difficult problems still exist in obtaining a measure of bearing error even if a reliable indication of the abnormal horizontal polarization level could be obtained from a dipole. The magnitude and phase of both the horizontal, $\overline{E}_h$, and vertical, $\overline{E}_v$, components must be known which requires another auxiliary antenna sensitive to the vertical component of the field. Both the amplitude and phase of the dipole and auxiliary antenna outputs must track over the required frequency range. Also, circuitry must be developed to measure the $\overline{E}_h/\overline{E}_v$ ratio and maintain broadband phase and amplitude tracking. The instantaneous

elevation angle-of-incidence must be known as well as the instantaneous ground reflection coefficients for both vertical and horizontal polarization. The reflection coefficients for vertical and horizontal polarization are essentially equal only for soil of high conductivity.

Assuming that all of the parameters were known, the computation would require extensive circuitry to calculate the products, trignometric functions, and ratios explicit in the expression for bearing error.

Even if a reliable estimate of bearing error could be obtained it would be difficult to determine whether the error is clockwise or counter-clockwise, i.e., there is no simple method to determine the instantaneous relative directions of the vertical and horizontal polarization vectors.

To summarize, there are several difficult problems present in the practical implementation of an "indicated compensation" technique. Indeed it is questionable whether the technique should be used -- even if it could be implemented -- in view of the fact that it may provide erroneous results under certain conditions. Also, the circuitry complexity is as great as, if not greater, than that connected with implementing total compensation.

2.4.4.3 Inverse Compensation

Abnormal horizontally polarized signals incident on the loop will obscure, broaden, and shift the null pattern. The present breadboard system uses techniques that remove or perturbate the bearing display when these conditions occur; hence, the operator is capable of ascertaining the character of the null pattern by observing the bearing display. It has been suggested that it may be possible to accentuate these effects of abnormal polarizations on the bearing display in order to more clearly indicate the presence of bearing errors. One possible method is to use an auxiliary antenna output that is combined with the loop output in such a manner that the presence of abnormal polarization accentuates the distortion of the antenna null pattern; hence, the absence of abnormal polarization can be more easily observed. It may be noted that this method is essentially the inverse of compensation techniques that use the output of auxiliary antennas to neutralize the effects of abnormal polarizations.

The following will discuss the factors involved in using a vertical monopole to accomplish inverse compensation. Consider the situation where the output of a vertical monopole is combined with that of a vertical loop. This loop-monopole configuration is familiar in that it produces a cardioid antenna pattern if the outputs are combined properly. For example, consider the general case where a signal,

$\bar{E}$, is incident on the loop with an angle of incidence, θ, and polarization tilt angle, ψ. With $\theta = 90^\circ$ and $\psi = 0^\circ$ and no inverse compensation, the loop pattern has a null when the plane of the loop coincides with the normal to the plane of propagation. With proper inverse compensation (the loop and monopole outputs are combined with the proper phase and amplitude), a cardioid pattern results with the null shifted 90°. Any finite ψ value will distort the cardioid null and indicate the presence of abnormal polarization. However, this is a trivial case in that the operation of interest is for ionospherically propagated signals with $\theta < 90^\circ$ and $\psi \neq 0^\circ$. In this case, the incident signal has three electric field components: (1) $\bar{E}_v$, which is vertical; (2) $\bar{E}_{h1}$, which lies in the direction of propagation; and (3) $\bar{E}_{h2}$, which lies in the plane perpendicular to the direction of propagation. In the conventional, uncompensated loop, $\bar{E}_{h1}$ produces no distortion of the null and produces no bearing shifts. With inverse compensation using the vertical monopole, the pattern is distorted by both $\bar{E}_{h1}$ and $\bar{E}_{h2}$. The distortion by $\bar{E}_{h1}$ is undesirable and precludes the use of inverse compensation by the vertical loop- monopole technique. For example, consider the case shown in figure 47. The loop output signal is proportional to

$$\bar{E}_\ell = K_1\bar{E}_v + K_2\bar{E}_{h1} = K_1\bar{E} \sin\theta + K_2\bar{E} \cos\theta \quad . \qquad (11)$$

Where K_1 and K_2 are functions of factors such as the loop size, ground reflection coefficients, height above ground, and wavelength. The monopole output is $\bar{E}_m = \bar{E}_v = K_3 E \sin\theta$ where K_3 is a function of the effective height of the monopole.

For a given θ, $\bar{E}_m$ can be made equal to $\bar{E}_\ell$ by proper adjustment of the combiner phase and amplitude to obtain the proper cardioid. However, when θ changes, the inverse compensation is incorrect since $\bar{E}_m$ can be made equal to $\bar{E}_\ell$ at only one θ value. K_1 and K_2 vary as a function of θ, further complicating the inverse compensation technique. With improper inverse compensation the cardioid pattern null is filled in, and so indicates an improper bearing when actually the bearing is correct. This is all due to $\bar{E}_{h1}$. Without inverse compensation, $\bar{E}_{h1}$ has no harmful effect on the null pattern and a true bearing would be indicated. In addition, the presence of a significant $\bar{E}_{h1}$ value is not restricted to ionospherically propagated signals because a ground wave signal can (and usually does) have a $\bar{E}_{h1}$ component due to a finite ground conductivity. Hence, the inverse compensation technique may produce erroneous performance under conditions where the uncompensated system would perform satisfactorily.

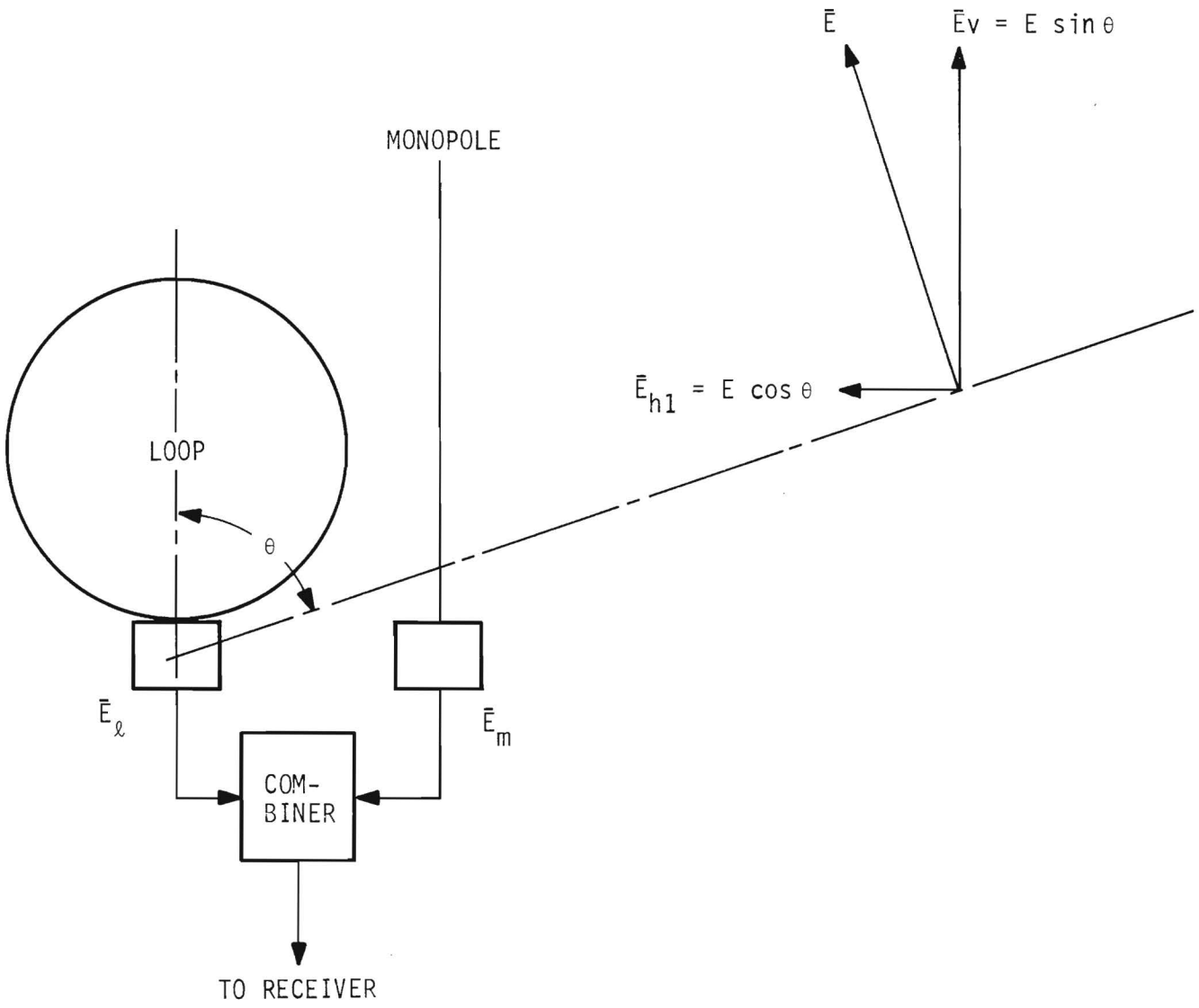

Figure 47. Diagram Illustrating Inverse Compensation.

To summarize, the inverse compensation technique using a vertical loop monopole combination does not appear practical due to the effects of $\underline{E}_{hl}$.

2.4.5 Low Impedance Loading for a Loop Antenna

The preceding discussion on compensated loop systems states that a high input impedance loading of a loop may be desirable. However, it is also interesting to consider the effects of low impedance loading even though practical implementation is difficult.

Figure 48 depicts the Thevenin equivalent circuit of a loop and the input impedance of the load. The radiation resistance is considered to be insignificant when compared to the impedance of L. C is the distributed capacitance of the transmission line between the loop and input stage. The Norton equivalent circuit of figure 48 is as shown in figure 49 where the current i is obtained from the relationship $Li = n\mu HA$. Several factors are evident from figure 49: (1) the effects of loop inductance and the distributed capacitance are negligible when shunted by a low impedance, Z_o, and (2) the current into Z_o is proportional to the absolute value of H rather than the rate-of-change. Hence, the loop output will not increase at a 6 dB/octave rate. Both of the above factors tend to reduce and stabilize amplitude and phase variations, which are major disturbing parameters in small-aperture loop antenna techniques.

Figure 49 points out another advantage of using a low impedance load. L is proportional to n^2; hence, i is inversely proportional to the number of loop turns. This is exactly opposite to the situation for a high input impedance load which requires n to be as large as possible. L is proportional to μ, implying that an increase in μ by using, for example, ferrite material will not be effective in increasing the pick-up factor.

To summarize, it appears that a low impedance load for a loop antenna may provide better overall performance than a high impedance load if it could be obtained in practice. A smaller number of turns can be used, and output amplitude and phase variations can be reduced.

2.4.6 Null Width Discriminator

This unit was designed to provide for operation on ICW signals by passing only those pulse outputs of the null detector with pulse widths between 5 and 15 milliseconds. It was estimated that (1) the pulses formed by on-off keying of the carrier would exceed the 15 msec width and be rejected, and that (2) the true null pulses would be in

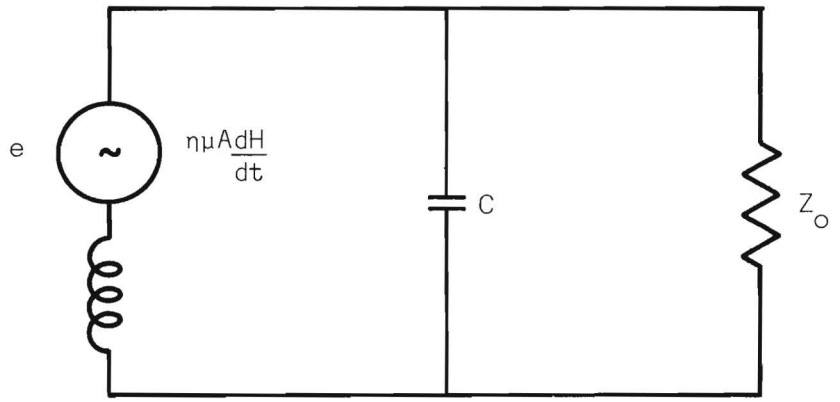

Figure 48. Thevenin Equivalent Circuit of Loop and Load, Z_o.

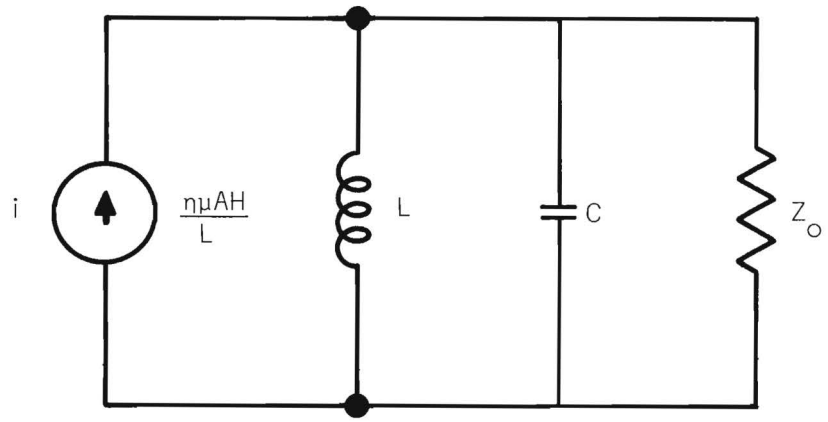

Figure 49. Norton Equivalent Circuit of Loop and Load, Z_o.

the 5-15 msec range and be passed on to intensity modulate the display. However, this did not occur in practice due to several factors. In some cases, the keying rates were sufficiently high to create pulse widths in the 5-15 millisecond range. Also, the keying pulses were not necessarily square waves. Hence, noise pulses occurring during the carrier transition time created false nulls. In some cases, the true nulls became partially synchronized with the carrier off-time. This was probably due to the fact that automatic keyers operating from and synchronized with a 60 Hz source were being used. The loop rotation rate (180 rpm) was also synchronized with 60 Hz; hence, a synchronous state developed between the nulls and the keying pulses. This synchronization was manifested by a stationary keying pattern on the bearing display scope with no bearing patterns present.

3.0 CONCLUSIONS AND RECOMMENDATIONS

3.1 Conclusions

Techniques to reduce bearing errors in HF vertical loop direction finders for ionospherically-propagated signals have been developed and proven effective by operational evaluation. Error reduction can be accomplished by using an auxiliary receiving channel to unblank a bearing display only when the time-variable characteristics of the incident signal produce minimum bearing errors. It has been determined that minimum bearing errors occur at or near the maxima (fade crest) of the vertical component of the incident signal when the bearing swing rate is a minimum.

Several modes of fade crest detection have been designed to optimize unblanking performance for a wide variety of signal and fade conditions. One allows for unblanking when the signal amplitude exceeds some selectable value above the average value. This mode performs best when the SNR is much greater than one and the fading is reasonably periodic with deep nulls (e.g., polarization fading). Other modes operate on the signal peaks and function independently of the average value of the signal. These modes perform best in the presence of multipath fading especially if there is a low SNR and/or low-level interference. Error reduction based solely on bearing swing rate is effective, primarily for polarization fading, as shown by an evaluation of a swing rate discriminator that provides for unblanking when eight consecutive bearings occur within a pre-set azimuth range.

The techniques have been implemented in an exploratory dual-channel HF/DF system and operationally evaluated under field conditions, primarily under transitional ionospheric conditions, on signals from 5 to 20 MHz over path lengths exceeding several hundred miles. Overall test results show that a large majority of the unblanked bearings can be restricted to within $\pm 15^{\circ}$ of the GCB for any signal or fade condition when the optimum mode of operation is used. Average bearing deviations of 10° or less are typical. These figures do not include corrections for site effects which tend to increase bearing error and deviation.

Operational comparison of the exploratory system and the AN/PRD-5 showed that the exploratory system's performance is better with bearing spreads, standard deviations, and RMS errors reduced by about one-half. Improvement is more significant in the presence of polarization fading with the ES producing about a 3 to 1 improvement. The exploratory system's mean bearing deviations are less by about a 2 to 1 factor.

Using a storage scope for the bearing display can greatly improve DF performance especially when used with auxiliary channel unblanking. Groups of bearings rapidly occurring at the crest of a fade cycle can be stored and subsequently recorded in a more optimum manner. The scope can also be used to average bearings that are fluctuating symmetrically over a small (e.g., 20°) azimuth region.

Mathmatical modeling of polarization fading was performed by postulating the detected envelope of the vertical component to be a full-wave, rectified sine wave. Fade crest unblanking levels relative to the average level were related to polarization tilt angle which was, in turn, converted to bearing error using the bearing error equations and an estimate of elevation angle of arrival. Hence, it was possible to predict approximate bearing spreads for specific unblanking levels relative to the average level. The model predicted the maximum reliable unblanking level to be about 3 dB above the average. Test data showed this to be correct. Measured spreads with polarization fading were somewhat larger than predicted; however, measured standard deviations were very close to the predicted spread values, implying the modeling to be a better predictor of standard deviation than absolute spread.

A similar polarization rotation modeling procedure was devised to predict bearing distribution and elevation angle of arrival. Also, methods were developed to obtain the same parameters directly from measured swing rate discriminator data. Comparisons of predicted and measured parameters showed very similar results. This is considered to be a significant result since polarization rotation normally presents a worst-case (almost hopeless) condition for loop DF systems; however, it appears that swing rate data obtained during periods of consistent polarization fading may possibly be used to obtain a measure of not only the azimuth angle-of-arrival but also the elevation angle-of-arrival.

Tests on transmissions experiencing polarization fading indicate that if the polarization rotation characteristics are uniform the statistical parameters describing the bearing distribution are also uniform. If the fade crest amplitudes are varying, the most accurate bearings apparently occur on the crests with the largest amplitudes.

Test data disclosed that bearings can be highly erroneous even though steady, sharp displays are present. This occurred in the presence of (1) polarization fading when the rotation ceased on the skirt or null of a vertical component fade cycle, and (2) lateral path deviation effects.

An analysis of compensated antenna techniques showed that real-time, optimum compensation is limited by the fact that major parameters vary as a function of time and frequency, and that automatic compensation for these variations cannot be easily implemented.

The specially-wound loop was ineffective in rejecting abnormally polarized fields. The doubly-loaded loop proved ineffective due to lowered pick-up factor.

Investigation using a null width discriminator for ICW operation proved ineffective primarily because of (1) false nulls created by noise pulses and certain high keying rates, and (2) synchronous keying.

A relatively large amount of test data were obtained on test transmissions experiencing polarization fading since it constitutes a

worst-case situation for loop systems; however, it should be stressed that polarization fading occurs less often than multipath fading.

3.2 Recommendations

It is recommended that the error reduction techniques developed on this project be used with operational loop HF/DF systems. Also, storage scopes and associated circuitry should be developed for use with DF systems.

Other general recommendations are as follows:

A. Develop Techniques for Interrupted Carrier Operation

Techniques for direction finding on modulations (on-off keying, burst, etc.) using interrupted carrier should be developed for use with the ES.

B. Additional Comparison with Other Operational HF Loop Antenna Direction Finding Systems

It may be desirable to conduct simultaneous operational performance tests with other types of military HF loop antenna direction finders such as crossed and spaced loop systems at an optimum site under a wide variety of propagation conditions.

C. Apply Fade Crest Detection and Swing Rate Discrimination to Other DF Systems

It is believed that the error reduction techniques developed for the rotating loop antenna could also be effectively used with other DF systems such as spaced loops, Adcocks, Wullenwebers, etc., since these systems are also effected, to varying degrees, by polarization and wave interference errors.

The techniques may also be applicable to DF systems operating in frequency ranges other than HF.

D. Investigate Adaptive DF Systems

The optimum error reduction mode of operation is selected by the operator based on the prevalent signal and fade characteristics. However, it is possible that this selection could be automated in order to obtain a DF system that continuously optimizes its mode of operation to the real-time signal characteristics.

E. Provide Visual Read-Out of the Time-Average of the Bearing Data

Since the average of a set of bearings increases in accuracy as the averaging time increases, a useful devise would be a continuous visual read-out of the up-to-date average of all previous bearings accumulated during a particular test, or specific

averaging intervals could be chosen either automatically or manually. Averaging is a natural extension of the techniques developed for the ES for converting bearing azimuth to a form of pulse position modulation. That is, the bearings azimuths are converted to pulses, such that the pulse position relative to a reference pulse is a function of bearing. Standard PPM to PAM converters followed by averaging circuitry and a calibrated read-out could be used to present a continuous bearing time-average.

F. Provide Strip-Chart Recording of Fade Amplitude-Time Characteristics

Even if no auxiliary channel unblanking is used, a strip-chart recording of the vertical component amplitude variations could be beneficial to a trained operator — especially if slow polarization fading is present. Fade crest detection could be done visually. Also, harmful fade moding could be noted. (Visual crest detection using a strip-chart recording was tried several times during periods of very slow polarization fading and appeared to be just as accurate as automatic unblanking.)

G. Perform Propagation Studies for Very Short Range (e.g., 100 km) Paths Using High Elevation Angle Transmitting Antennas

During the course of this project a considerable amount of the unclassified literature on HF propagation was reviewed. It was noted that relatively little work has been done defining the propagation characteristics of a short-path link using ionospheric propagation. It is submitted that, with the advent of HF antennas especially designed with a high-elevation angle maxima (e.g., 60° -90°), more and more short range transmissions will be via the ionosphere especially if the terrain features produce high ground-wave absorption. It has been shown on this project that the propagation conditions have a major effect on selecting the optimum mode for DF operation. Therefore, in order to develop systems to properly DF on high elevation angle signals it is necessary to have a knowledge of the basic propagation characteristics such as principal propagation and fading modes (polarization or multipath), fade rates and statistical distributions, phase stability, and long-and short-term variations.

H. Train DF Operators As to the Relationships Between Bearing Errors and Propagation Effects

It has been shown that large bearing errors can occur in small-aperture systems even though the displayed bearing appears to be a good, acceptable bearing. However, a trained operator may be able to correlate bearing and propagation characteristics to avoid these highly erroneous readings.

4.0 REFERENCES

References Cited

1. Howard, F. S. and Wood, F. M., "Note on the Bearing Error and Sensitivity of a Loop Antenna in an Abnormally Polarized Field", Proceedings of the IRE, April 1944, pp. 231-233.

2. Hayden, E. C., "Some Basic Problems In the Determination of the Direction of Arrival of Radio Waves", University of Illinois, ONR Project No. NR 371-61, September 1958.

3. Ionospheric Radio Propagation, National Bureau of Standards, Circular 462.

4. Norton, K. A., "The Polarization of Downcoming Ionospheric Radio Waves", Report in Connection with NBS Project Sponsored by the National Defense Research Committee.

5. Pierce, J. N., "Theoretical Limitations on Frequency and Time Diversity for Fading Binary Transmissions", Report No. ERD-TR-60-169, Air Force Cambridge Research Laboratories, AD 245 723, July 1960.

6. Banerji, R. B., "Some Studies on Random Fading Characteristics", Proceedings Physical Society, London, 66 BN2, p. 105, February 1953.

7. Hancock, J. C., and Weiner, D. D., "Channel Characteristics", Frequency, pp. 12-16, November-December 1963

8. Khastgir, S. R. and Ray, A. K., "On the Intensity Variations of the Downcoming Wireless Waves From the Ionosphere", Indian Journal of Physics, pp. 283-292, June 1940.

9. Huntington, C. F., "A Proposed Tropospheric Scatter Communications Equipment Configuration for Time Diversity Reception", Technical Note RADC-TN-59-304, AD 231 258, December 1959.

10. Mitra, S. N., "Statistical Analysis of Fading of a Single Downcoming Wave from the Ionosphere", Proc. IEE, Vol. 96, Part III, pp. 505-507, November 1949.

11. McNicol, R. W. E., "The Fading of Radio Waves of Medium and High Frequencies", Proc. IEE, Vol. 96, Part III, pp. 517-524, November 1959

12. Goldberg, B., "Communications Systems 300 kc/s - 30 mc/s - MF/HF", IEEE Annual Communications Convention Record, 1965, pp. 713-724.

13. Hayden, E. C., "Correlation of D/F Errors with Ionospheric Radio Propagation Phenomena", University of Illinois, Technical Report 2, Contract AF 30(602)-2413, March 1962.

14. Kanellakos, D. P., "Origin and Location of Ionospheric Perturbations Affecting the Frequency and Bearing of HF Radio Waves", Stanford Electronics Laboratory, Nonr-225(33), November 1962.

15. Wale, H. A. and Delves, L. M., "Some Relations Between the Bearing and Amplitude of a Fading Radio Wave", J. Atmos, Terr. Phys. 43, pp. 72-85, 1958.

16. Salamon, R. K., et al, "Fading Multipath and Direction of Arrival Studies for HF Communications", NBS Report 7206, NBS Boulder Laboratories, Boulder, Colorado, 15 December 1961.

17. Gething, P. J. D., "High-Frequency Direction Finding", Proc. IEEE, January 1966.

18. "A Study of High Frequency Directional Propagation Over a 450 Km East-to-West Path", University of Illinois, AD 625 413.

19. Bailey, A. D., and Sydnor, R. L., "An Investigation of Signal Amplitude to Bearing Deviation Correlation as a Function of Time in HF Radio Direction Finding", Technical Report No. 13, Contract Nonr 1834(02), 1 July 1956, University of Illinois.

20. Detert, David G., "An Investigation of Large Scale Ionospheric Disturbances Observed in a Radiolocation Experiment", Technical Report No. 28, Contract Nonr 1834(02), September 1965. University of Illinois, Urbana, Illinois.

21. Whiteside, H. and King, R. W. P., "The Loop Antenna as a Probe", Trans. IEEE, Vol. AP-12, No. 3, pp. 291-297, May 1964.

Additional References

1. Travers, P. N. and Hixon, S. M., "Abstracts of the Available Literature on Radio Direction Finding 1899-1965", Southwest Research Institute, San Antonio, Texas, 1 July 1966.
(This is an excellent reference including abstracts on approximately 6000 documents, reports, papers, etc.)

2. Remmler, O. D., "Bibliography on Direction Finding and Related Ionsopheric Propagation Topics 1955-1961", NBS Technical Note No. 127.

3. Raytheon Co., "Studies in Ionospheric Propagation", 31 June 1961, Final Report, AF 19(604)-5230, AD 268 270.

4. Dearden, E. W., "Field Aligned Ionization Irregularities", Report No. 1,AD 294 723, University of Queensland, Brisbane, Austraila, AF 64(500)-9.

5. Sandretto, P. C., Principles of Aeronautical Radio Engineering, McGraw-Hill Book Company, Inc., New York 1942.

6. Haber, F., "Generation of Standard Fields in Shielded Enclosures", Proceedings of the IRE, Vol. 42, pp. 1693-1698, November 1954.

7. Villard, O. G. and Yeh, K. C., "A Proposed Technique For Improving The Intelligibility of Voice Radio in Auroral Flutter Fading", Technical Note AFCRC-TN-58-644, AD 230 694, October 1958.

8. Hutchinson, H. P., "Short-Period Sky-Wave Fading of CW Emissions", U. S. Army Signal Corps, Office of Chief Signal Officer, Washington, D. C.

9. Koch, J. W., Harding, W. B. and Jansen R. J., "Fading Rate Recorder for Propagation Research", Electronics, pp. 78-80, December 18, 1959.

10. General Dynamics, Inc., "Evaluation of New High Frequency Radio Communications Equipment", Signal Corps. Contract No. DA 36-039 SC-78309, AD 272 565, January 1962.

11. Steele, J. G., "HF Backscatter from Terrain with Trees", Stanford Electronics Laboratory, Stanford University, ONR Contract Nonr-225 (64), NR 088019 and ARPA Order 196-65, AD 482 575, April 1966.

12. Ernst, E. W., et al, "Studies in Time Averaging and Wave Interference in Radio Direction Finding", Radiolocation Research Laboratory, University of Illinois, RRL Publication No. 312, Technical Report No. 2, AD 636 791, July 1966.

13. Hedlund, D. A. and Edwards, L. C., "Polarization Fading Over an Oblique Incidence Path", IRE Trans. on Antennas and Propagation, pp. 21-25, January 1958.

14. Glaser, J. and Faber, L., "Evaluation of Polarization Diversity Performance", Proc. IRE, pp. 1774-1778, December 1953.

15. Grisdale, G. L., Morris, J. G. and Palmer, D. S., "Fading of Long Distance Radio Signals and a Comparison of Space and Polarization Diversity Reception in the 6-18 mc/s Range", Proc. IEE, 104B pp. 39-51, 1957.

16. Terman, F. E. and Petit, J. M., "The Compensated Loop Direction Finder", Proc. IRE, Vol. 33, pp. 307-318, May 1945.

17. Grush, H. L., "An Investigation of a Digital Bearing Computer for a Small Aperture Radio DF System", ONR Project NR 371-161, Technical Report No. 27, University of Illinois, Urbana, Illinois, June 1965, AD 623 177.

18. Syndor, R. L., "An Investigation of Space Diversity Radio DF", ONR Project NR 371-161, Technical Report No. 17, University of Illinois, Urbana, Illinois, April 1962, AD 286 032.

19. Ernst, E. W., et al, "Studies in Time Averaging and Wave Interference in Radio DF", RRL Publ. No. 312, Technical Report No. 2, University of Illinois, Urbana, Illinois, July 1966, AD 636 791.

20. Bailey, A. D., Dyson, J. D. and Hayden, E. C., "Studies and Investigation Leading to the Design of a Radio DF System for the MF-HF-VHF Range", First Quarterly Report, Contract DA 36-039 SC-87264, University of Illinois, Urbana, Illinois, October 1961, AD 271 531.

21. Bailey, A. D., Dyson, J. D. and Hayden, E. C., "Studies and Investigation Leading to the Design of a Radio DF System for the MF-HF-VHF Range", Final Report, Contract No. DA 35-039 SC-84525, University of Illinois, Urbana, Illinois , June 1961, AD 267 087.

22. David, F., et al, "Analytical and Experimental Study of Correlation Functions Over HF Circuits", Final Report, Contract DA 28-043 AMC-00145 (E), Communications Systems, Inc., Paramus, N. J., November 1965, AD 626 905.

23. Tupper, B. C. and Shaver, H. N., "HF Communication Effects: Experimental Justification of the Gaussian Channel Model", Final Report, Contract DA 36-039 SC-87197, Stanford Research Institute , Menlo Park, California, August 1965, AD 800 339.

24. Bowen, E. D., et al, "Transequatorial F- Layer Propagation Study", Technical Report No. RADC-TR-66-504, Contract AF 30(602)-3379, Symth Research Associates, September 1966, AD 800 339.

25. Tveten, L. H., et al, "Propagation Studies for RFD", Volume II, Technical Report No. RADC-TR-66-504, Contract AF 30(602)-2488, Institute for Telecommunication Sciences and Aeronomy, October 1966, AD 803 851.

26. Chapman, R., et al, "Dispersive Characteristics of the Ionosphere", Final Technical Report No. RADC-TR-66-211, Contract AF 30(602)-3360, General Electric Co., Syracuse, N. Y., August 1966, AD 800 851.

Contract DA 28-043 AMC-01207(E) Reports

1. Quarterly Report No. 1, 1 March to 31 May 1965, AD 469 961L
2. " " No. 2, 1 June to 31 August 1965, AD 473 847L
3. " " No. 3, 1 September to 30 November 1965, AD 477 074L
4. " " No. 4, 1 December 1965 to 30 April 1966, AD 486 325L
5. " " No. 5, 1 May to 31 July 1966, AD 488 963L

Contract DA 28-043 AMC-01207(E) Reports (Continued)

6. Quarterly Report No. 6, 1 August to 31 October 1966
7. " " No. 7, 1 November 1966 to January 1967.

APPENDIX A

TEST TRANSMISSIONS

Listed below are the test transmissions showing location and code.

Station	Code	Location
Radio Austria	AUS	Vienna, Aus.
BBC	BBC	Daventry, Eng.
Radio Netherlands	BON	Bonaire, Carib.
Radio Budapest	BUD	Budapest, Hung.
VOA	BY	Bethany, Ohio
Radio Canada	CAN	Sackville, NB
VOA	DEL	Delano, Calif.
VOA	DIX	Dixon, Calif.
VOA	GRE	Greenville, N. C.
Radio Haiti	HAI	Haiti
Radio Havana	HAV	Havana, Cuba
Radio Moscow	MOS	Moska, USSR
Radio Mexico	MEX	Mexico, DF
Radio Panama	PAN	Panama Canal Zone
Radio Prague	PRA	Prague, Czech.
HCJB	QUI	Quito, Ecu.
Radio Italy	RAI	Rome, Italy
Radio S. Africa	RSA	Johannesburg, S. A.
KGEI	SAN	San Francisco, Calif.
Radio Switzerland	SBC	Berne, Swiz.
Radio Sofia	SOF	Sofia, Bulgaria
Radio Vatican	VAT	Vatican City
WWV	WWV	Boulder City, Colo.

Listed below are the groupings of the test transmissions referenced in the main body of the report. The nomenclature following the station and frequency specifies the number of tests and time period. For example, under Group 1 by HAV 6.1 MHz the 2D, 2M means that two tests were performed during the daytime period and two during the morning period. The letter N indicates a nighttime period.

Group 1

HAV	6.1 MHz	2D, 2M	NY	15.4 MHz	1D
HAV	9.5 MHz	1M	QUI	11.7 MHz	2M
HAV	15.2 MHz	1D	WWV	10 MHz	4D
MEX	15.1 MHz	1D	WWV	15 MHz	1D
NY	9.7 MHz	1N			

Group 2

BON	9.4 MHz	1N	HAV	5.9 MHz	1D
BON	11.8 MHz	1M	HAV	6.1 MHz	2D, 2M
BON	15.2 MHz	1D	HAV	15.2 MHz	2D
BY	11.9 MHz	1M	HAV	17.6 MHz	1M
CAN	9.6 MHz	1D	MOS	7.1 MHz	2D
CAN	15.4 MHz	2D	NY	15.4 MHz	2D
GRE	9.5 MHz	1D	NY	17.8 MHz	1D
GRE	9.7 MHz	1D, 1N	QUI	17.8 MHz	2D
GRE	11.7 MHz	1D	WWV	10 MHz	2D, 1N
GRE	15.4 MHz	1D	WWV	15 MHz	4D, 3M
HAI	11.8 MHz	1M			

Group 3

BBC	11.8 MHz	1D	HAV	15.2 MHz	2D
BON	11.8 MHz	2M	HAV	17.6 MHz	1M
CAN	9.6 MHz	1D	MEX	15.1 MHz	1D
CAN	15.4 MHz	2D	NY	9.7 MHz	1N
GRE	9.5 MHz	1M	NY	15.4 MHz	1D, 1M

Group 3 (Continued)

HAI	11.8 MHz	1M	NY	17.8 MHz	1D
HAV	6.1 MHz	2D, 2M, 1N	QUI	11.7 MHz	1M, 2M
HAV	9.5 MHz	2M	WWV	10 MHz	2D, 2M
			WWV	15 MHz	4D, 2M

Group 4

BY	6.1 MHz	1M	MOS	7.1 MHz	3N
CAN	15.4 MHz	1M	NY	15.4 MHz	1D
GRE	11.7 MHz	2D	QUI	15.4 MHz	1D
GRE	9.5 MHz	1M	QUI	17.8 MHz	1D
HAV	15.2 MHz	2D	WWV	10 MHz	1D, 1N
HAV	6.1 MHz	1D, 2M	WWV	15 MHz	2D, 2M

Group 5

BBC	6.1 MHz	2N	HAV	9.5 MHz	1D, 1M, 3N
BBC	7.2 MHz	3N	HAV	15.2 MHz	7D
BBC	9.4 MHz	4N	HAV	17.6 MHz	1M, 1N
BON	9.4 MHz	2N	MEX	15.1 MHz	1D
BON	9.6 MHz	1N	MOS	7.1 MHz	7N
BON	11.8 MHz	2M	MOS	9.7 MHz	2N
BON	15.2 MHz	1D	NY	9.7 MHz	1N
BY	6.1 MHz	4N	NY	15.4 MHz	8D
BY	9.6 MHz	1N	NY	17.8 MHz	7D
BY	11.9 MHz	1M	QUI	9.7 MHz	3N
CAN	9.4 MHz	3N	QUI	11.7 MHz	3M
CAN	9.6 MHz	1D, 2N	QUI	17.8 MHz	2D
CAN	15.4 MHz	3D	RAI	9.4 MHz	1N
DEL	9.5 MHz	2M	RAI	9.6 MHz	1N
DEL	17.8 MHz	2N	RSA	9.7 MHz	1N

Group 5 (Continued)

DIX	11.8 MHz	1D	RSA	11.8 MHz	1N
DIX	17.7 MHz	1N	SBC	9.5 MHz	1N
HAI	11.8 MHz	2M	VAT	9.7 MHz	1N
HAV	5.9 MHz	1D	WWV	10 MHz	10D, 5N
HAV	6.1 MHz	5D, 4M, 5N	WWV	15 MHz	6D, 3M, 1N
HAV	7.1 MHz	1N			

Group 6

AUS	9.7 MHz	1N	HAV	6.1 MHz	1D, 1M, 6N
BBC	6.1 MHz	2N	HAV	9.5 MHz	1D, 1M
BBC	7.2 MHz	1N	HAV	15.2 MHz	1D
BBC	9.2 MHz	2N	MOS	7.1 MHz	2N
BBC	9.6 MHz	5N	MOS	9.7 MHz	5N
BBC	11.8 MHz	1N	NY	9.7 MHz	1D, 2N
BON	9.4 MHz	1N	NY	15.4 MHz	2D, 1N
BON	9.6 MHz	3N	PAN	9.0 MHz	1N
BON	11.9 MHz	3M	PRA	7.1 MHz	1N
BUD	11.9 MHz	1M	PRA	9.7 MHz	1N
BY	6.1 MHz	3N	QUI	9.7 MHz	2N
BY	9.6 MHz	2N	RAI	9.4 MHz	1N
BY	11.9 MHz	1M	RSA	11.8 MHz	2N
CAN	9.4 MHz	1N	SAN	15.2 MHz	1N
CAN	9.6 MHz	4N	SBC	9.5 MHz	3N
CAN	17.8 MHz	1D	WWV	5 MHz	2N
DEL	9.5 MHz	2M	WWV	10 MHz	2M, 6N
DEL	17.8 MHz	1N	WWV	15 MHz	3D, 1M, 1N
DIX	9.5 MHz	1M			

Group 7

BY	9.6 MHz	4N	NY	9.7 MHz	1D
CAN	17.8 MHz	1D	NY	15.4 MHz	1D

Group 7 (Continued)

GRE	9.5 MHz	3D, 14M, 1N	QUI	9.7 MHz	1M
GRE	9.7 MHz	1D, 2N	WWV	10 MHz	1D
GRE	11.7 MHz	8D, 4N	WWV	15 MHz	1D
HAV	6.1 MHz	3N	WWV	20 MHz	1D
MEX	15.1 MHz	1D			

Group 8

BY	6.1 MHz	1N	MEX	15.1 MHz	1D
BY	9.6 MHz	4N	NY	15.4 MHz	2D
GRE	9.5 MHz	1D, 29M, 2N	QUI	15.1 MHz	1M
GRE	9.7 MHz	1D, 2N	WWV	10 MHz	1D
GRE	11.7 MHz	9D, 6N	WWV	15 MHz	2D
HAV	6.1 MHz	2N	WWV	20 MHz	1D

Group 9

BBC	7.2 MHz	1N	DIX	9.5 MHz	1M
CAN	9.4 MHz	1N	GRE	9.4 MHz	1N
CAN	17.8 MHz	1D	WWV	10 MHz	1M
DEL	9.5 MHz	1M	WWV	15 MHz	2D, 1N

Group 10

BBC	6.1 MHz	2N	GRE	9,5 MHz	2N
BY	6.1 MHz	2N	GRE	9.7 MHz	2N
BY	9.6 MHz	1N	HAV	6.1 MHz	1N
CAN	9.6 MHz	1N	WWV	15 MHz	1D
GRE	6.2 MHz	2N	NY	15.4 MHz	4D

Group 11

MOS	7.1 MHz	1N
QUI	9.7 MHz	1N
WWV	10 MHz	1N

Group 12

BBC	7.2 MHz	1N	MOS	7.1 MHz	1N
BBC	9.6 MHz	1N	NY	9.7 MHz	1D

Group 12 (Continued)

BON	9.6 MHz	1N	NY	15.4 MHz	1D
CAN	9.6 MHz	1N	QUI	9.7 MHz	1N
DEL	17.8 MHz	1N	SBC	9.5 MHz	1N
GRE	6.2 MHz	1N	WWV	10 MHz	1N
HAV	6.1 MHz	2D, 1N	WWV	15 MHz	2D
HAV	15.2 MHz	2D			

Group 13

BON	9.6 MHz	1N	HAV	6.1 MHz	1D
BY	11.9 MHz	1M	MOS	9.6 MHz	1N
BUD	11.9 MHz	1N	RSA	11.9 MHz	2N

Group 14

BY	6.1 MHz	1N	GRE	9.7 MHz	1D
BY	9.6 MHz	1N	HAV	6.1 MHz	1N
CAN	9.6 MHz	1N	HAV	15.4 MHz	2D
GRE	6.2 MHz	1N	NY	15.4 MHz	1D

Group 15

BY	9.6 MHz	2N	QUI	15.2 MHz	1M
GRE	9.5 MHz	2D, 5M, 1N	WWV	15 MHz	1D
GRE	11.7 MHz	2D, 2N			

Group 16

BY	6.1 MHz	1N	GRE	11.7 MHz	3D, 5N
BY	9.6 MHz	1N	QUI	15.1 MHz	1M
GRE	9.5 MHz	1D, 5M, 1N	WWV	15 MHz	1D
GRE	9.7 MHz	1D			

Group 17

DEL	9.5 MHz	2M	MOS	9.7 MHz	1N
DIX	9.5 MHz	1M	WWV	10 MHz	2M, 2N
HAV	9.5 MHz	1D, 1M	WWV	15 MHz	1D, 1M

Group 18

DEL	9.5 MHz	1M	WWV	10 MHz	1M
DIX	9.5 MHz	1M	WWV	15 MHz	1D

Group 19

GRE	9.5 MHz	2D, 5M, 1N

Group 20

GRE	9.5 MHz	2D, 5M, 1N

Group 21

GRE	11.7 MHz	2D, 2N

Group 22

GRE	11.7 MHz	3D, 5N

Group 23

BY	6.1 MHz	1N	GRE	17.8 MHz	3D
GRE	9.5 MHz	1D, 1M, 1N	HAV	6.1 MHz	2N
GRE	9.7 MHz	1D	NY	15.4 MHz	1D
GRE	6.2 MHz	1N	NY	9.7 MHz	1D
GRE	11.9 MHz	1D	NY	17.8 MHz	2D
GRE	11.8 MHz	1D	WWV	15 MHz	1M

Group 24

GRE	11.8 MHz	2D, 2N	NY	11.9 MHz	1D
GRE	9.5 MHz	6M	NY	15.4 MHz	1D
GRE	11.9 MHz	1D	WWV	15 MHz	1M
GRE	17.8 MHz	4D			

Group 25

GRE	9.5 MHz	1D, 4M	NY	17.6 MHz	2D
HAV	6.1 MHz	1N	NY	17.8 MHz	2D
NY	9.7 MHz	1D	WWV	15 MHz	1N, 2D
NY	11.9 MHz	2D	WWV	20 MHz	4D
NY	15.4 MHz	2N, 1D			

APPENDIX B

SWING RATE DISCRIMINATOR (SRD) DESCRIPTION

Figure B1 shows a functional block diagram of the circuit that was used to implement the SRD. Note that three signals are inserted into this system: the azimuth reference pulses, the bearing null pulses, and unblanking pulses. The unblanking pulses are obtained from other portions of the DF system (see figure 8). The time relationship between the azimuth reference pulses and the bearing null pulses was explained in Section 2.3.6.2. Observe from figure 8 that the bearing null pulse chain would closely resemble a pulse position modulation (PPM) waveform for a swinging bearing. In the discussion of SRD operation which follows, reference should be made to the functional block diagram of figure B1.

The bearing sampler circuit in conjunction with the trigger amplifier, 180 ms ramp generator, 180 ms gate, and pulse generator is effectively a PPM demodulator. Figure B2 illustrates the operation of this portion of the SRD circuitry. The time position (which is the azimuth information) of the first bearing pulse relative to the preceeding azimuth reference pulse is converted into a dc level at the bearing sampler output. The level of the dc signal is directly proportional to the azimuth difference between the reference pulse and the first bearing pulse. The second bearing pulse, which corresponds to the reciprocal bearing null, is removed in the 180 ms gate. If the azimuth position of two successive gated bearing pulses differ, then the resultant dc levels will differ correspondingly. If any bearing pulses are missing, as could occur during signal fades, the dc voltage remains at the level determined by the last received bearing pulse. Note that the bearing sampler circuit along with its associated circuits provides a continuous dc analog of the bearing azimuth position relative to the reference azimuth position.

The reference sampler circuit and its related circuits as shown in figure B3 act basically as a sample and hold circuit. Whenever the reference sampler circuit is discharged by activation of the reference discharge gate, a new sample is automatically obtained. This sample, which again is a dc analog of the bearing azimuth position, is held until the next activation of the reference discharge gate. Note that the reference sampling circuit holds a given sample until the reference discharge gate is activated, while the bearing sampler circuit obtains a new sample each time a gated bearing pulse is received. A steady bearing will produce equal dc levels out of the reference sampler and bearing sampler.

The dc analog signals of bearing positions from the reference sampler and bearing sampler circuits are fed into the three circuits shown in figure B4. The differential amplifier effectively subtracts the reference sampler voltage from the bearing sampler voltage.

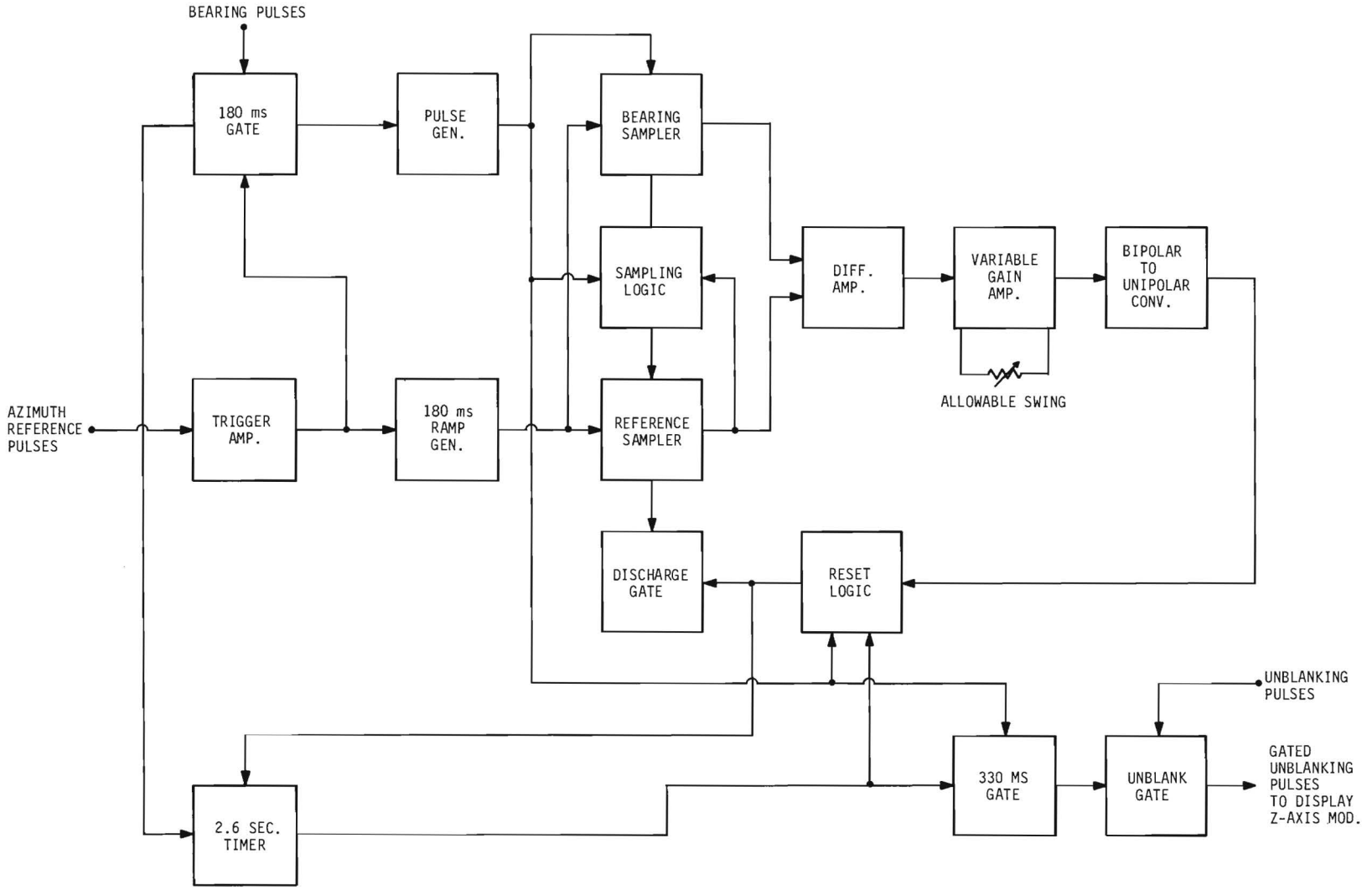

Figure B1. Functional Block Diagram of Swing Rate Discriminator.

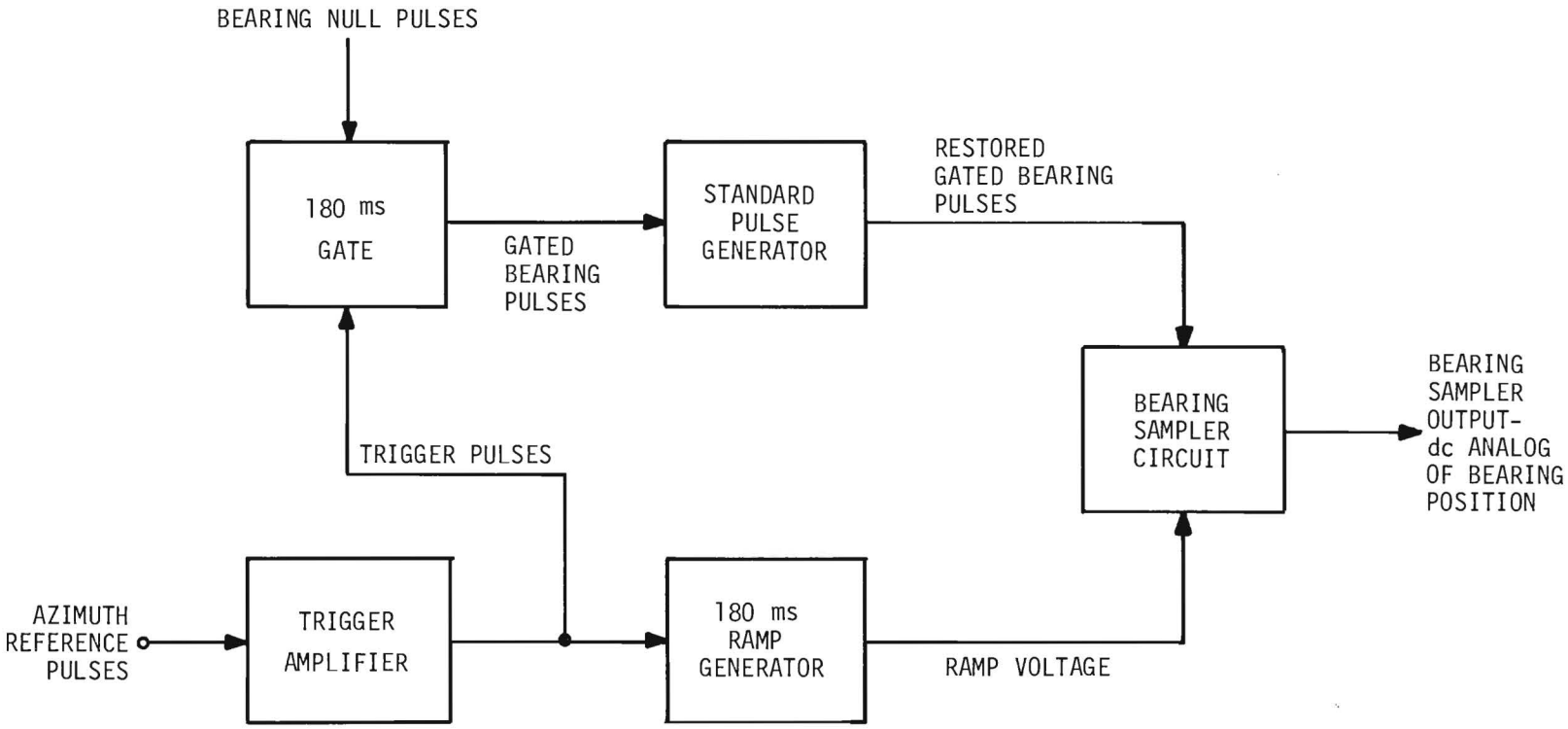

Figure B2. Bearing Sampler and Related Circuits.

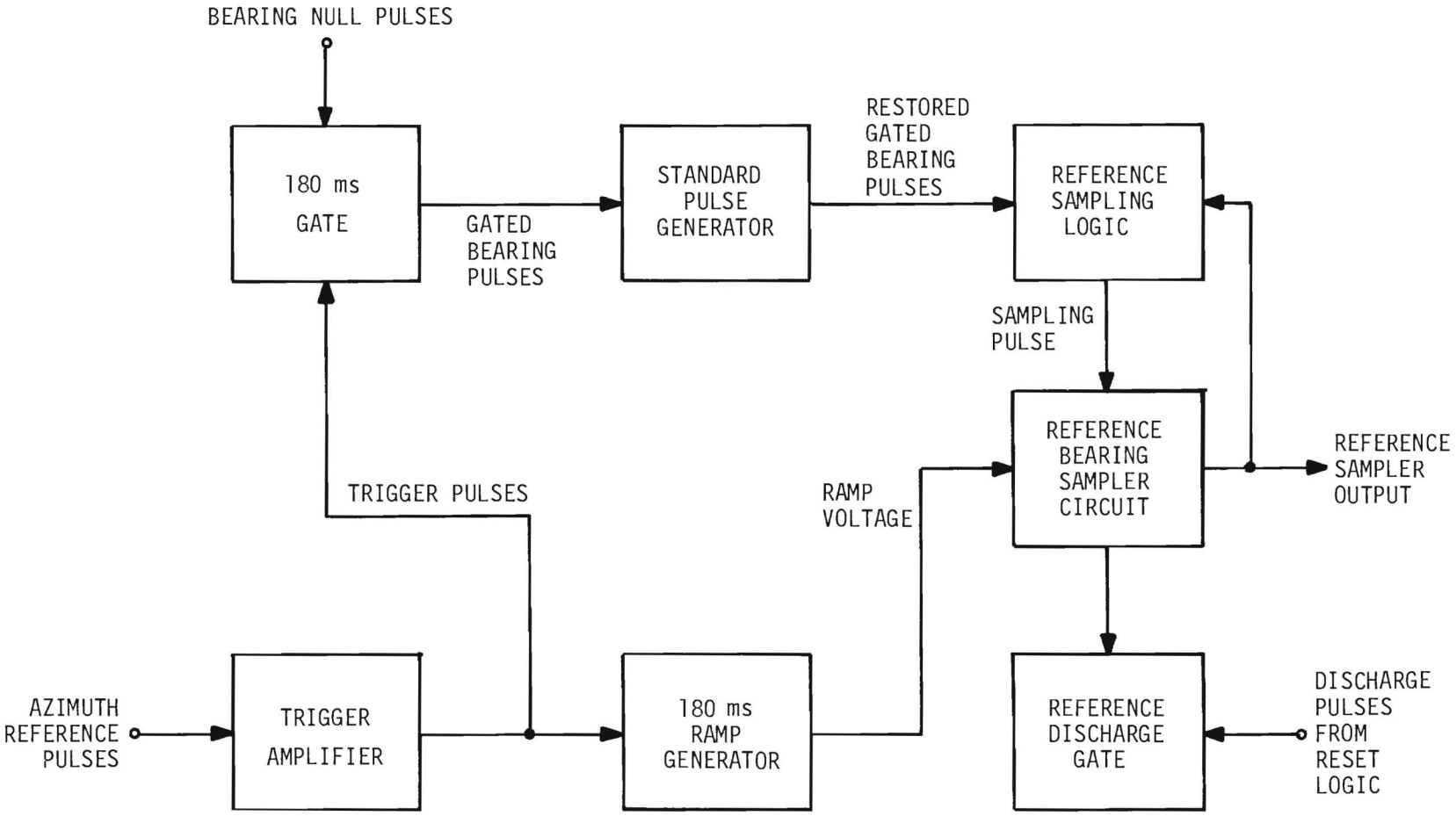

Figure B3. Reference Sampler and Related Circuits.

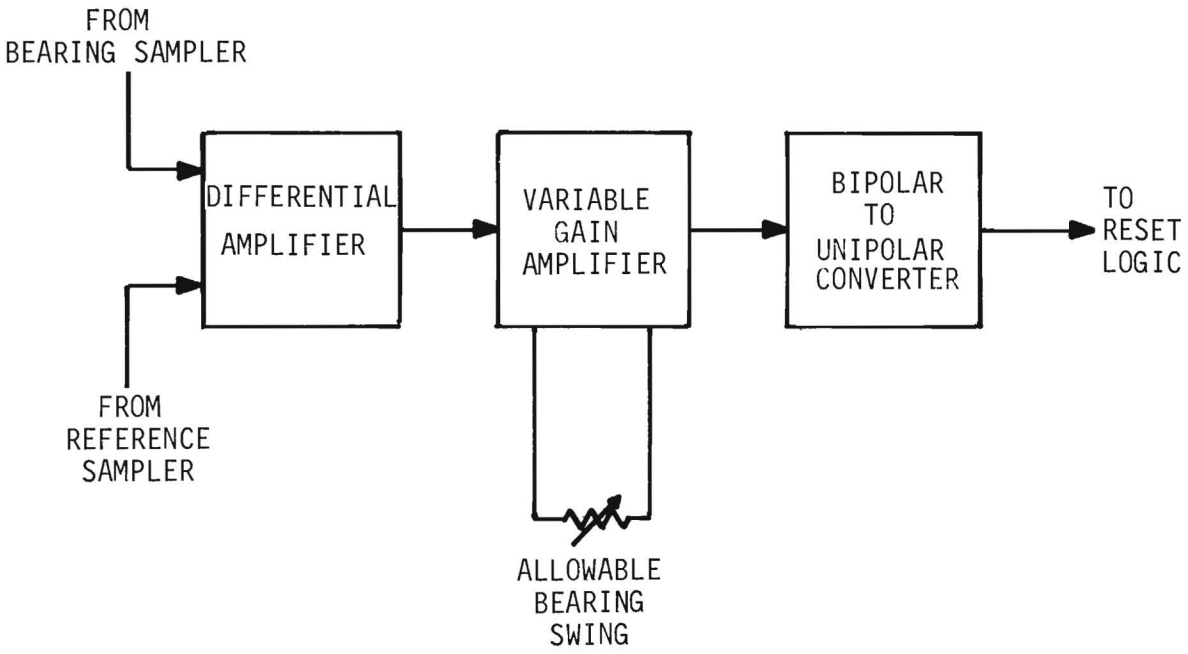

Figure B4. Comparison Circuits.

Thus, the differential amplifier output is proportional to the difference in bearing positions. The output of the differential amplifier is amplified by the variable gain amplifier and fed to the bipolar to unipolar converter. As will become clear later, the gain of the variable gain amplifer determines the amount of swing rate discrimination that the SRD provides. The bipolar signal out of the variable gain amplifier is converted to a unipolar signal by the bipolar-to-unipolar converter. The combined circuits of figure B4 produce an output which is proportional to the absolute value of the difference between the reference sampler and bearing sampler outputs. Moreover, the proportionality factor depends on the circuit gain. Under steady bearing conditions the output of the circuits of figure B4 will be zero.

The four remaining circuits of the SRD shown in figure B5 perform the essential timing and logic operations for the SRD circuit. The reset logic circuit is basically on OR-gate circuit where one input leg may be inhibited by the output of the bipolar to the unipolar converter. If the output of the bipolar to unipolar converter is near zero, the gated bearing pulses do not appear at the output of the reset logic circuit. If the bipolar to unipolar converter output is sufficiently large, the gated bearing pulses appear at the output of the reset logic circuit. Any time that a timer pulse occurs, it also occurs at the output of the reset logic circuit. The output pulses of the reset logic circuit are used to activate the reference discharge gate; therefore, if any bearing sample differs from the reference sample by more than the amount determined by the gain of the variable gain amplifier, the reference discharge gate is activated and a new reference sample is obtained. The timer circuit of figure B5 determines the number of sample bearings to be compared to a given reference sample. The timer circuit is reset whenever a pulse is received from the reset logic circuit, and is started again when the next reference azimuth pulse is received. After starting, the timer is unaffected by additional azimuth pulses and can be stopped by either one of two conditions. First, any time that a reset pulse is received from the reset logic circuit, the timer will stop and commence again at the next reference azimuth pulse. Second, if no reset pulses are received, the timer will stop automatically after eight loop scans have occurred and will generate a timer output pulse. As before, the timer is re-started by a reference azimuth pulse. Note that a timer output pulse is generated only if the timer receives no reset pulses during eight loop scans. The occurrence of a timer output pulse indicates that eight sample bearings have differed from a reference sample bearing by no more than the allowable swing setting of the variable gain amplifier. Whenever a timer pulse occurs, the 355 ms gate opens and allows the next gated bearing pulse to pass to the unblanking gate. Since the 355 ms gate remains open for only 355 ms (one loop scan period), only one gated bearing pulse reaches the unblanking gate. Whenever the unblanking gate receives a bearing pulse,

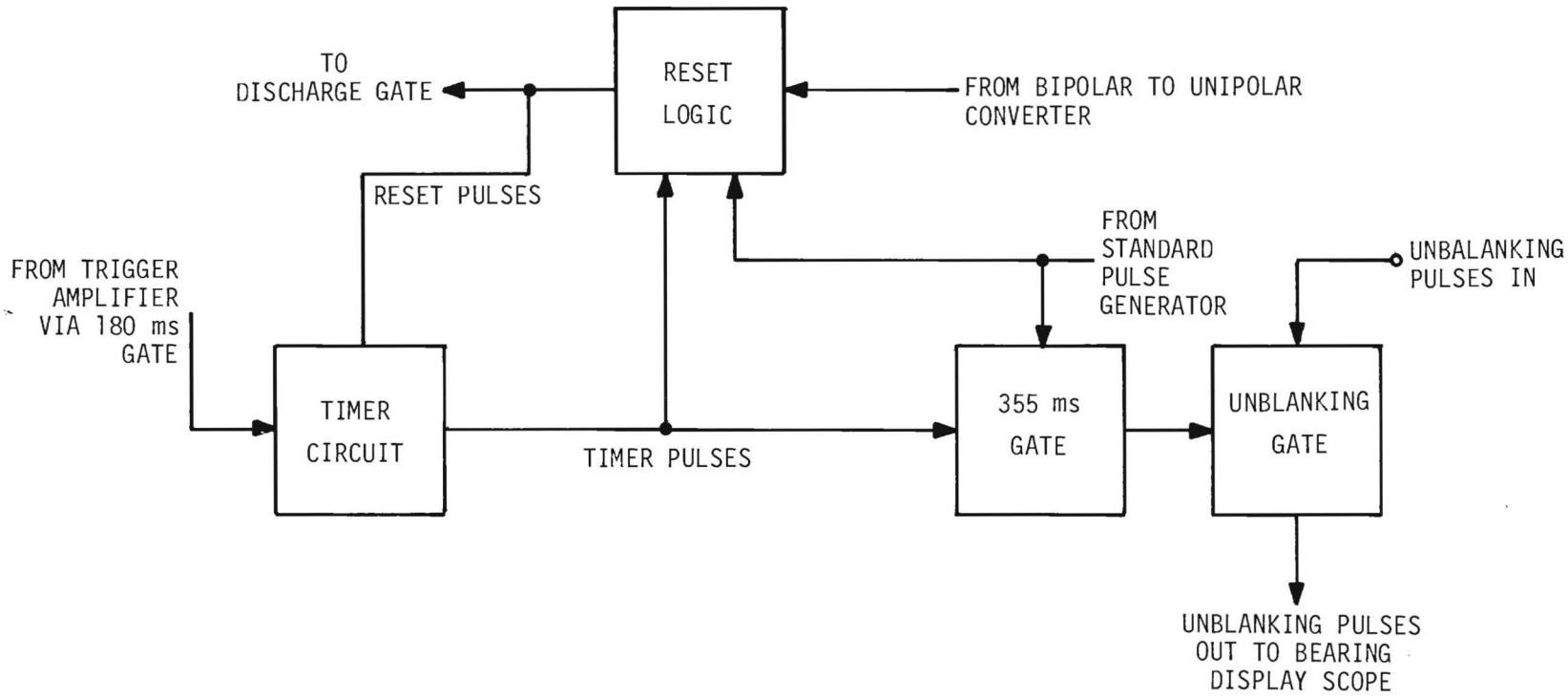

Figure B5. Timing and Logic Circuits.

it allows unblanking pulses to unblank the bearing display oscilloscopes for one loop scan period. Note that the display oscilloscope is unblanked only if eight successive bearings are within the allowable tolerance determined by the allowable swing setting.

Since polarization rotation periods and vertical angles of arrival are time variables, it was unnecessary to calibrate the allowable swing control precisely. This control was made continuously variable from approximately 0 to 20 degrees. Thus, the SRD will accept only those bearings whose rotation rates lie in the range 0 to 20 degrees per eight loop scans. Time-wise these rotation rates lie in the range 0 to 7 degrees per second.

Figure B6 shows a schematic diagram of the swing rate discriminator circuit. The encircled letters refer to the waveforms of figure B7 and figure B8. The sequence of events listed below for two conditions of operation summarize the operational characteristics of the SRD circuit. For Case 1 the waveforms of figure B7 should be referenced, and for Case II the waveforms of figure B8 should be referenced.

Case I: Eight successive bearing samples differ from an initial reference bearing sample by less than the allowable swing setting. This case results from a steady bearing or a bearing whose swing rate is low. Figure B7 illustrates waveforms for case 1 and a bearing with low swing rate. The indexed numerals along the time scale of figure B7 indicate the timing of the events listed below.

1. A dc voltage analog of bearing position is obtained on each loop scan. See waveform K.
2. A dc voltage analog of a reference bearing position is obtained at an arbitrary time. (The sample time coincides with a gated bearing pulse, but the exact time depends on past history). See waveform M.
3. A reference azimuth pulse starts the timer circuit. See waveforms A and H.
4. Each bearing sample for eight successive loop scans is compared to the reference sample and the difference remains within the allowable swing setting. See waveform U.
5. The timer circuit completes its cycle and delivers a pulse which discharges the reference sampler circuit and activates the 355 ms gate. See waveforms I, W, and V.
6. The timer circuit is re-started at the occurrence of reference azimuth pulse. See waveforms A and H.
7. The next gated bearing pulse (waveform F) causes a new reference sample to be obtained (waveform M), resets the timer circuit (waveform H), and opens the unblanking gate (waveform P) for one loop scan. The display oscilloscope is unblanked for one loop scan.

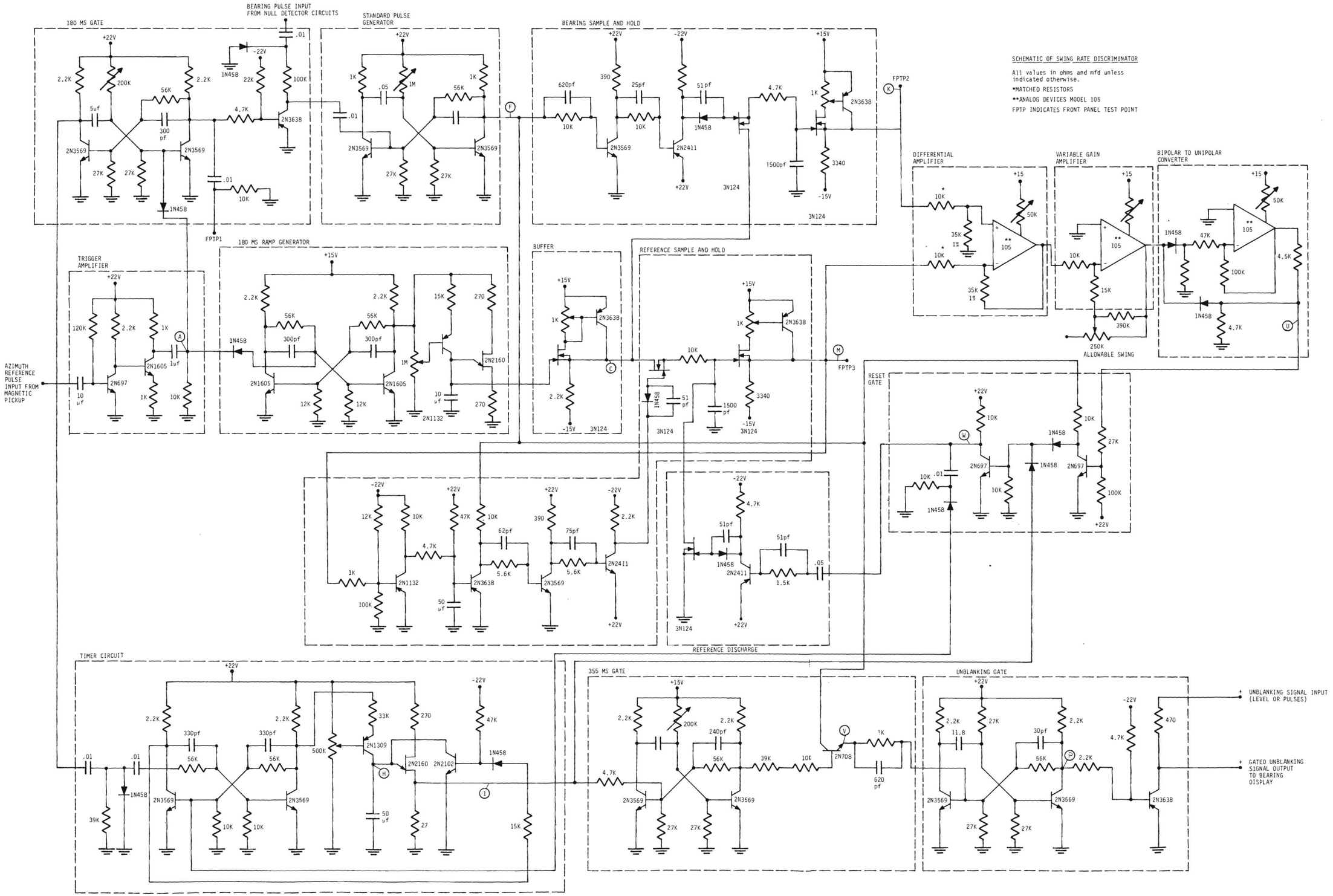

Figure B6. Swing Rate Discriminator Schematic

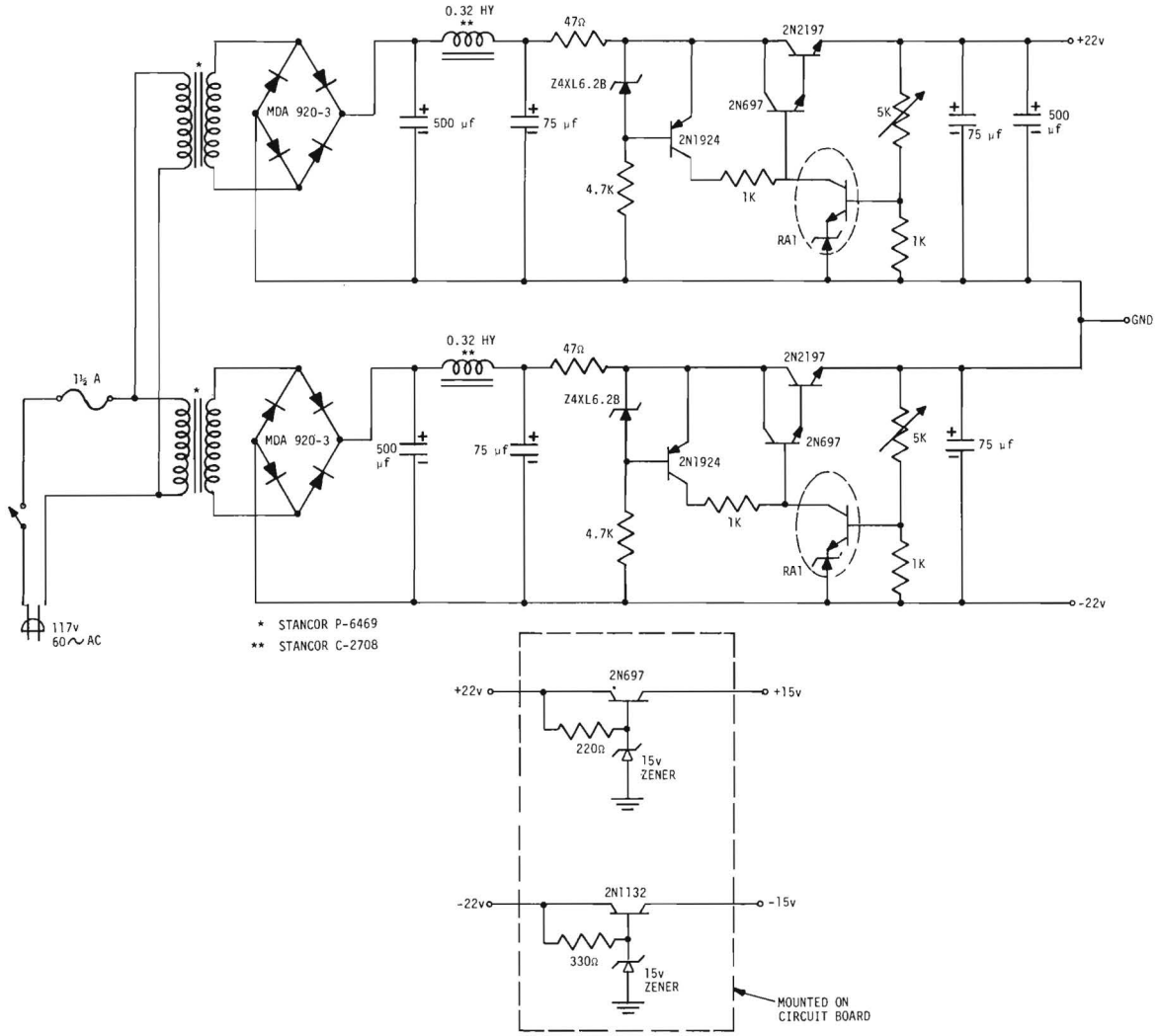

Figure B6 (Continued). Swing Rate Discriminator Schematic.

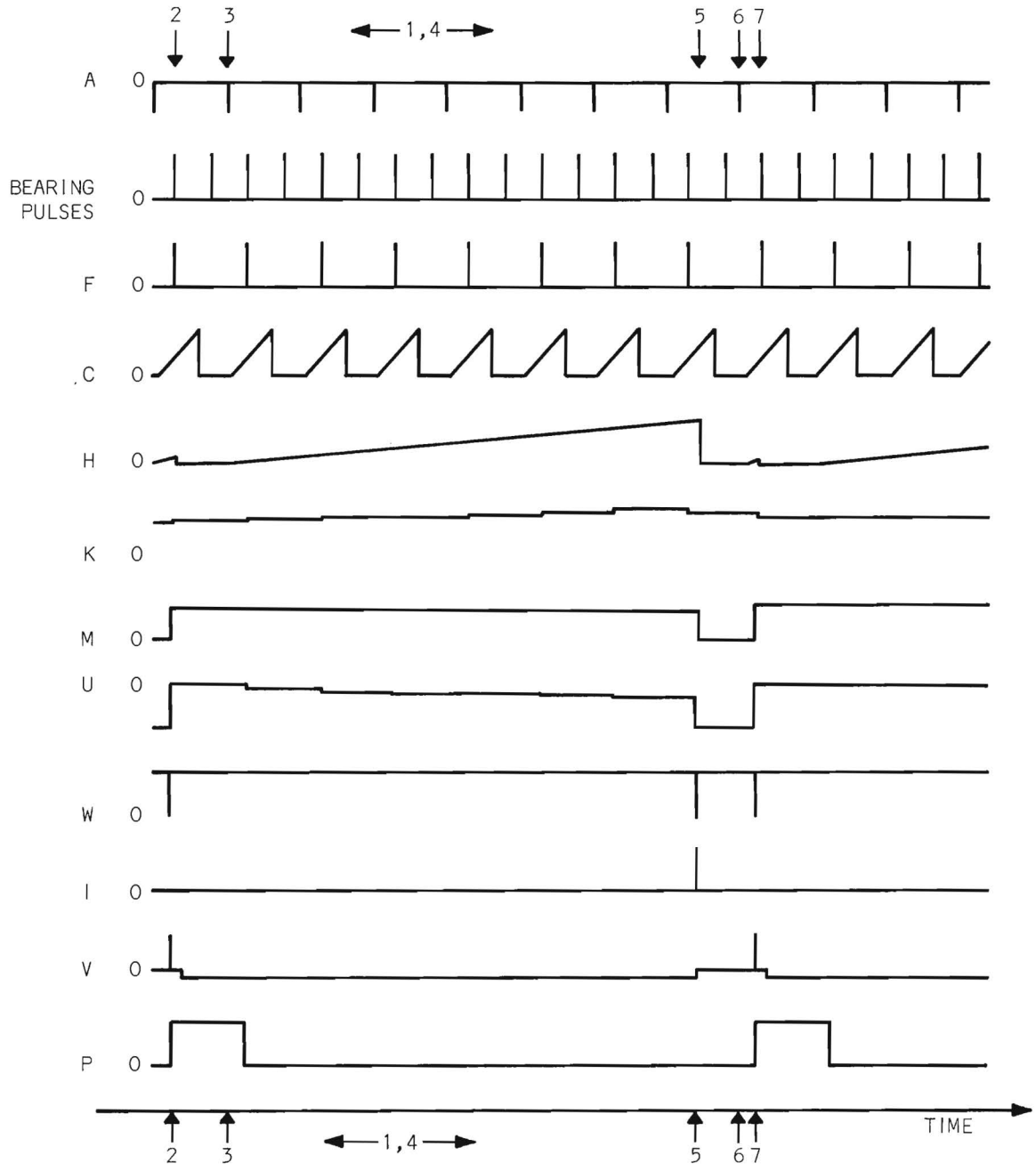

Figure B7. SRD Waveforms for Slowly Swinging Bearing - Case I.

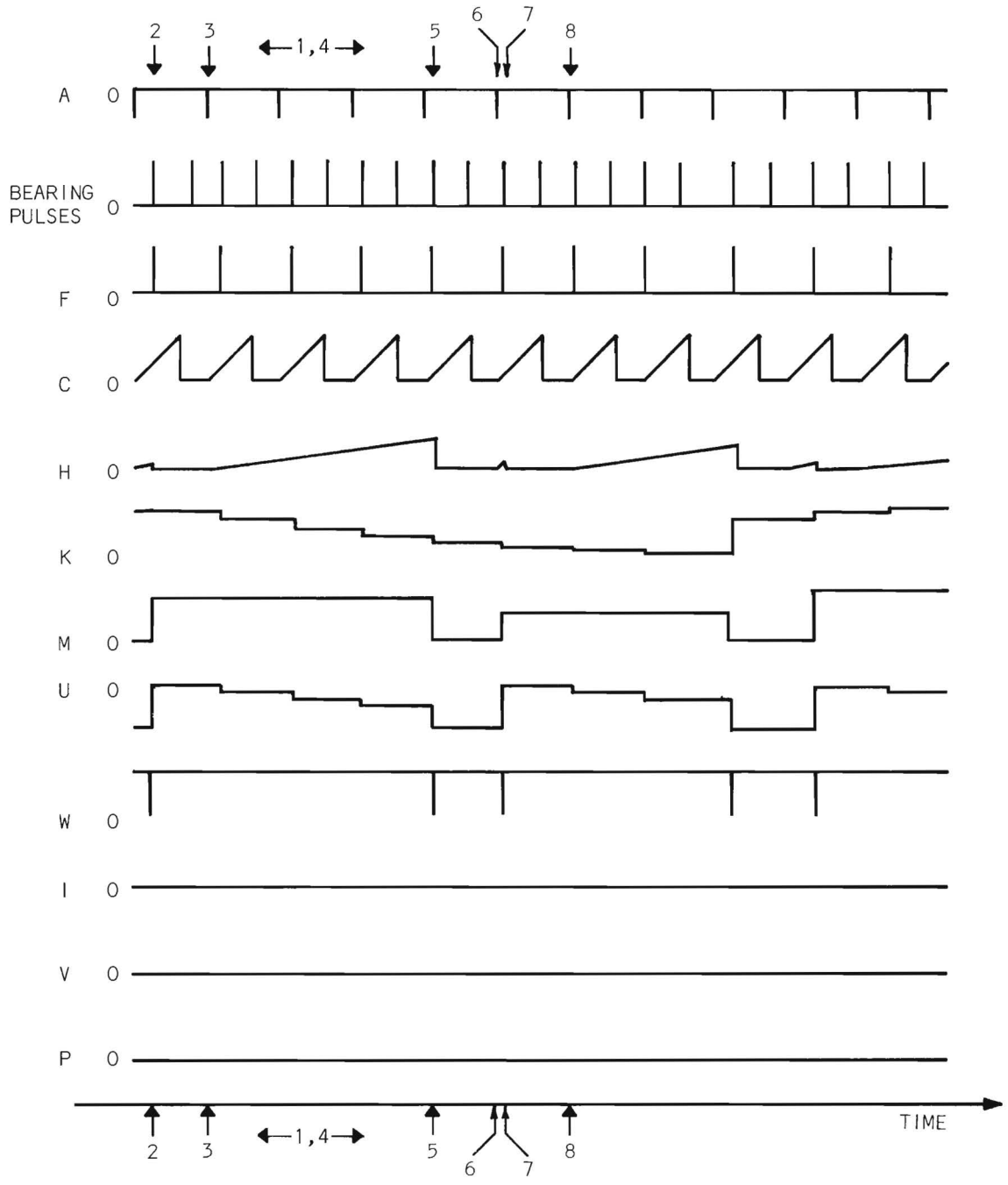

Figure B8. SRD Waveforms for Bearing with Large Swing - Case II.

8. Steps 1 through 7 are repeated as long as the maximum variation of eight successive bearings is within the allowable swing setting. Note that a new reference sample is obtained at the end of eight loop scans, thus, a slowly swinging (or rotating) bearing will be displayed.

NOTE: A bearing that is within the allowable swing setting for only eight scans will not necessarily be displayed. If the reference sample is obtained on the third scan, for example, the bearing may appear to be acceptable for only five scans. If the bearing is within the allowable swing setting for at least sixteen scans, a bearing will always be displayed.

Case II: Eight successive bearing samples differ from an initial reference sample by more than the allowable swing setting. This case results from a bearing whose swing rate is high. Figure B8 illustrates waveforms for case II. The indexed numerals along the time scale of figure B8 indicate the timing of the events listed below.

1. A dc voltage analog of bearing position is obtained on each loop scan. See waveform K.
2. A dc voltage analog of a reference bearing position is obtained at an arbitrary time. (The sample time coincides with a gated pulse, but the exact time depends on past history). See waveform M.
3. A reference azimuth pulse starts the timer circuit. See waveforms A and H.
4. Before eight successive scans have occurred, the difference between the reference sample and one of the bearing samples will exceed the allowable swing setting. See waveform U.
5. The reset gate allows the next gated bearing pulse (waveform F) to discharge the reference sampler and reset the timer circuit. See waveforms W and H.
6. The next reference azimuth pulse re-starts the timer circuit. See waveforms A and H.
7. The next gated bearing pulse (waveform F) causes a new reference sample to be obtained and resets the timer circuit. See waveforms, F, M, and H.
8. The next reference azimuth pulse re-starts the timer circuit. See waveforms A and H.
9. Steps 1 through 8 are repeated as long as the bearing deviation exceeds the allowable swing setting before eight loop scans have occurred. Note that the timer

circuit is never allowed to complete its cycle under these conditions, thus, the display oscilloscope is not unblanked for rapidly swinging bearings.

NOTE: It should be noted that the second gated bearing pulse which is evident in waveform W of figures B7 and B8 does not discharge the reference sampler. The reference discharge circuit and reference sample circuit are designed so that the sampling function overrides the discharge pulse whenever these two events occur simultaneously.

APPENDIX C

TEST SITE FACILITIES, ENVIRONS, AND EQUIPMENT

Figure C1 is an exterior view of the trailer containing the equipment and shows the location of the loop and auxiliary antennas on the roof. This view is toward the north. Figures C2, C3, C4 and C5 depict the environs to the north, east, south, and west, respectively. Figure C6 shows the equipment. The loop and auxiliary receivers are located in the rack to the left. In the rack to the right, the top scope is a general-purpose scope; the next scope displays the raw bearing display; the third scope from the top is the storage scope which displays the processed bearings. The fourth unit from the top is the main unit containing the detection and logic circuitry. The fifth unit from the top is the meter panel used for the monitoring of current and voltage. The sixth unit from the top is the power supply.

Figure C7 is a photograph of the loop scan mechanism with the one-foot square loop. Figure C8 shows the auxiliary channel whip (foreground) and the signal strength recorder whip(background).

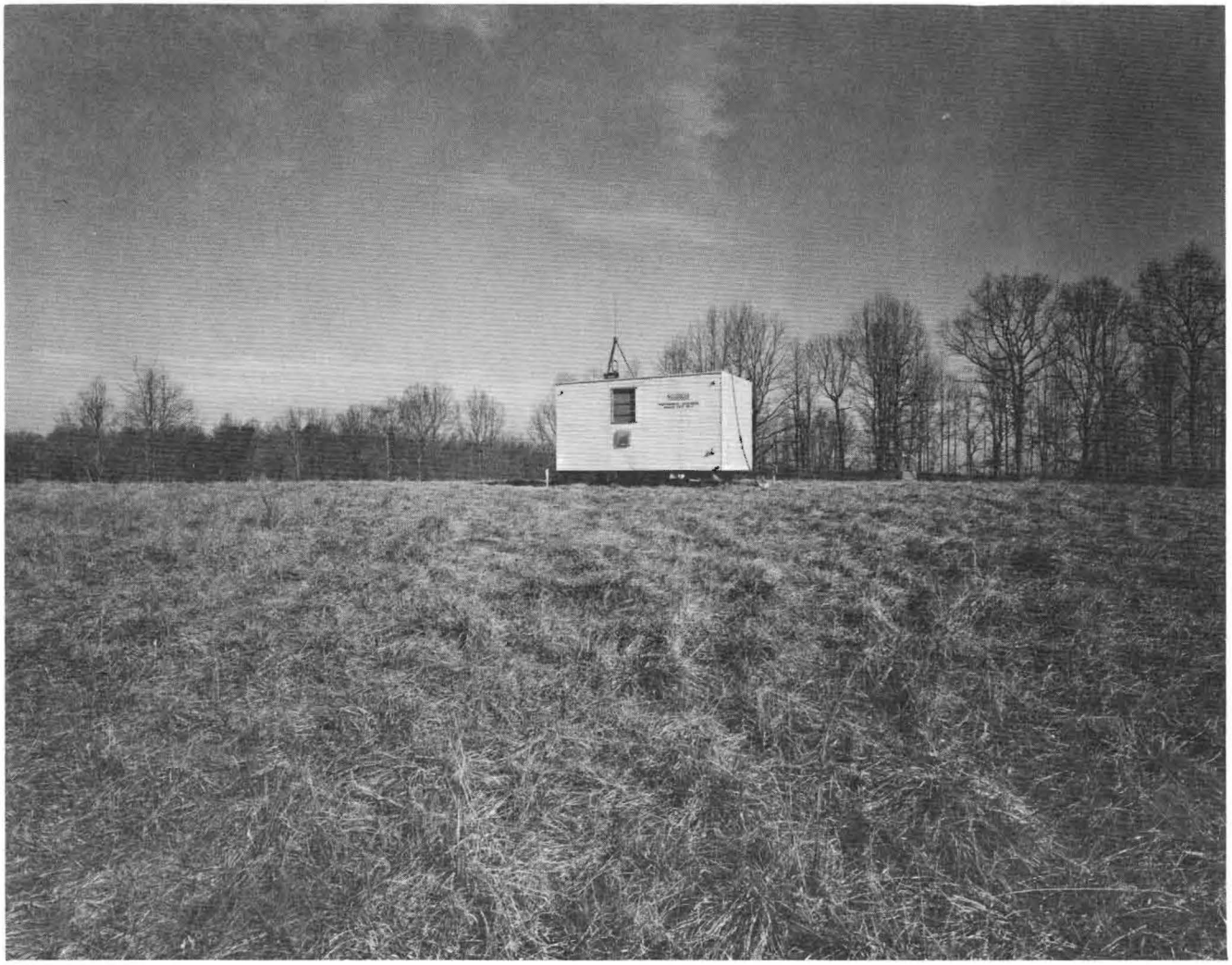

Figure C1. Exterior View of Trailer.

Figure C2. Test Site Environs - North View.

Figure C3. Test Site Environs - East View.

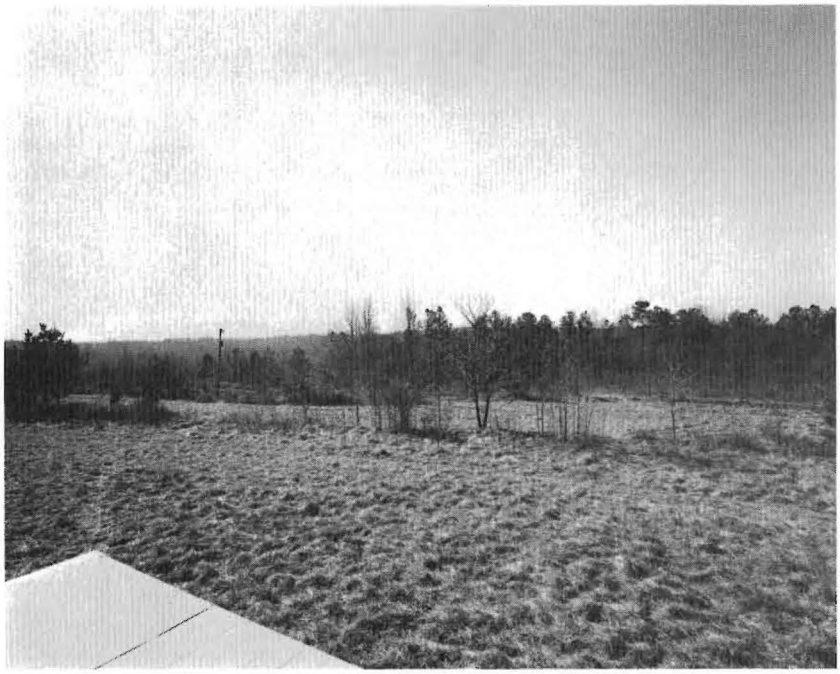

Figure C4. Test Site Environs - South View.

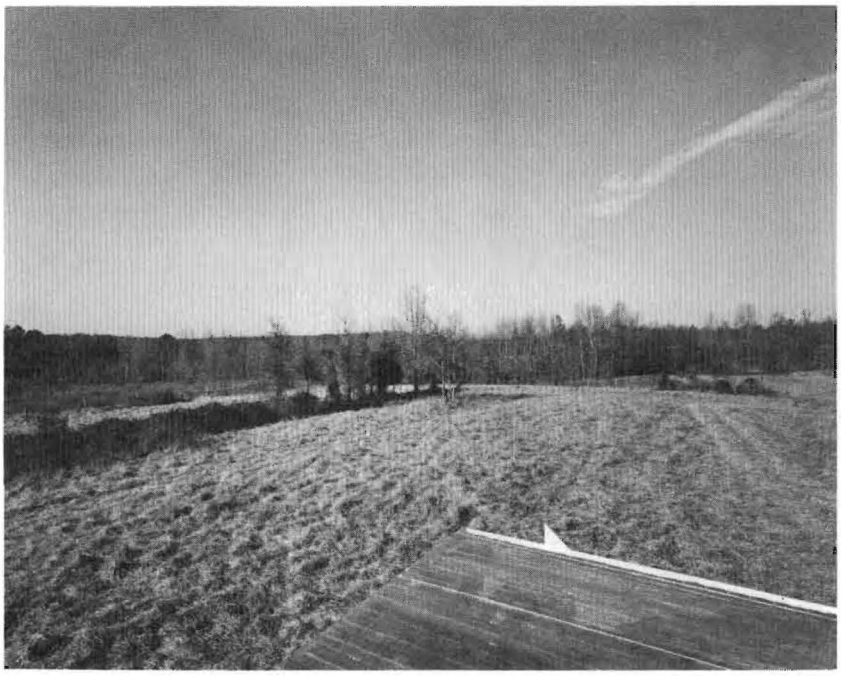

Figure C5. Test Site Environs - West View.

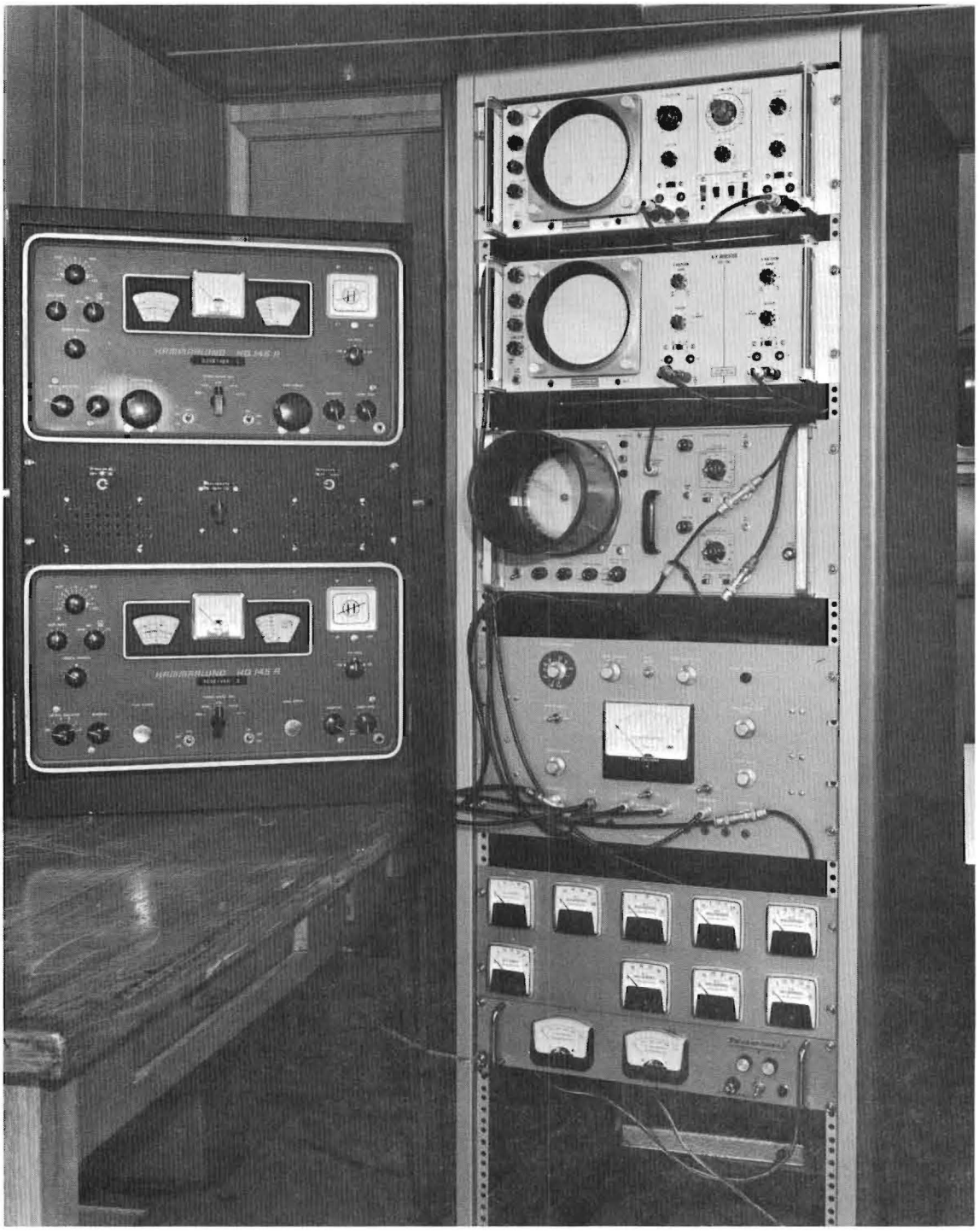

Figure C6. Photograph of Equipment.

Figure C7. Loop Scan Mechanism.

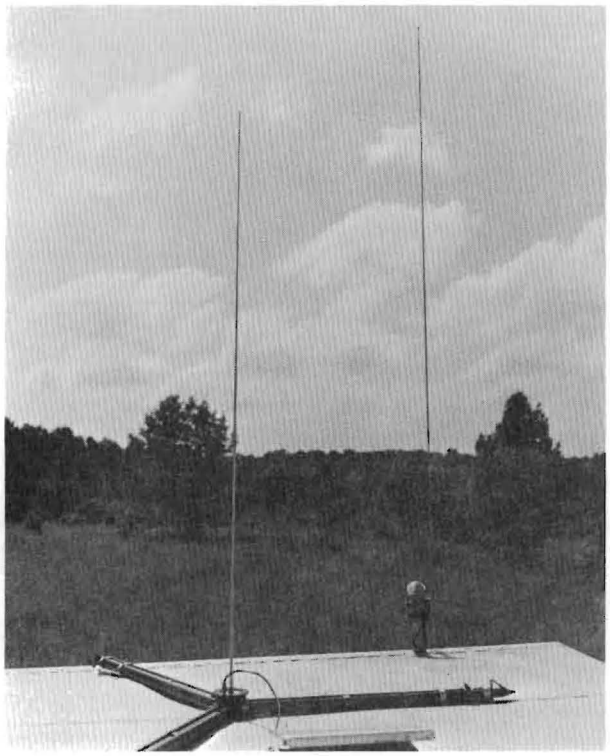

Figure C8. Auxiliary Channel and Signal Strength Recorder Whips.

DISTRIBUTION LIST FOR FINAL REPORT on CONTRACT NO. DA 28-043 AMC-01207(E)

No. of Copies	To
20	Director, National Security Agency, Attn: TDL, Fort George Meade, Maryland, 20755
1	Office of Assistant Secretary of Defense, (Research and Engineering), Attn: Technical Library, Rm 3E1065, Washington, D. C., 20315
1	Chief of Naval Research, Attn: Code 427, Department of the Navy, Washington, D. C., 20325
1	Naval Ships Systems Command Technical Library, Attn: Code 6312, Main Navy Building, Room 1528, Washington, D. C., 20325
1	Chief, Bureau of Ships, Attn: Code 686B, Department of the Navy, Washington, D. C., 20325
1	Chief, Bureau of Ships, Attn: Code 454, Department of the Navy, Washington, D. C., 20360
1	Director, U. S. Naval Research Laboratory, Attn: Code 2027, Washington, D. C., 20390
1	Commanding Officer and Director, U. S. Navy Electronics Laboratory, Attn: Library, San Diego, California, 92101
1	Commander, U. S. Naval Ordnance Laboratory, White Oak, Silver Spring, Maryland, 20390
1	AFSC Scientific/Technical Liaison Office, U. S. Naval Air Development Center, Johnsville, Pennsylvania
1	Headquarters, U. S. Air Force, Attn: AFCIN, Washington, D. C. 20325
1	Rome Air Development Center, Attn: RAALD, Griffiss Air Force Base, New York, 13442
1	Headquarters, Strategic Air Command, Attn: DOCE, Offuit Air Force Base, Nebraska, 68113
1	Systems Engineering Group (SEPIR), Wright-Patterson Air Force Base, Ohio, 45453
1	Electronic Systems Division (AFSC), Scientific and Technical Info Div. (ESTI), L. G. Hanscom Field, Bedford, Massachusetts, 01731
1	Air Force Cambridge Research Laboratories, Attn: CRXL-R, L. G. Hanscom Field, Bedford, Massachusetts, 01731

No. of Copies	To
1	Commanding General, U. S. Army Electronics Command, Attn: AMSEL-10-T, Fort Monmouth, New Jersey 07703
1	Commanding General, U. S. Army Electronics Command, Attn: AMSEL-RD-DR, Fort Monmouth, New Jersey 07703
1	Commanding General, U. S. Army Electronics Command, Attn: AMSEL-RD-ADT, Fort Monmouth, New Jersey 07703
1	Commanding General, U. S. Army Electronics Command, Attn: AMSEL-RD-ADO-RHA, Fort Monmouth, New Jersey 07703
1	Commanding General, U. S. Army Electronics Command, Attn: AMSEL-RD-LNA, Fort Monmouth, New Jersey 07703
1	Commanding General, U. S. Army Electronics Command, Attn: AMSEL-RD-LNR, Fort Monmouth, New Jersey 07703
1	Commanding Officer, U. S. Army Electronics R & D Activity, Attn: SELWS-AJ, White Sands, New Mexico 88002
1	Chief, U. S. Army Electronics Laboratories, Mountain View Office, P. O. Box 205, Mountain View, California 94042
1	Chief, U. S. Army Electronics Intelligence, Materiel Development Office, Attn: AMSEL-RD-IMC, Fort Holabird, Maryland 21219
1	Chief, U. S. Army Electronics Laboratories, Willow Run Office, The University of Michigan, P. O. Box 618, Ann Arbor, Michigan 48107
1	USAEL Liaison Office, Aeronautical Systems Division, Attn: ASDL-9, Wright-Patterson AF Base, Ohio 45433
1	USAEL Liaison Officer, Rome Air Development Center, Attn: RAOL, Griffiss Air Force Base, New York 13442
1	U. S. National Bureau of Standards, Boulder Laboratories, Attn: Library, Boulder, Colorado
1	NASA Representative, Scientific and Technical Information Facility, P. O. Box 5700, Bethedsa, Maryland 20014
1	Commanding General, U. S. Army Electronics Command, Attn: AMSEL-WL-C, Fort Monmouth, New Jersey

No. Of Copies	To
1	U. S. Air Force Security Service, Attn: ESD, San Antonio, Texas
1	Headquarters, Research and Technology Division, Attn: RTH Bolling A. F. Base, Washington, D. C. 20325
2	Chief of Research and Development, Department of the Army, Washington, D. C. 20315
1	OFC of the Chief of Communications-Electronics, Attn: OCC-E, Department of the Army, Washington, D. C. 20315
1	OFC of the Chief of Communications-Electronics, Attn: CCEES-1A, Department of the Army, Washington, D. C., 20315
2	Commanding General, U. S. Army Material Command, Attn: R & D Directorate, Washington, D. C. 20315
1	Headquarters, U. S. Army Continental Army Command, Fort Monroe, Virginia
1	Commanding General, U. S. Army Combat Developments Command, Attn: CDCMR-E, Fort Belvoir, Virginia 22060
1	Commanding General, U. S. Army Combat Developments Command, Communications-Electronics Agency, Fort Huachuca, Arizona
2	Chief, U. S. Army Security Agency, Attn: ACofS, 64 (Technical Library), Arlington Hall Station, Arlington, Virginia 22207
1	Deputy President, U. S. Army Security Agency Board, Arlington Hall Station, Arlington, Virginia 22207
1	Commanding Officer, U. S. Army Security Agency Processing Center, Vint Hill Farms Station, Warrenton, Virginia 22186
1	Commanding Officer, Harry Diamond Laboratories, Connecticut Ave and Van Ness St., N. W., Washington, D. C. 20438
2	Command Officer, U. S. Army Engineer R & D Laboratories, Attn: Stinfo Branch, Fort Belvoir, Virginia
1	Commanding General, U. S. Army Electronic Proving Ground Attn: Technical Library, Fort Huachuca, Arizona 85613
5	Commanding General, U. S. Army Electronics Command, Attn: AMSEL-WL-S, Fort Monmouth, New Jersey 07703
1	USAECOM Commodity Management Office, Attn: AMSEL-EW, Fort Monmouth, New Jersey 07703

UNCLASSIFIED

Security Classification

DOCUMENT CONTROL DATA - R&D

(Security classification of title, body of abstract and indexing annotation must be entered when the overall report is classified)

1. ORIGINATING ACTIVITY *(Corporate author)*
Georgia Institute of Technology, Atlanta, Georgia

2a. REPORT SECURITY CLASSIFICATION
Unclassified

2b. GROUP

3. REPORT TITLE

ERROR REDUCTION IN LOOP DIRECTION FINDERS

4. DESCRIPTIVE NOTES *(Type of report and inclusive dates)*
Final Report - 1 March 1965 to 30 June 1967

5. AUTHOR(S) *(Last name, first name, initial)*

Jenkins, Herndon H., Jr., and Moss, Richard W.

6. REPORT DATE	7a. TOTAL NO. OF PAGES	7b. NO. OF REFS
September 1967	146	54

8a. CONTRACT OR GRANT NO.
DA 28-043 AMC-01207(E)

b. PROJECT NO.
5A6-79191-D902

c. Task No. 01

d. Sub-task No. 03

9a. ORIGINATOR'S REPORT NUMBER(S)
A-842-8

9b. OTHER REPORT NO(S) *(Any other numbers that may be assigned this report)*
ECOM-01207-F

10. AVAILABILITY/LIMITATION NOTICES U. S. Military agencies may obtain copies of this report directly from Dir. NSA, Attn: TDL, Fort George Meade, Md., 20755. Other qualified users shall request through U. S. Army Electronics Command, AMSEL-WL-S, Fort Monmouth, New Jersey 07703.

11. SUPPLEMENTARY NOTES

12. SPONSORING MILITARY ACTIVITY
U. S. Army Electronics Command
AMSEL-WL-S
Fort Monmouth, New Jersey

13. ABSTRACT Techniques for reducing bearing errors in vertical loop HF direction finders for ionospherically propagated signals were developed and operationally evaluated. The investigation was concerned with the determination of specific characteristics of the incident signal and the subsequent use of these characteristice to restrict the display of the bearing information to theconditions that produce minimum bearing error.

The techniques were implemented in an exploratory dual-channel HF/DF system. The main channel produced a bearing display from the output of a rotating vertical loop; the auxiliary channel unblanked the bearing display when conditions were favorable for minimum bearing errors. A storage scope was also used for bearing display and memory.

Analyses of the error producing effects in loop systems showed that: (1) minimum bearing errors can be expected at or near the maxima of the vertical component of the incident signal; and (2) steady bearings normally possess less error than swinging bearings. Unblanking information was obtained by either detecting the fade crests of the vertical component of the incident signal or by using a swing rate discriminator to determine a steady bearing condition. Several modes of fade crest detection were included to optimize performance for a wide variety of signal and fade conditions.

DD FORM 1 JAN 64 1473

Unclassified
Security Classification

14. KEY WORDS	LINK A		LINK B		LINK C	
	ROLE	WT	ROLE	WT	ROLE	WT
Direction Finding Ionospheric Waves HF Propagation Loop Antennas Fading Characteristics Storage Scopes Polarization Fading Multipath Fading Elevation Angle-of-Arrival Bearing Swing Rates Operational Evaluation						

INSTRUCTIONS

1. ORIGINATING ACTIVITY: Enter the name and address of the contractor, subcontractor, grantee, Department of Defense activity or other organization *(corporate author)* issuing the report.

2*a*. REPORT SECURITY CLASSIFICATION: Enter the overall security classification of the report. Indicate whether "Restricted Data" is included. Marking is to be in accordance with appropriate security regulations.

2*b*. GROUP: Automatic downgrading is specified in DoD Directive 5200.10 and Armed Forces Industrial Manual. Enter the group number. Also, when applicable, show that optional markings have been used for Group 3 and Group 4 as authorized.

3. REPORT TITLE: Enter the complete report title in all capital letters. Titles in all cases should be unclassified. If a meaningful title cannot be selected without classification, show title classification in all capitals in parenthesis immediately following the title.

4. DESCRIPTIVE NOTES: If appropriate, enter the type of report, e.g., interim, progress, summary, annual, or final. Give the inclusive dates when a specific reporting period is covered.

5. AUTHOR(S): Enter the name(s) of author(s) as shown on or in the report. Enter last name, first name, middle initial. If military, show rank and branch of service. The name of the principal author is an absolute minimum requirement.

6. REPORT DATE: Enter the date of the report as day, month, year; or month, year. If more than one date appears on the report, use date of publication.

7*a*. TOTAL NUMBER OF PAGES: The total page count should follow normal pagination procedures, i.e., enter the number of pages containing information.

7*b*. NUMBER OF REFERENCES: Enter the total number of references cited in the report.

8*a*. CONTRACT OR GRANT NUMBER: If appropriate, enter the applicable number of the contract or grant under which the report was written.

8*b*, 8*c*, & 8*d*. PROJECT NUMBER: Enter the appropriate military department identification, such as project number, subproject number, system numbers, task number, etc.

9*a*. ORIGINATOR'S REPORT NUMBER(S): Enter the official report number by which the document will be identified and controlled by the originating activity. This number must be unique to this report.

9*b*. OTHER REPORT NUMBER(S): If the report has been assigned any other report numbers *(either by the originator or by the sponsor)*, also enter this number(s).

10. AVAILABILITY/LIMITATION NOTICES: Enter any limitations on further dissemination of the report, other than those imposed by security classification, using standard statements such as:

(1) "Qualified requesters may obtain copies of this report from DDC."

(2) "Foreign announcement and dissemination of this report by DDC is not authorized."

(3) "U. S. Government agencies may obtain copies of this report directly from DDC. Other qualified DDC users shall request through _____."

(4) "U. S. military agencies may obtain copies of this report directly from DDC. Other qualified users shall request through _____."

(5) "All distribution of this report is controlled. Qualified DDC users shall request through _____."

If the report has been furnished to the Office of Technical Services, Department of Commerce, for sale to the public, indicate this fact and enter the price, if known.

11. SUPPLEMENTARY NOTES: Use for additional explanatory notes.

12. SPONSORING MILITARY ACTIVITY: Enter the name of the departmental project office or laboratory sponsoring *(paying for)* the research and development. Include address.

13. ABSTRACT: Enter an abstract giving a brief and factual summary of the document indicative of the report, even though it may also appear elsewhere in the body of the technical report. If additional space is required, a continuation sheet shall be attached.

It is highly desirable that the abstract of classified reports be unclassified. Each paragraph of the abstract shall end with an indication of the military security classification of the information in the paragraph, represented as *(TS), (S), (C), or (U)*.

There is no limitation on the length of the abstract. However, the suggested length is from 150 to 225 words.

14. KEY WORDS: Key words are technically meaningful terms or short phrases that characterize a report and may be used as index entries for cataloging the report. Key words must be selected so that no security classification is required. Identifiers, such as equipment model designation, trade name, military project code name, geographic location, may be used as key words but will be followed by an indication of technical context. The assignment of links, roles, and weights is optional.